HARNESSING MESENCHYMAL STEM CELLS AND CD200 TO FABRICATE IMMUNE-EVADING BIOMATERIALS FOR THERAPEUTIC APPLICATIONS

A Dissertation

Presented in Partial Fulfillment of the Requirements for the

Degree of Doctor of Philosophy

with a

Major in Biological Engineering

in the

College of Graduate Studies

University of Idaho

by

Jun Zhang

Major Professor: Ching-An Peng, Ph.D.

Committee Members: Nathan Schiele, Ph.D.; Jill L. Johnson, Ph.D.;

Darren A. Thompson, Ph.D.

Department Administrator: Ching-An Peng, Ph.D.

May 2019

AUTHORIZATION TO SUBMIT DISSERTATION

This dissertation of Jun Zhang, submitted for the degree of Doctor of Philosophy with a major in Biological Engineering and titled "HARNESSING MESENCHYMAL STEM CELLS AND CD200 TO FABRICATE IMMUNE-EVADING BIOMATERIALS FOR THERAPEUTIC APPLICATIONS," has been reviewed in final form. Permission, as indicated by the signatures and dates given below, is now granted to submit final copies to the College of Graduate Studies for approval.

Major Professor: _____ Date: _____
　　　　　　　　　Ching-An Peng, Ph.D.

Committee Members: _____ Date: _____
　　　　　　　　　Nathan Schiele, Ph.D.

　　　　　　　　　_____ Date: _____
　　　　　　　　　Jill L. Johnson, Ph.D.

　　　　　　　　　_____ Date: _____
　　　　　　　　　Darren A. Thompson, Ph.D.

Department
Administrator: _____ Date: _____
　　　　　　　　　Ching-An Peng, Ph.D.

ABSTRACT

Mesenchymal stem cells (MSCs) are multipotent stromal cells derived from bone-marrow. Antioxidants such as ascorbic acid and have been supplemented into the medium of MSCs to enhance the proliferation and differentiation of MSCs. In this study, astaxanthin, a highly potent and lipid soluble antioxidant extracted from green algae *Haematococcus pluvialis*, was encapsulated by methoxy polyethylene glycol-polycaprolactone (mPEG-PCL) polymeric micelles to increase its aqueous solubility. Astaxanthin encapsulated mPEG-PCL was supplemented in the culture medium and chondrogenic, adipogenic and osteogenic differentiation medium to enhance the proliferation and differentiation of human MSCs. A thermo-sensitive polymer poly(N-isopropylacrylamide) (PNIPAAm) surface was then used to culture and harvest MSCs with a temperature switch. As a result, astaxanthin enhanced not only the proliferation of MSCs but also the differentiation of MSCs. Also, MSCs can be harvested from PNIPAAm surface without using trypsin. Due to the intrinsic tumor-tropic feature of MSCs, MSCs are used in cancer therapy for drug and gene delivery. Carbon nanotubes (CNTs) are used in photothermal therapy because they can absorb near infrared (NIR) radiation and release heat. In this study, CNTs were anchored on the surfaces of human MSCs as a cell-based tumor-targeted system for potential application in photothermal therapy. As a result, CNT-tagged MSCs were able to migrate toward the chemoattractant SDF-1α when the amount of CNT on MSCs was no more than the threshold value 4.26 ng CNT per cell. MSCs also possess immunosuppressive properties. CD200 is an anti-inflammatory transmembrane glycoprotein expressed on MSC surfaces. The interaction between CD200 and its receptor CD200R has known to reduce macrophage activation and chronic inflammation. In this study, CD200 was appended on the surface of nano- and micro-sized polystyrene particles to reduce macrophage phagocytosis. A polyethylene glycol (PEG)/CD200 co-immobilized biomaterial surface was also fabricated for reduced macrophage attachment. The results demonstrated that CD200 modification decreased macrophage phagocytic activities for both nano- and micro-sized particles. PEG/CD200 co-immobilized surface showed delayed macrophage attachment as well as reduced interleukin-6 and TNF-α secretion from macrophages.

ACKNOWLEDGEMENTS

DEDICATION

This work is dedicated to my beloved wife Binqi Li, who has been constantly supporting and encouraging me throughout my Ph.D. study. To my lovely daughter Grace J. Zhang for being my little angel.

TABLE OF CONTENTS

LIST OF FIGURES

Chapter 1. Introduction

1.1 General Introduction

      Mesenchymal stem cells (MSCs) are multi-potent cells derived from bone marrow. MSCs are widely used in tissue engineering and regenerative medicine because of they are able to self-renew and differentiate into multi-lineage cells. Human MSCs can differentiate into mesodermal lineage such as adipocytes, osteocytes and chondrocytes (Sarugaser et al. 2009, Caplan 2007). Moreover, MSCs possess immunomodulatory properties (Iyer and Rojas 2008). MSCs are able to home to sites of injury and respond to injuries in similar manner as the immune system responds to foreign pathogens (Dimarino, Caplan, and Bonfield 2013). Studies have shown that MSCs can suppress modulate immune responses of T cells (Selmani et al. 2008), B cells (Corcione et al. 2006), dendritic cells (Zhang et al. 2004), macrophages (Nemeth et al. 2009), etc. Due to the easy accessibility and their unique properties, MSCs have shown great potentials in tissue regeneration and wound healing during clinical applications (Nasef et al. 2007, Chen et al. 2008, Hayashi et al. 2008).

      MSCs can be expanded *in vitro* and then differentiated into adipocytes, osteocytes and chondrocytes under different cultural conditions (Pittenger et al. 1999). MSCs within 5 passages can generally be used for clinical applications (Jiang et al. 2017). Clinical studies show that passage 1-2 MSCs demonstrated improved patient survival than passage 3-4 cells (Jiang et al. 2017). However, the proliferative capability and potency of MSCs declines gradually with passaging. Elevated level of reactive oxygen species (ROS) could cause stem cells to lose their self-renewal property (Jang and Sharkis 2007). Therefore, obtaining sufficient cell number during in vitro expansion is crucial for transplantation (Bellayr et al. 2014).

      The primary focus of this dissertation is to use human MSCs and CD200 protein to fabricate immune-evading biomaterials for therapeutic applications. The first part of this dissertation focuses on the proliferation and differentiation of human MSCs *in vitro*. Antioxidants such as ascorbic acid and N-acetylcysteine (NAC) have been used to enhance the proliferation and differentiation of human MSCs (Fan et al. 2011, Choi et al. 2008). In this dissertation, a potent antioxidant astaxanthin will be used to enhance *in*

vitro proliferation and differentiation of human MSCs. Traditionally, mammalian cells cultured *in vitro* are harvested by enzymatic treatment such as trypsin-EDTA. However, enzymatic treatment could disrupt the extracellular matrix (ECM) and make the MSCs lose their differentiated phenotypes (Yang et al. 2012). Poly(N-isopropylacrylamide) (PNIPAAm) is a temperature-sensitive polymer. Human MSCs harvested from PNIPAAm-modified surfaces have shown higher cell viability, better proliferation, and stronger differentiation than MSCs harvested by trypsinization after three cell passages (Yang et al. 2012). In this study, surface of tissue culture petri dish will be modified with PNIPAAm coating through polydopamine film. Polydopamine film can be prepared with a simple dip coating method, and PNIPAAm film can be produced without using any special instrument. Human MSCs will be harvested from PNIPAAm-*g*-polydopamine surface with a temperature switch.

The second part of this dissertation focuses on the use of human MSCs and carbon nanotubes (CNTs) for a potential tumor-targeted system. MSCs are used as cell carriers for cancer therapy because of their tumor-homing capability (Kucerova et al. 2013, Roger et al. 2010). CNTs are used in photothermal therapy because they can absorb near infrared (NIR) light and release heat (Wang et al. 2011, Kam et al. 2005). In this study, CNTs will be anchored on the surface of human MSCs through biotin-streptavidin binding. This cell-based tumor-targeted system can efficiently deliver CNTs to tumor cites and has the potential for photothermal therapy.

The third part of this dissertation focuses on CD200 protein modified 2D and 3D biomaterial surface for the fabrication of immune-evading biomaterials. CD200 is a widely expressed anti-inflammatory transmembrane glycoprotein in the immunoglobin superfamily (Clark et al. 1985). CD200 is expressed on the surfaces of T cells, B cells, and dendritic cells (Barclay et al. 2002). CD200 interacts with its receptor CD200R, which is expressed on the surface myeloid cells such as macrophages, neutrophils, and microglia(Hoek et al. 2000). The CD200-CD200R interaction has shown to inhibit macrophage activation (Koning et al. 2010) and reduce chronic inflammation (Elward and Gasque 2003, Kim et al. 2014, Varnum et al. 2015). CD200 is also expressed on the surface of MSCs. Co-culturing CD200 positive MSCs with macrophages has shown to suppress macrophage inflammatory responses (Pietilä et al. 2012). In this study, nano-

and micro-sized polystyrene 3D particles will be modified with CD200-core streptavidin fusion protein in order to reduce macrophage phagocytosis through CD200-CD200R interaction. Furthermore, polyethylene glycol (PEG) is a hydrophilic polymer used to reduce non-specific protein adsorption on biomaterial surface. Also, a PEG/CD200 co-immobilized 2D biomaterial surface will be fabricated in order to reduce macrophage attachment as well as proinflammatory cytokine secretion.

1.2 The Effect of Antioxidant on MSC Proliferation and Differentiation

Antioxidants have shown to enhance the in vitro proliferation and differentiation of stem cells by decreasing reactive oxygen species (ROS) levels and increasing the expression of antioxidant enzymes (Denu and Hematti 2016). MSC proliferation has also been improved by supplementing culture medium with antioxidants such as ascorbic acid, phenyl-α-tert-butylnitrone and N-acetylcysteine (NAC) (Fan et al. 2011, Choi et al. 2008). For example, ascorbic acid 2-phosphate has shown to enhance the proliferation of MSCs at the concentration of 250 mM (Choi et al. 2008). The same group also showed that ascorbic acid 2-phosphate promoted adipogenic and osteogenic differentiation of MSCs at the concentration of 250 mM and 50 mM, respectively (Choi et al. 2008).

Astaxanthin is a potent antioxidant derived from green microalgae, *Haematococcus pluvialis* (Figure 1.1). The activity of astaxanthin is reported to be ten times higher than various carotenoids such as lutein, α-carotene and β-carotene (Naguib 2000). Kim *et al.* reported that astaxanthin could improve the proliferation as well as adipogenic and osteogenic differentiation of neural stem cells (Kim et al. 2010). In their study, astaxanthin was prepared as a stock solution in dimethyl sulfoxide (DMSO) due to the low aqueous solubility of astaxanthin. However, using DMSO certainly is an issue when applying astaxanthin for *in vivo* applications (Galvao et al. 2014). Also, the effect of astaxanthin on chondrogenic differentiation remains undiscovered. In this study, the effects of astaxanthin on mesodermal trilineage differentiation (i.e., adipogenesis, chondrogenesis and osteogenesis) of human MSCs will be investigated. The potential effect of astaxanthin on chondrogenesis can be used in cartilage repair and regeneration.
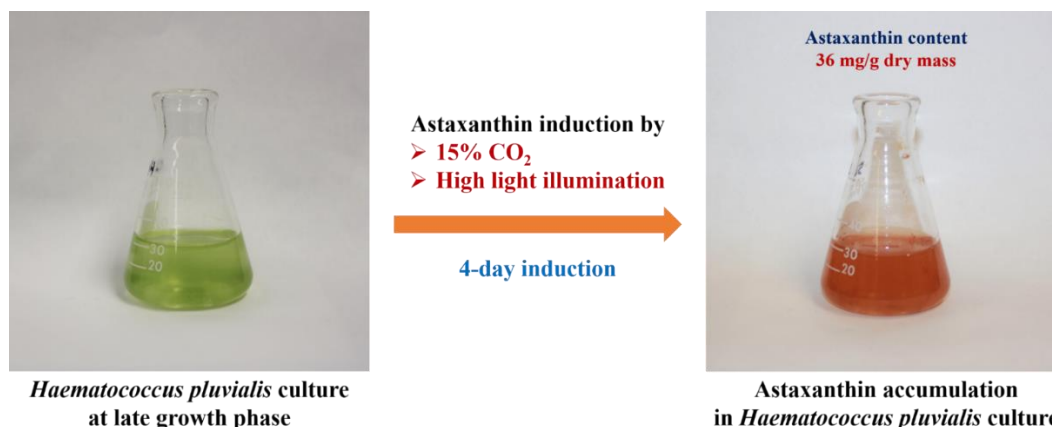
Figure 1.1. Induction of astaxanthin production by highlight illumination and 15% CO_2 in green algae *Haematococcus pluvialis* cells.

1.3 Harvesting MSCs from Poly(N-isopropylacrylamide) Surface

PNIPAAm is an extensively studied thermo-sensitive polymer with a lower critical solution temperature (LCST) of 32°C in aqueous solution (Heskins and Guillet 1968). PNIPAAm is hydrophobic when the temperature is higher than 32°C, and it becomes hydrophilic as the temperature falls below LCST. At the temperature of 37°C, MSCs are able to proliferate on hydrophobic surface; when temperature is lowered below LCST, the surface becomes hydrophilic and cells are allowed to detach from the surface without using enzymatic treatment such as trypsin (Figure 1.2). In this way, PNIPAAm modified surfaces have been used to harvest high-density cell sheets without disrupting the extracellular matrix proteins (Dalsin and Messersmith 2005). Polydopamine is an ultrathin but robust film, and it can be used to modify the surfaces of a vast range of materials. Polydopamine film can be used as a versatile platform for surface functionalization and biomolecule immobilization (Cui et al. 2012, Rivera and Messersmith 2012, Lee, Rho, and Messersmith 2009). The advantage of polydopamine chemistry is that polydopamine film can be prepared by a simple dip coating method, and it can be formed on substrates of almost any shape and any material without the need for any special instrument. In this study, a PNIPAAm-*g*-polydopamine film coated biomaterial surface will be fabricated to culture and harvest human MSCs.
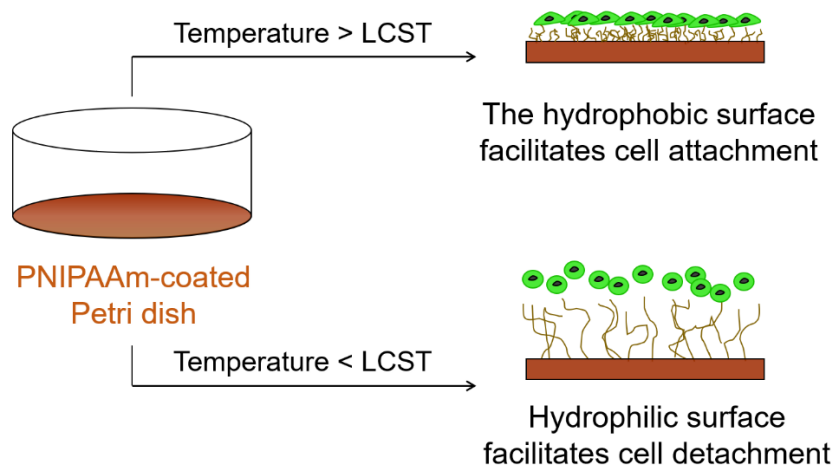
Figure 1.2. Schematic drawing of mammalian cell harvesting from temperature-responsive polymer PNIPAAm modified Petri dish surface.

1.4 Migration of Carbon Nanotubes Anchored MSCs under Chemotatic Gradient

There have been increasing interests in using MSCs as vehicles for drug and gene delivery due to their intrinsic tumor-tropic, immunosuppressive and anti-inflammatory properties (Roger et al. 2010, Kidd et al. 2009, Nasef et al. 2007, Iyer and Rojas 2008, Li et al. 2016). Carbon nanotubes (CNTs) have been extensively studied in photothermal therapy (PTT) due to their ability of absorbing near infrared (NIR) radiation and releasing heat (Wang et al. 2011, Kam et al. 2005). Compared to traditional chemotherapeutic drugs, PTT with nanoparticles such as CNTs have the advantage of low toxicity and less injuries to nonmalignant cells and tissues (Son, Hong, and Lee 2016, Peer et al. 2007). However, efficient delivery of nanoparticles to tumor sites remains challenging. There have been increasing interests in using human MSCs as cell carriers for cancer therapy (Kucerova et al. 2013, Roger et al. 2010). Compared to other types of carriers, MSCs have the advantage of low immunogenicity and intrinsic tumor-tropism (Lee et al. 2014, Kidd et al. 2009). There have been increasing interests in using MSCs to deliver nanoparticles for cancer therapy. For example, gold nanoparticles (AuNPs) internalized MSCs have been used in PTT for enhanced tumor-targeting efficiency (Kang et al. 2015), but no attempts have been made to deliver CNTs to tumor sites by MSCs. In this study, CNTs will be anchored on the surfaces of MSCs to create a tumor-targeted system for potential applications in PTT (Figure 1.3).
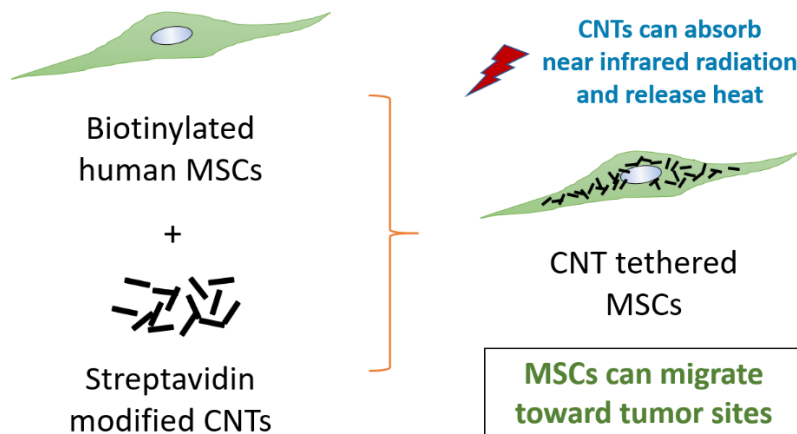
Figure 1.3. Schematic drawing of attaching CNTs to the surface of human MSCs.

1.5 CD200-CD200 Receptor Interaction

MSCs have drawn great interests in the treatment of immune diseases due to their immunosuppressive properties (Singer and Caplan 2011). MSCs have shown to significantly inhibit the proliferation of T cells, B cells, dendritic cells and natural killer cells (Di Nicola et al. 2002, Deng et al. 2005, Jiang et al. 2005, Spaggiari et al. 2006, Tse et al. 2003). Immunosuppressive soluble factors such as TGF-β, HGF, PGE2, IDO, galectin-1 and iNOS are secreted by MSCs (Sotiropoulou et al. 2006, Meisel et al. 2004, Aggarwal and Pittenger 2005, Opitz et al. 2009, Di Nicola et al. 2002, Lepelletier et al. 2010). CD200 is confirmed to be expressed on MSC surface. The level of CD200 on MSCs varies depending on the donor of MSCs (Pietilä et al. 2012). Pietila *et al.* have co-cultured MSCs with macrophages and showed that MSCs suppressed inflammatory responses of macrophages (Pietilä et al. 2012). CD200 has shown to interact with its receptor CD200R and thus sending an immunosuppressive signal to suppress immune cell activation (Najar et al. 2012). CD200 positive MSCs have also shown to suppress osteoclast formation (Varin et al. 2013). These studies suggest that CD200 positive MSCs exert immunosuppressive properties that down-regulate immune cell responses through CD200-CD200R interaction.

CD200, a.k.a. OX-2, is an anti-inflammatory transmembrane glycoprotein in the immunoglobin superfamily (Clark et al. 1985). The total structure of CD200 is ~50 kDa, with an extracellular domain, a transmembrane domain and a short cytoplasmic domain.

CD200 is expressed on a variety of cells including T cells, B cells, dendritic cells, etc (Barclay et al. 2002). CD200 reacts with its receptor, CD200 receptor (CD200R), which is expressed on the surface myeloid cells such as macrophages, neutrophils, and microglia (Hoek et al. 2000, Wright et al. 2000). The locations of CD200 and CD200R expression suggest their regulatory role in myeloid cell functions. CD200-CD200R interaction has shown to transmit an inhibitory signal that downregulates macrophage activity (Hoek et al. 2000). Several other studies supported the inhibitory role of CD200-CD200R signal in the activation of macrophages and dendritic cells (Rosenblum et al. 2004, Gorczynski et al. 1999, Taylor et al. 2005, Gorczynski, Yu, and Clark 2000).

CD200 has been used to reduce macrophages activation as well as inflammatory responses. Kim *et al.* have made CD200 modified biomaterials by treating avidin-coated plates with biotinylated CD200 protein (Kim et al. 2014). They found that CD200 coated biomaterial has suppressed macrophage activation and inflammatory responses. In 2017, the same group modified surfaces of poly(lactic-co-glycolic acid) (PLGA) biomaterials with CD200, and CD200 suppressed secretion of proinflammatory cytokine TNF-α and enhanced secretion of the anti-inflammatory cytokine IL-10 (Chen et al. 2017).

CD200 is also able to modulate macrophage phagocytosis through the interaction of CD200 and CD200R. Hayakawa *et al.* showed that administration with CD200 restrains macrophage phagocytosis of oligodendrocyte precursor cells by downregulating toll-like receptor 4 signaling (Hayakawa et al. 2016). In another study, increased phagocytosis in microglial cells was observed in CD200-deficient mice (Lyons et al. 2017). These studies show that CD200-CD200R interaction plays an inhibitory role in macrophage phagocytosis.

The ability of CD200 to modulate macrophage phagocytosis is similar to the interaction of CD47 with its receptor signal regulatory protein alpha receptor (SIRPα). CD47 is a ubiquitously expressed transmembrane glycoprotein known as "marker of self". Similar to CD200, CD47 is a transmembrane glycoprotein widely ubiquitously expressed on a variety of cells such as red blood cells and T cells (Blazar et al. 2001, Oldenborg et al. 2000). Its receptor SIRPα is mainly expressed on the surface of myeloid cells. The immune system recognizes invaders because foreign objects do not have "marker of self" on their surfaces (Oldenborg et al. 2000). The extracellular domain of

CD47 signals the macrophages "do not eat me" by interacting with SIRPα expressed on myeloid cells such as macrophages (Soto-Pantoja et al. 2013). The expression of CD47 on aged red blood cells is lowered, and this results in phagocytosis of red blood cells by macrophages (Blazar et al. 2001). Surface modification with CD47 protein has shown to prolong the circulation of therapeutic particles in blood, thereby promoting drug delivery to tumors by diminishing macrophage-mediated phagocytic clearance via CD47-SIRPα interaction (Rodriguez et al. 2013, Qie et al. 2016). However, the effect of CD200 protein on evading macrophage phagocytosis remains undiscovered. In this study, micro- and nano-sized particles will be modified with CD200 protein in order to avoid macrophage phagocytosis (Figure 1.4).
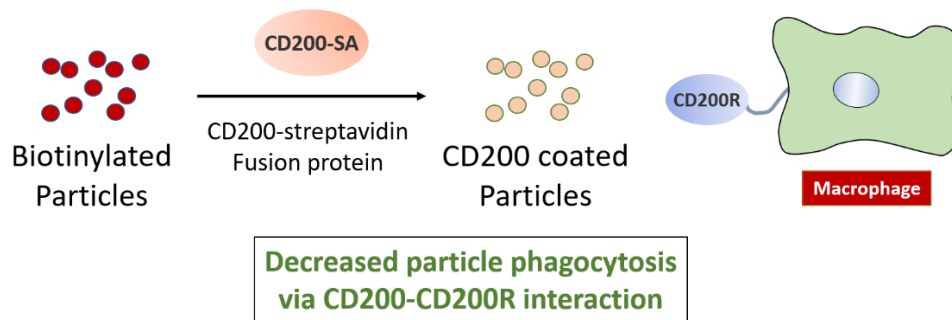
Figure 1.4. Schematic drawing of decreased macrophage phagocytosis by coating biotinylated particles with CD200-streptavidin fusion protein.

1.6 CD200 Modified Biomaterials for Reduced Inflammatory Response

Implantation of medical device in vivo elicits a series of interactions including injury, blood-biomaterial interaction, acute and chronic inflammation, foreign body reactions, wound healing processes and fibrous capsule formation (Anderson, Rodriguez, and Chang 2008, Sheikh et al. 2015). Foreign body reactions are one of the major causes of medical device failure. Upon implantation of biomaterials, a series of foreign body reactions take place. They include protein and platelet adsorption, macrophage adhesion, formation of foreign body giant cells, etc (Anderson, Rodriguez, and Chang 2008).

Macrophages play essential roles in foreign body reactions. Macrophages are myeloid immune cells that can detect foreign invaders. They are able to engulf microbes and foreign particles in the process of phagocytosis. In the early stage of implantation,

fibrinogen and other proteins bind non-specifically to the surface of medical device. This leads to acute inflammation and recruitment of macrophages to medical device surface (Tang and Eaton 1993, Tang et al. 1996). When activated, macrophages will fuse and form giant cells on biomaterial surface (Zhao et al. 1991). Activated macrophages can secret a wide array of cytokines including TNF-α, interleukin 1 beta (IL-1β), interleukin-6 (IL-6), interleukin-10 (IL-10), transforming growth factor β (TGF-β), etc (Jones et al. 2007, Fujiwara and Kobayashi 2005). Adherent macrophages and foreign body giant cells could eventually cause failure of the medical device such as biomaterial degradation, cracking of implanted device, fibrous thickening, etc (Anderson, Rodriguez, and Chang 2008, Zhao et al. 1990, Sutherland et al. 1993, Zhao et al. 1991, Stark, Gobel, and Jaeger 1990).

Traditionally, hydrophilic polymer polyethylene glycol (PEG) is used on biomaterial surface to reduce protein adsorption and prevent cell adhesion on biomaterial surface (Hashi et al. 2010, VandeVondele, Voros, and Hubbell 2003). Surface modification with polyethylene glycol (PEG) has shown improved blood compatibility and reduction in platelet adhesion (Uchida et al. 2000). Moreover, the use of PEG as a space linker can effectively reduce the non-specific adsorption of proteins and enhance the anticoagulant effect of the surface (Hashi et al. 2010, VandeVondele, Voros, and Hubbell 2003). However, the effect of PEG at reducing macrophage activation is moderate, and PEG may even promote proinflammatory cytokine secretion from macrophages (Lynn, Kyriakides, and Bryant 2010). Macrophage inflammatory responses is not dependent solely on protein adsorption (Kim, Chen, and Liu 2016). Other factors such as surface chemical and topology of the biomaterial may also affect macrophage inflammatory responses (Anderson, Rodriguez, and Chang 2008, Refai et al. 2004).

CD47 functionalized biomaterial surface has shown the ability to reduce inflammatory cell adhesion and activation (Finley et al. 2012). Recently, Finley *et al.* showed CD47 immobilized biomaterials can reduce the attachment of inflammatory cell and platelets through CD47-SIRPα interaction (Stachelek et al. 2011). In their study, avidin was first immobilized onto their PU and PVC films. Then, biotinylated CD47 was appended to the surfaces due to the strong binding of avidin to biotin. However, avidin is produced in the eggs of birds, and it may cause immunogenicity problems. Using

streptavidin can solve the problem of immunogenicity because streptavidin is originated from *Streptomyces avidinii* bacteria. Kim et al. have also made CD200 coated biomaterial surface for reduced macrophage activation (Kim et al. 2014). In their study, avidin-coated plate was treated with biotinylated CD200 to make CD200 coated surface. They observed reduced activation of macrophages on CD200 modified surface. In this study, a PEG/CD200 co-immobilized surface was fabricate for reduced macrophage responses (Figure 1.5).
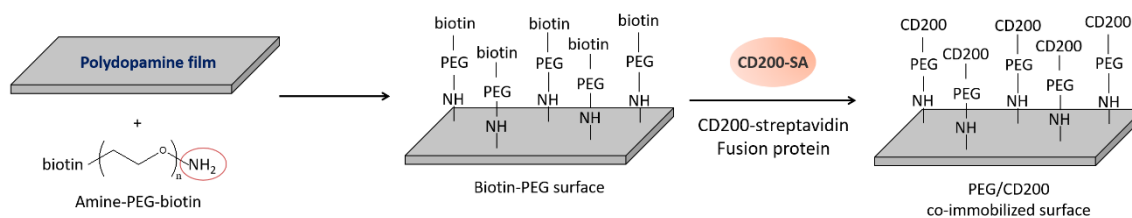
Figure 1.5. Schematic drawing of the fabrication of PEG/CD200 co-immobilized surface from polydopamine coated surface.

1.7 Rationale and Specific Aims

Specific Aim 1

Astaxanthin will be extracted from green algae *Haematococcus pluvialis* and encapsulated by methoxy polyethylene glycol-polycaprolactone (mPEG-PCL) polymeric micelles. *In vitro* cultures of human MSCs will be supplemented with astaxanthin encapsulated MPEG-PCL polymeric micelles to enhance the proliferation of MSCs. Adipogenic, osteogenic and chondrogenic differentiation medium of MSCs will be supplemented with astaxanthin encapsulated MPEG-PCL polymeric micelles. Adipocytes, osteocytes and chondrocytes will be stained with Oil Red O, Alizarin Red and Alcian Blue, respectively. The effect of astaxanthin on MSC differentiation will be evaluated.

Specific Aim 2

PNIPAAm is a thermo-sensitive polymer widely used in the area of cell/tissue engineering due to the reversible phase transition at its lower critical solution temperature (LCST) around 32°C. A simple two-step method will be developed to produce PNIPAAm surfaces using polydopamine as a platform and free radical polymerization. Human

MSCs will be cultured on PNIPAAm grafted cell culture surface and harvested by decreasing the temperature from 37°C to room temperature.

Specific Aim 3

MSCs are used as vehicles for the drug and gene delivery to tumor cites due to their intrinsic tumor-tropic feature. CNTs are used in photothermal therapy due to their ability of absorbing near infrared (NIR) radiation and releasing heat. In this study, CNTs will be functionalized with streptavidin and anchored on the surfaces of biotinylated human MSCs for a cell-based tumor-targeted system. The amount of CNTs on MSC surfaces will be optimized to retain the migration capability of MSCs. The migration of CNT-anchored MSCs will be evaluated by transwell migration assay.

Specific Aim 4

MSCs have shown to have immunosuppressive properties by modifying both innate and adaptive immune systems. CD200 is a widely expressed membrane glycoprotein in the immunoglobulin family. CD200 positive MSCs have shown to interact with its receptor CD200R which is expressed on the surface of myeloid lineage cells. The CD200-CD200R interaction has shown to suppress the activation of macrophages. The surface of nano-sized and micro-sized particles will be modified with CD200 protein. THP-1 induced macrophages will be treated with control particles as well as CD200 coated particles to evaluate the effect of CD200 on macrophage phagocytosis.

Specific Aim 5

CD200 and PEG will be modified on biomaterial surface through polydopamine film coating. J774A.1 macrophages will be seeded on control as well as CD200 coated surface to assess the effect of CD200 on macrophage attachment. IL-6 and TNF-α secreted from J774A.1 macrophages on CD200 coated surfaces will be evaluated by enzyme-linked immunosorbent assay (ELISA).

1.8 References

Aggarwal, S., and M. F. Pittenger. 2005. "Human mesenchymal stem cells modulate allogeneic immune cell responses." *Blood* 105 (4):1815-22.

Anderson, James M., Analiz Rodriguez, and David T. Chang. 2008. "Foreign body reaction to biomaterials." *Seminars in immunology* 20 (2):86-100.

Barclay, A. Neil, Gavin J. Wright, Gary Brooke, and Marion H. Brown. 2002. "CD200 and membrane protein interactions in the control of myeloid cells." *Trends in Immunology* 23 (6):285-290.

Bellayr, I. H., J. G. Catalano, S. Lababidi, A. X. Yang, J. L. Lo Surdo, S. R. Bauer, and R. K. Puri. 2014. "Gene markers of cellular aging in human multipotent stromal cells in culture." *Stem Cell Res Ther* 5 (2):59.

Blazar, B. R., F. P. Lindberg, E. Ingulli, A. Panoskaltsis-Mortari, P. A. Oldenborg, K. Iizuka, W. M. Yokoyama, and P. A. Taylor. 2001. "CD47 (integrin-associated protein) engagement of dendritic cell and macrophage counterreceptors is required to prevent the clearance of donor lymphohematopoietic cells." *J Exp Med* 194 (4):541-9.

Caplan, A. I. 2007. "Adult mesenchymal stem cells for tissue engineering versus regenerative medicine." *J Cell Physiol* 213 (2):341-7.

Chen, Esther Y., Shu-Hui Chu, Lanny Gov, Yoon Kyung Kim, Melissa B. Lodoen, Andrea J. Tenner, and Wendy F. Liu. 2017. "CD200 modulates macrophage cytokine secretion and phagocytosis in response to poly(lactic-co-glycolic acid) microparticles and films." *J. Mater. Chem. B* 5 (8):1574-1584.

Chen, Liwen, Edward E. Tredget, Philip Y. G. Wu, and Yaojiong Wu. 2008. "Paracrine factors of mesenchymal stem cells recruit macrophages and endothelial lineage cells and enhance wound healing." *PloS one* 3 (4):e1886-e1886.

Choi, K. M., Y. K. Seo, H. H. Yoon, K. Y. Song, S. Y. Kwon, H. S. Lee, and J. K. Park. 2008. "Effect of ascorbic acid on bone marrow-derived mesenchymal stem cell proliferation and differentiation." *J. Biosci. Bioeng.* 105 (6):586-94.

Clark, M. J., J. Gagnon, A. F. Williams, and A. N. Barclay. 1985. "MRC OX-2 antigen: a lymphoid/neuronal membrane glycoprotein with a structure like a single immunoglobulin light chain." *Embo j* 4 (1):113-8.

Corcione, A., F. Benvenuto, E. Ferretti, D. Giunti, V. Cappiello, F. Cazzanti, M. Risso, F. Gualandi, G. L. Mancardi, V. Pistoia, and A. Uccelli. 2006. "Human mesenchymal stem cells modulate B-cell functions." *Blood* 107 (1):367-72.

Cui, J., Y. Yan, G. K. Such, K. Liang, C. J. Ochs, A. Postma, and F. Caruso. 2012. "Immobilization and intracellular delivery of an anticancer drug using mussel-inspired polydopamine capsules." *Biomacromolecules* 13 (8):2225-8.

Dalsin, Jeffrey L., and Phillip B. Messersmith. 2005. "Bioinspired antifouling polymers." *Materials Today* 8 (9):38-46.

Deng, W., Q. Han, L. Liao, S. You, H. Deng, and R. C. Zhao. 2005. "Effects of allogeneic bone marrow-derived mesenchymal stem cells on T and B lymphocytes from BXSB mice." *DNA Cell Biol* 24 (7):458-63.

Denu, Ryan A., and Peiman Hematti. 2016. "Effects of Oxidative Stress on Mesenchymal Stem Cell Biology." *Oxid. Med. Cell. Longev.* 2016:2989076.

Di Nicola, M., C. Carlo-Stella, M. Magni, M. Milanesi, P. D. Longoni, P. Matteucci, S. Grisanti, and A. M. Gianni. 2002. "Human bone marrow stromal cells suppress T-lymphocyte proliferation induced by cellular or nonspecific mitogenic stimuli." *Blood* 99 (10):3838-43.

Dimarino, Amy M., Arnold I. Caplan, and Tracey L. Bonfield. 2013. "Mesenchymal stem cells in tissue repair." *Frontiers in immunology* 4:201-201.

Elward, K., and P. Gasque. 2003. ""Eat me" and "don't eat me" signals govern the innate immune response and tissue repair in the CNS: emphasis on the critical role of the complement system." *Mol. Immunol.* 40 (2-4):85-94.

Fan, G., L. Wen, M. Li, C. Li, B. Luo, F. Wang, L. Zhou, and L. Liu. 2011. "Isolation of mouse mesenchymal stem cells with normal ploidy from bone marrows by reducing oxidative stress in combination with extracellular matrix." *BMC Cell. Biol.* 12:30.

Finley, M. J., L. Rauova, I. S. Alferiev, J. W. Weisel, R. J. Levy, and S. J. Stachelek. 2012. "Diminished adhesion and activation of platelets and neutrophils with CD47 functionalized blood contacting surfaces." *Biomaterials* 33 (24):5803-11.

Fujiwara, N., and K. Kobayashi. 2005. "Macrophages in inflammation." *Curr Drug Targets Inflamm Allergy* 4 (3):281-6.

Galvao, J., B. Davis, M. Tilley, E. Normando, M. R. Duchen, and M. F. Cordeiro. 2014. "Unexpected low-dose toxicity of the universal solvent DMSO." *Faseb J.* 28 (3):1317-30.

Gorczynski, R. M., M. S. Cattral, Z. Chen, J. Hu, J. Lei, W. P. Min, G. Yu, and J. Ni. 1999. "An immunoadhesin incorporating the molecule OX-2 is a potent immunosuppressant that prolongs allo- and xenograft survival." *J. Immunol.* 163 (3):1654-60.

Gorczynski, R. M., K. Yu, and D. Clark. 2000. "Receptor engagement on cells expressing a ligand for the tolerance-inducing molecule OX2 induces an immunoregulatory population that inhibits alloreactivity in vitro and in vivo." *J. Immunol.* 165 (9):4854-60.

Hashi, C. K., N. Derugin, R. R. Janairo, R. Lee, D. Schultz, J. Lotz, and S. Li. 2010. "Antithrombogenic modification of small-diameter microfibrous vascular grafts." *Arterioscler Thromb Vasc Biol* 30 (8):1621-7.

Hayakawa, K., L. D. Pham, J. H. Seo, N. Miyamoto, T. Maki, Y. Terasaki, S. Sakadzic, D. Boas, K. van Leyen, C. Waeber, K. W. Kim, K. Arai, and E. H. Lo. 2016. "CD200 restrains macrophage attack on oligodendrocyte precursors via toll-like receptor 4 downregulation." *J. Cereb. Blood Flow. Metab.* 36 (4):781-93.

Hayashi, Y., S. Tsuji, M. Tsujii, T. Nishida, S. Ishii, H. Iijima, T. Nakamura, H. Eguchi, E. Miyoshi, N. Hayashi, and S. Kawano. 2008. "Topical implantation of mesenchymal stem cells has beneficial effects on healing of experimental colitis in rats." *J Pharmacol Exp Ther* 326 (2):523-31.

Heskins, M, and J. E Guillet. 1968. "Solution properties of poly(N-isopropylamide)." *J. E. Macromol. Sci. Chem. A* 2 (8):1441-1455.

Hoek, R. M., S. R. Ruuls, C. A. Murphy, G. J. Wright, R. Goddard, S. M. Zurawski, B. Blom, M. E. Homola, W. J. Streit, M. H. Brown, A. N. Barclay, and J. D. Sedgwick. 2000. "Down-regulation of the macrophage lineage through interaction with OX2 (CD200)." *Science* 290 (5497):1768-71.

Iyer, S. S., and M. Rojas. 2008. "Anti-inflammatory effects of mesenchymal stem cells: novel concept for future therapies." *Expert Opin Biol Ther* 8 (5):569-81.

Jang, Y. Y., and S. J. Sharkis. 2007. "A low level of reactive oxygen species selects for primitive hematopoietic stem cells that may reside in the low-oxygenic niche." *Blood* 110 (8):3056-63.

Jiang, Tongmeng, Guojie Xu, Qiuyan Wang, Lihui Yang, Li Zheng, Jinmin Zhao, and Xingdong Zhang. 2017. "In vitro expansion impaired the stemness of early passage mesenchymal stem cells for treatment of cartilage defects." *Cell Death & Disease* 8 (6):e2851.

Jiang, X. X., Y. Zhang, B. Liu, S. X. Zhang, Y. Wu, X. D. Yu, and N. Mao. 2005. "Human mesenchymal stem cells inhibit differentiation and function of monocyte-derived dendritic cells." *Blood* 105 (10):4120-6.

Jones, J. A., D. T. Chang, H. Meyerson, E. Colton, I. K. Kwon, T. Matsuda, and J. M. Anderson. 2007. "Proteomic analysis and quantification of cytokines and chemokines from biomaterial surface-adherent macrophages and foreign body giant cells." *J Biomed Mater Res A* 83 (3):585-96.

Kam, N. W., M. O'Connell, J. A. Wisdom, and H. Dai. 2005. "Carbon nanotubes as multifunctional biological transporters and near-infrared agents for selective cancer cell destruction." *Proc. Natl. Acad. Sci. U S A* 102 (33):11600-5.

Kang, S., S. H. Bhang, S. Hwang, J. K. Yoon, J. Song, H. K. Jang, S. Kim, and B. S. Kim. 2015. "Mesenchymal Stem Cells Aggregate and Deliver Gold Nanoparticles to Tumors for Photothermal Therapy." *ACS Nano* 9 (10):9678-90.

Kidd, S., E. Spaeth, J. L. Dembinski, M. Dietrich, K. Watson, A. Klopp, V. L. Battula, M. Weil, M. Andreeff, and F. C. Marini. 2009. "Direct evidence of mesenchymal stem cell tropism for tumor and wounding microenvironments using in vivo bioluminescent imaging." *Stem Cells* 27 (10):2614-23.

Kim, J. H., S. W. Nam, B. W. Kim, W. J. Kim, and Y. H. Choi. 2010. "Astaxanthin improves the proliferative capacity as well as the osteogenic and adipogenic differentiation potential in neural stem cells." *Food Chem. Toxicol.* 48 (6):1741-5.

Kim, Y. K., R. Que, S. W. Wang, and W. F. Liu. 2014. "Modification of biomaterials with a self-protein inhibits the macrophage response." *Adv. Healthc. Mater.* 3 (7):989-94.

Kim, Yoon Kyung, Esther Y. Chen, and Wendy F. Liu. 2016. "Biomolecular strategies to modulate the macrophage response to implanted materials." *J. Mater. Chem. B* 4 (9):1600-1609.

Koning, N., M. van Eijk, W. Pouwels, M. S. Brouwer, D. Voehringer, I. Huitinga, R. M. Hoek, G. Raes, and J. Hamann. 2010. "Expression of the inhibitory CD200 receptor is associated with alternative macrophage activation." *J. Innate. Immun.* 2 (2):195-200.

Kucerova, L., S. Skolekova, M. Matuskova, M. Bohac, and Z. Kozovska. 2013. "Altered features and increased chemosensitivity of human breast cancer cells mediated by adipose tissue-derived mesenchymal stromal cells." *BMC Cancer* 13:535.

Lee, H., J. Rho, and P. B. Messersmith. 2009. "Facile Conjugation of Biomolecules onto Surfaces via Mussel Adhesive Protein Inspired Coatings." *Adv Mater* 21 (4):431-434.

Lee, Miyoung, Sang Young Jeong, Jueun Ha, Miyeon Kim, Hye Jin Jin, Soon-Jae Kwon, Jong Wook Chang, Soo Jin Choi, Wonil Oh, Yoon Sun Yang, Jae-Sung Kim, and Hong Bae Jeon. 2014. "Low immunogenicity of allogeneic human umbilical cord blood-derived mesenchymal stem cells in vitro and in vivo." *Biochem. Biophys. Res. Commun.* 446 (4):983-989.

Lepelletier, Y., S. Lecourt, A. Renand, B. Arnulf, V. Vanneaux, J. P. Fermand, P. Menasche, T. Domet, J. P. Marolleau, O. Hermine, and J. Larghero. 2010. "Galectin-1 and semaphorin-3A are two soluble factors conferring T-cell immunosuppression to bone marrow mesenchymal stem cell." *Stem Cells Dev* 19 (7):1075-9.

Li, Min, Fangrong Zhang, Kerong Chen, Cheng Wang, Yujie Su, Yuan Liu, Jianping Zhou, and Wei Wang. 2016. "Nanoparticles and mesenchymal stem cells: a win-win alliance for anticancer drug delivery." *RSC Advances* 6 (43):36910-36922.

Lynn, A. D., T. R. Kyriakides, and S. J. Bryant. 2010. "Characterization of the in vitro macrophage response and in vivo host response to poly(ethylene glycol)-based hydrogels." *J Biomed Mater Res A* 93 (3):941-53.

Lyons, A., A. M. Minogue, R. S. Jones, O. Fitzpatrick, J. Noonan, V. A. Campbell, and M. A. Lynch. 2017. "Analysis of the Impact of CD200 on Phagocytosis." *Mol. Neurobiol.* 54 (7):5730-5739.

Meisel, R., A. Zibert, M. Laryea, U. Gobel, W. Daubener, and D. Dilloo. 2004. "Human bone marrow stromal cells inhibit allogeneic T-cell responses by indoleamine 2,3-dioxygenase-mediated tryptophan degradation." *Blood* 103 (12):4619-21.

Naguib, Y. M. 2000. "Antioxidant activities of astaxanthin and related carotenoids." *J. Agric. Food Chem.* 48 (4):1150-4.

Najar, M., G. Raicevic, F. Jebbawi, C. De Bruyn, N. Meuleman, D. Bron, M. Toungouz, and L. Lagneaux. 2012. "Characterization and functionality of the CD200-CD200R system during mesenchymal stromal cell interactions with T-lymphocytes." *Immunol Lett* 146 (1-2):50-6.

Nasef, A., N. Mathieu, A. Chapel, J. Frick, S. Francois, C. Mazurier, A. Boutarfa, S. Bouchet, N. C. Gorin, D. Thierry, and L. Fouillard. 2007. "Immunosuppressive effects of mesenchymal stem cells: involvement of HLA-G." *Transplantation* 84 (2):231-7.

Nemeth, K., A. Leelahavanichkul, P. S. Yuen, B. Mayer, A. Parmelee, K. Doi, P. G. Robey, K. Leelahavanichkul, B. H. Koller, J. M. Brown, X. Hu, I. Jelinek, R. A. Star, and E. Mezey. 2009. "Bone marrow stromal cells attenuate sepsis via prostaglandin E(2)-dependent reprogramming of host macrophages to increase their interleukin-10 production." *Nat Med* 15 (1):42-9.

Oldenborg, P. A., A. Zhelezynak, Y. F. Fang, C. F. Lagenaur, H. D. Gresham, and F. P. Lindberg. 2000. "Role of CD47 as a marker of self on red blood cells." *Science* 288 (5473):2051-4.

Opitz, C. A., U. M. Litzenburger, C. Lutz, T. V. Lanz, I. Tritschler, A. Koppel, E. Tolosa, M. Hoberg, J. Anderl, W. K. Aicher, M. Weller, W. Wick, and M. Platten. 2009. "Toll-like receptor engagement enhances the immunosuppressive properties of human bone marrow-derived mesenchymal stem cells by inducing indoleamine-2,3-dioxygenase-1 via interferon-beta and protein kinase R." *Stem Cells* 27 (4):909-19.

Peer, Dan, Jeffrey M. Karp, Seungpyo Hong, Omid C. Farokhzad, Rimona Margalit, and Robert Langer. 2007. "Nanocarriers as an emerging platform for cancer therapy." *Nat. Nanotech.* 2:751.

Pietilä, Mika, Siri Lehtonen, Elina Tuovinen, Kaarina Lähteenmäki, Saara Laitinen, Hannu-Ville Leskelä, Antti Nätynki, Juha Pesälä, Katrina Nordström, and Petri Lehenkari. 2012. "CD200 Positive Human Mesenchymal Stem Cells Suppress TNF-Alpha Secretion from CD200 Receptor Positive Macrophage-Like Cells." *PLoS ONE* 7 (2):e31671.

Pittenger, M. F., A. M. Mackay, S. C. Beck, R. K. Jaiswal, R. Douglas, J. D. Mosca, M. A. Moorman, D. W. Simonetti, S. Craig, and D. R. Marshak. 1999. "Multilineage potential of adult human mesenchymal stem cells." *Science* 284 (5411):143-7.

Qie, Y., H. Yuan, C. A. von Roemeling, Y. Chen, X. Liu, K. D. Shih, J. A. Knight, H. W. Tun, R. E. Wharen, W. Jiang, and B. Y. Kim. 2016. "Surface modification of nanoparticles enables selective evasion of phagocytic clearance by distinct macrophage phenotypes." *Sci. Rep.* 6:26269.

Refai, A. K., M. Textor, D. M. Brunette, and J. D. Waterfield. 2004. "Effect of titanium surface topography on macrophage activation and secretion of proinflammatory cytokines and chemokines." *J Biomed Mater Res A* 70 (2):194-205.

Rivera, J. G., and P. B. Messersmith. 2012. "Polydopamine-assisted immobilization of trypsin onto monolithic structures for protein digestion." *J Sep Sci* 35 (12):1514-20.

Rodriguez, Pia L., Takamasa Harada, David A. Christian, Diego A. Pantano, Richard K. Tsai, and Dennis E. Discher. 2013. "Minimal "Self" Peptides That Inhibit Phagocytic Clearance and Enhance Delivery of Nanoparticles." *Science* 339 (6122):971-975.

Roger, M., A. Clavreul, M. C. Venier-Julienne, C. Passirani, L. Sindji, P. Schiller, C. Montero-Menei, and P. Menei. 2010. "Mesenchymal stem cells as cellular vehicles for delivery of nanoparticles to brain tumors." *Biomaterials* 31 (32):8393-401.

Rosenblum, M. D., E. B. Olasz, K. B. Yancey, J. E. Woodliff, Z. Lazarova, K. A. Gerber, and R. L. Truitt. 2004. "Expression of CD200 on epithelial cells of the murine hair follicle: a role in tissue-specific immune tolerance?" *J. Invest. Dermatol.* 123 (5):880-7.

Sarugaser, Rahul, Lorraine Hanoun, Armand Keating, William L. Stanford, and John E. Davies. 2009. "Human Mesenchymal Stem Cells Self-Renew and Differentiate According to a Deterministic Hierarchy." *PLoS ONE* 4 (8):e6498.

Selmani, Z., A. Naji, I. Zidi, B. Favier, E. Gaiffe, L. Obert, C. Borg, P. Saas, P. Tiberghien, N. Rouas-Freiss, E. D. Carosella, and F. Deschaseaux. 2008. "Human leukocyte antigen-G5 secretion by human mesenchymal stem cells is required to suppress T lymphocyte and natural killer function and to induce CD4+CD25highFOXP3+ regulatory T cells." *Stem Cells* 26 (1):212-22.

Sheikh, Zeeshan, Patricia J. Brooks, Oriyah Barzilay, Noah Fine, and Michael Glogauer. 2015. "Macrophages, Foreign Body Giant Cells and Their Response to Implantable Biomaterials." *Materials (Basel, Switzerland)* 8 (9):5671-5701.

Singer, N. G., and A. I. Caplan. 2011. "Mesenchymal stem cells: mechanisms of inflammation." *Annu Rev Pathol* 6:457-78.

Son, Kuk Hui, Jeong Hee Hong, and Jin Woo Lee. 2016. "Carbon nanotubes as cancer therapeutic carriers and mediators." *Int. J. Nanomedicine* 11:5163-5185.

Sotiropoulou, P. A., S. A. Perez, A. D. Gritzapis, C. N. Baxevanis, and M. Papamichail. 2006. "Interactions between human mesenchymal stem cells and natural killer cells." *Stem Cells* 24 (1):74-85.

Soto-Pantoja, D. R., E. V. Stein, N. M. Rogers, M. Sharifi-Sanjani, J. S. Isenberg, and D. D. Roberts. 2013. "Therapeutic opportunities for targeting the ubiquitous cell surface receptor CD47." *Expert Opin. Ther. Targets* 17 (1):89-103.

Spaggiari, G. M., A. Capobianco, S. Becchetti, M. C. Mingari, and L. Moretta. 2006. "Mesenchymal stem cell-natural killer cell interactions: evidence that activated NK cells are capable of killing MSCs, whereas MSCs can inhibit IL-2-induced NK-cell proliferation." *Blood* 107 (4):1484-90.

Stachelek, S. J., M. J. Finley, I. S. Alferiev, F. Wang, R. K. Tsai, E. C. Eckells, N. Tomczyk, J. M. Connolly, D. E. Discher, D. M. Eckmann, and R. J. Levy. 2011. "The effect of CD47 modified polymer surfaces on inflammatory cell attachment and activation." *Biomaterials* 32 (19):4317-26.

Stark, G. B., M. Gobel, and K. Jaeger. 1990. "Intraluminal cyclosporine A reduces capsular thickness around silicone implants in rats." *Ann Plast Surg* 24 (2):156-61.

Sutherland, K., J. R. Mahoney, 2nd, A. J. Coury, and J. W. Eaton. 1993. "Degradation of biomaterials by phagocyte-derived oxidants." *J Clin Invest* 92 (5):2360-7.

Tang, L., and J. W. Eaton. 1993. "Fibrin(ogen) mediates acute inflammatory responses to biomaterials." *J Exp Med* 178 (6):2147-56.

Tang, L., T. P. Ugarova, E. F. Plow, and J. W. Eaton. 1996. "Molecular determinants of acute inflammatory responses to biomaterials." *J Clin Invest* 97 (5):1329-34.

Taylor, Neil, Karen McConachie, Claudia Calder, Rosemary Dawson, Andrew Dick, Jonathon D. Sedgwick, and Janet Liversidge. 2005. "Enhanced tolerance to autoimmune uveitis in CD200-deficient mice correlates with a pronounced Th2 switch in response to antigen challenge." *J. Immunol.* 174 (1):143-154.

Tse, W. T., J. D. Pendleton, W. M. Beyer, M. C. Egalka, and E. C. Guinan. 2003. "Suppression of allogeneic T-cell proliferation by human marrow stromal cells: implications in transplantation." *Transplantation* 75 (3):389-97.

Uchida, K., M. Yamato, E. Ito, O. H. Kwon, A. Kikuchi, K. Sakai, and T. Okano. 2000. "Two different types of nonthrombogenic surfaces: PEG suppresses platelet adhesion ATP-independently but HEMA-St block copolymer requires ATP consumption of platelets to prevent adhesion." *J Biomed Mater Res* 50 (4):585-90.

VandeVondele, S., J. Voros, and J. A. Hubbell. 2003. "RGD-grafted poly-L-lysine-graft-(polyethylene glycol) copolymers block non-specific protein adsorption while promoting cell adhesion." *Biotechnol Bioeng* 82 (7):784-90.

Varin, A., C. Pontikoglou, E. Labat, F. Deschaseaux, and L. Sensebe. 2013. "CD200R/CD200 inhibits osteoclastogenesis: new mechanism of osteoclast control by mesenchymal stem cells in human." *PLoS One* 8 (8):e72831.

Varnum, M. M., T. Kiyota, K. L. Ingraham, S. Ikezu, and T. Ikezu. 2015. "The anti-inflammatory glycoprotein, CD200, restores neurogenesis and enhances amyloid phagocytosis in a mouse model of Alzheimer's disease." *Neurobiol Aging* 36 (11):2995-3007.

Wang, C. H., S. H. Chiou, C. P. Chou, Y. C. Chen, Y. J. Huang, and C. A. Peng. 2011. "Photothermolysis of glioblastoma stem-like cells targeted by carbon nanotubes conjugated with CD133 monoclonal antibody." *Nanomedicine: NBM* 7 (1):69-79.

Wright, G. J., M. J. Puklavec, A. C. Willis, R. M. Hoek, J. D. Sedgwick, M. H. Brown, and A. N. Barclay. 2000. "Lymphoid/neuronal cell surface OX2 glycoprotein recognizes a novel receptor on macrophages implicated in the control of their function." *Immunity* 13 (2):233-42.

Yang, L., F. Cheng, T. Liu, J. R. Lu, K. Song, L. Jiang, S. Wu, and W. Guo. 2012. "Comparison of mesenchymal stem cells released from poly(N-isopropylacrylamide) copolymer film and by trypsinization." *Biomed Mater* 7 (3):035003.

Zhang, W., W. Ge, C. Li, S. You, L. Liao, Q. Han, W. Deng, and R. C. Zhao. 2004. "Effects of mesenchymal stem cells on differentiation, maturation, and function of human monocyte-derived dendritic cells." *Stem Cells Dev* 13 (3):263-71.

Zhao, Q., M. P. Agger, M. Fitzpatrick, J. M. Anderson, A. Hiltner, K. Stokes, and P. Urbanski. 1990. "Cellular interactions with biomaterials: in vivo cracking of pre-stressed Pellethane 2363-80A." *J Biomed Mater Res* 24 (5):621-37.

Zhao, Q., N. Topham, J. M. Anderson, A. Hiltner, G. Lodoen, and C. R. Payet. 1991. "Foreign-body giant cells and polyurethane biostability: in vivo correlation of cell adhesion and surface cracking." *J Biomed Mater Res* 25 (2):177-83.

**Chapter 2. Enhanced Proliferation and Differentiation of Mesenchymal Stem Cells
by Astaxanthin-Encapsulated Polymeric Micelles**

2.1 Abstract

Astaxanthin is a highly potent antioxidant which can be extracted from
Haematococcus pluvialis when cultivated and induced at high stress conditions. Due to
astaxanthin's hydrophobicity, methoxy polyethylene glycol-polycaprolactone (mPEG-
PCL) copolymer was synthesized to form polymeric micelles for the encapsulation of
astaxanthin. Astaxanthin-loaded polymeric micelles were then used to examine the effect
on the proliferation and differentiation of human mesenchymal stem cells (MSCs).
Dynamic light scattering (DLS) and Fourier transform infrared spectroscopy (FT-IR)
confirmed astaxanthin was encapsulated into mPEG-PCL micelles. Astaxanthin loading
and encapsulation efficiency, determined by UV/Vis spectroscopy, were 3.27% and
96.67%, respectively. After 48 h, a total of 87.31% of astaxanthin was released from the
polymeric micelles. The drug release profile was better fit by the Michaelis-Menten type
model than the power law model. The MSC culture results showed that culture medium
supplemented with 0.5 μg/mL astaxanthin-encapsulated polymeric micelles led to a
26.3% increase in MSC proliferation over an 8-day culture period. MSC differentiation
results showed that 20 ng/mL astaxanthin-encapsulated polymeric micelles enhanced
chondrogenesis, adipogenesis and osteogenesis of MSCs by 106%, 33% and 182%,
respectively.

2.2 Introduction

Mesenchymal stem cell (MSC) has been widely used in tissue engineering and
regenerative medicine due to its unique properties of self-renewal and multipotency
(Sarugaser et al. 2009). Rapid in vitro expansion of MSCs is crucial for clinical
applications (Wang, Qu, and Zhao 2012). Increased reactive oxygen species (ROS) levels
have been shown to reduce the self-renewal ability and proliferation of MSCs (Denu and
Hematti 2016). Antioxidants are known to enhance *in vitro* proliferation of adipose-
derived MSCs by regulation of cyclin-dependent kinase (CDK) and CDK inhibitor levels
(Sun et al. 2013). Proliferation of human and mouse bone marrow-derived MSCs have

also been improved by supplementing culture medium with antioxidants such as ascorbic acid 2-phosphate, phenyl-α-tert-butylnitrone and N-acetylcysteine (Fan et al. 2011, Choi et al. 2008). Moreover, supplementation of ascorbic acid 2-phosphate also enhanced adipogenesis and osteogenesis of bone marrow-derived MSCs (Choi et al. 2008).

Astaxanthin is a lipid soluble, dark red carotenoid found in various aquatic animals (Guerin, Huntley, and Olaizola 2003). It has been mainly used as a color additive in animal and fish feed, providing the flesh of aquatic animals a pink to red-orange color (Higuera-Ciapara, Felix-Valenzuela, and Goycoolea 2006). Astaxanthin is also a very potent antioxidant, with activity ten times higher than various carotenoids such as lutein, α-carotene and β-carotene (Naguib 2000). The polyene chain and long conjugated double bonds are the reason for such strong antioxidant activity of astaxanthin (Yang, Kim, and Lee 2013). Kim et al. reported that astaxanthin could improve the proliferation of neural stem cells; in addition, adipogenic and osteogenic differentiation of neural stem cells were also enhanced by astaxanthin (Kim et al. 2010). In their study, astaxanthin was prepared as a stock solution in dimethyl sulfoxide (DMSO) due to its low solubility in water. However, using DMSO certainly is an issue when applying astaxanthin for *in vivo* applications (Galvao et al. 2014). Also, the effect of astaxanthin on chondrogenic differentiation remains unexplored. In this study, the effects of astaxanthin on mesodermal trilineage differentiation (i.e., adipogenesis, chondrogenesis and osteogenesis) of human MSCs were investigated together for the first time.

Astaxanthin production can be induced in microalgae *Haematococcus pluvialis,* one of the richest known sources of natural astaxanthin, is subjected to stressful conditions such as salinity, nitrogen deficiency, and light (Kobayashi 2000, Fabregas et al. 2001). In this study, the accumulation of astaxanthin was induced by the combination of high light stimulus and 15% CO_2 aeration (Christian et al. 2018), and astaxanthin was extracted from *H. pluvialis* using mechanical disruption with DMSO (Boussiba and Vonshak 1991). After being extracted from *H. pluvialis*, a liquid-liquid extraction method was used to extract astaxanthin from DMSO to ether for obtaining astaxanthin powder by rotary evaporation.

Because poor water solubility of astaxanthin limits its applications, various carriers have been used to enhance the aqueous solubility of astaxanthin (Lockwood,

O'Malley, and Mosher 2003, Yuan et al. 2013, Tachaprutinun et al. 2009, Anarjan et al. 2014, Hama et al. 2012). Polymeric micelle as an effective nanocarrier which has not been attempted for the encapsulation of astaxanthin. In this study, methoxypolyethylene glycol-polycaprolactone (mPEG-PCL), a biocompatible self-assembled diblock copolymer containing hydrophilic mPEG and hydrophobic PCL (Adams, Lavasanifar, and Kwon 2003, Gou et al. 2009), was synthesized to exam its entrapment capacity of astaxanthin in aqueous medium. The hydrophilic mPEG can protect the inner core from the aqueous environment, and the hydrophobic PCL is able to encapsulate poorly water-soluble astaxanthin. The chemical structure of astaxanthin-encapsulated mPEG-PCL micelles was characterized by Fourier transform infrared spectroscopy (FT-IR). The size of the micelles was measured by dynamic light scattering (DLS). UV/Vis absorbance spectrum was used to determine encapsulation efficiency and drug loading. The release profile of astaxanthin from mPEG-PCL micelles was also obtained. The cultures of human bone marrow-derived MSCs were treated with various dosage of astaxanthin-encapsulated polymeric micelles to evaluate the effect of astaxanthin on the proliferation of MSCs. Astaxanthin was also supplemented in adipogenesis, osteogenesis and chondrogenesis differentiation medium of MSCs. The effect of astaxanthin on MSC differentiation was evaluated.

2.3 Materials and methods

2.3.1 Materials

Haematococcus pluvialis (UTEX 2505) and MES-Volvox medium were purchased from the Culture Collection of Algae (UTEX, Austin, TX, USA). Astaxanthin standard, DMSO, acetone, methanol, 2,2'-azino-bis (3-ethylbenzthiazoline-6-sulphonic acid (ABTS), methoxypolyethylene glycol (mPEG; MW = 2,000), Tin(II) 2-ethylhexanoate (Sn(Oct)2), acetone, dichloromethane (DCM), phosphotungstic acid, rhodamine B and penicillin-streptomycin were purchased from Sigma-Aldrich (St. Louis, MO, USA). Anhydrous ether, ammonium persulfate (APS), acetic acid, potassium hydroxide (KOH) and absolute methanol were purchased from J.T. Baker (Philipsburg, NJ, USA). ε-CL was purchased from Acros Organics (Geel, Belgium). Spectra/Por dialysis membrane tube (MW cutoff of 3.5 kD) was purchased from Spectrum Labs

(Rancho Dominguez, CA, USA). Human bone marrow-derived mesenchymal stem cells were purchased from RoosterBio (Frederick, MD, USA). Minimum essential medium alpha medium (αMEM), L-glutamine and 0.25% trypsin/EDTA solution were purchased from Fisher Scientific (Waltham, MA, USA). Fetal bovine serum (FBS) was purchased from Gibco (Grand Island, NY, USA). AdipoLife DfKt-2 Adipogenesis Medium Kit, OsteoLife Complete Osteogenesis Medium, ChondroLife Complete Chondrogenesis Medium, Oil Red O Staining Kit, 2% Alizarin Red Stain and Alcian Blue Staining Kit were purchased from Lifeline Cell Technology (Frederick, MD, USA).

2.3.2 Extraction of astaxanthin from *H. pluvialis* culture

Cultivation of *H. pluvialis* microalgal cells and the induction of astaxanthin were as reported previously (Christian et al. 2018). Briefly, *H. pluvialis* were cultivated in MES-volvox medium in Erlenmeyer flasks under 80 µmol m^{-2}s^{-1} light intensity (low light) for 8 days. At day 9, the light intensity was increased to 300 µmol m^{-2}s^{-1} (high light) and 15% CO_2 balanced with air was aerated into the culture to induce astaxanthin accumulation. The microalgal cells were cultivated for another two days at high light intensity and 15% CO_2 stress conditions.

Extraction of astaxanthin from *H. pluvialis* has been previously described (Boussiba, Fan, and Vonshak 1992). Briefly, the cells were harvested by centrifugation (4,500 rpm, 5 min), and re-suspended in 5 mL of 5% (w/v) KOH in 30% methanol. The cells were then heated in a 70°C water bath to destroy the chlorophyll. The cells were centrifuged again (4,500 rpm, 5 min) and then treated with 10 mL of DMSO with 5 drops of acetic acid. The cell suspensions were bath sonicated for 2 min three times with intervals of 30 s. The cells were then heated in the 70°C water bath for 5 min. The cells were heated repeatedly until they were completely white and finally centrifuged at 4,500 rpm for 5 min. The color of the cells was observed by Leica DMI3000 B microscope equipped with Leica EC3 digital color camera (Leica Microsystems, Wetzlar, Germany). The extracted astaxanthin in DMSO was stored at 4°C for further use.

2.3.3 Extraction of astaxanthin from DMSO to ether

DMSO was mixed with water to determine the optimal DMSO:water ratio for

astaxanthin extraction to ether. 3 mL of astaxanthin solution was prepared in DMSO containing 1%, 3%, 5%, 10%, 20%, 30%, 40%, and 50% water, respectively. 3 mL of ether was then added on top of all the prepared astaxanthin solutions. The mixture was fully mixed by vigorous shaking until the color of bottom layer (DMSO) turned from red to colorless. The UV/Vis absorbance spectrum of astaxanthin in DMSO/water mixture was recorded before and after extraction by a SpectraMax M2e Microplate Reader (Molecular Devices, Sunnyvale, CA, USA). The absorbance of astaxanthin in DMSO at 492 nm before extraction was taken as A_0. The absorbance of astaxanthin in DMSO at 492 nm after extraction was taken as A_1. The extraction efficiency was determined by equation 2.1:

$$astaxanthin\ extraction\ yield\ (\%) = \frac{A_0 - A_1}{A_0} \times 100 \qquad (2.1)$$

An astaxanthin standard curve was constructed by making serial dilutions of astaxanthin standard solutions in DMSO. The concentrations of astaxanthin solutions were correlated with UV/Vis absorbance readings at 492 nm. Astaxanthin in ether was then dried by a rotary evaporator (IKA, RV 10, Staufen, Germany) at 40°C.

2.3.4 Production of mPEG-PCL copolymer

The production of mPEG-PCL copolymer has been described by Sawdon *et al.* (Sawdon and Peng 2014). Briefly, 50 mg of mPEG (molecular weight of 2,000) was mixed with 2.25 mL of ε-CL in the ultrasonication bath for 5 min at ambient temperature. $Sn(Oct)_2$ (0.5 wt% of ε-CL) was added into the mixture, and the solution was transferred into a 3-necked round-bottom flask. The system was immersed in an oil bath at 140°C and continuously purged with nitrogen for 24 h. The crude product was allowed to cool to the ambient temperature, dissolved in DCM, and precipitated by treating the solution with cold methanol.

2.3.5 Encapsulation of astaxanthin by mPEG-PCL polymeric micelles

Ten mg of mPEG-PCL was dissolved in 2 mL of acetone. An excess amount (5 mg) of astaxanthin was added into the solution and placed in an ultrasonication bath for 5 min. The mixture was added dropwise into 10 mL of DI water under ultrasonication. Acetone in the solution was removed by rotary evaporation at 60°C. The final micelle

product was passed through a 0.45-µm filter. The amount of encapsulated astaxanthin was determined by UV/Vis spectroscopy and the astaxanthin standard curve. Drug loading (DL) was calculated by equation 2.2:

$$DL = \frac{Amount\ of\ encapsulated\ astaxanthin}{Amount\ of\ polymer + Amount\ of\ encapsulated\ astaxanthin} \times 100\% \qquad (2.2)$$

The encapsulation efficiency (EE) was determined by loading 0.3 mg of astaxanthin into 10 mg of mPEG-PCL micelles. The amount of encapsulated astaxanthin was determined by UV/Vis spectroscopy, and EE was calculated by equation 2.3:

$$EE = \frac{Amount\ of\ encapsulated\ astaxanthin}{Amount\ of\ original\ astaxanthin} \times 100\% \qquad (2.3)$$

2.3.6 ABTS scavenging activity

The ABTS scavenging activity of astaxanthin extracts was evaluated using a previously describe method (Re et al. 1999). Briefly, 7 mM ABTS was mixed with equal volume of 2.4 mM APS, and the reaction mixture was allowed to react for 12 h at room temperature in the dark. The mixture was then diluted with deionized water, and the UV/Vis absorbance reading at 734 nm was taken as K_0. 1 mL of ABTS solution was mixed with 1 mL of astaxanthin solutions of different concentrations (10 – 100 µg/mL), and the reaction mixture was vortexed for 10 s. After 6 min, the UV/Vis absorbance reading at 734 nm was taken as K_1. The ABTS radical scavenging activity was determined by equation 2.4:

$$ABTS\ scavenging\ activity\ (\%) = \frac{K_0 - K_1}{K_0} \times 100 \qquad (2.4)$$

OD_{734} readings of astaxanthin-encapsulated polymeric micelles were measured to determine the ABTS scavenging activity.

2.3.7 Characterization of astaxanthin-encapsulated mPEG-PCL polymeric micelles

The chemical structure of commercial astaxanthin, mPEG-PCL micelles, and astaxanthin-encapsulated mPEG-PCL micelles was characterized by FT-IR. FT-IR spectra were recorded by Spectrum One ATR/FTIR Spectrometer (Perkin Elmer, Waltham, MA, USA). The particle size distribution of the mPEG-PCL micelles was determined by dynamic light scattering (DLS) using a Nano ZS Zetasizer (Malvern Panalytical,

Westborough, MA, USA). The TEM samples were prepared by adding 10 µL of 1 mg/mL mPEG-PCL micelle solution onto a Formvar grid (Ted Pella, Redding, CA, USA) for 5 min and excess solution was wicked off. The samples were negatively stained with 10 µL phosphotungstic acid solution (2 wt%) for 10 s and excess solution was wicked off. Transmission electron microscopy (TEM) image of mPEG-PCL micelles was taken by JEM-4000FX (JEOL, Tokyo, Japan) at 80 kV.

2.3.8 Astaxanthin release profile

Two mL astaxanthin-encapsulated mPEG-PCL micelle solution was placed in a Spectra/Por dialysis tube. The dialysis tube was then immersed in 500 mL 1X phosphate buffered saline (PBS) at ambient temperature. At specified time intervals, 100 µL of sample was removed from the dialysis tube and the absorbance at 492 nm was measured. The amount of astaxanthin released was quantified using the astaxanthin standard curve. All experiments were carried out in triplicate.

In order to identify the in vitro release mechanism of astaxanthin from mPEG-PCL micelles, the power law and the Michaelis-Menten model were used to fit the release profile. In the power law model, the *in vitro* drug release data were fit into equation 2.5:

$$\frac{M_t}{M_\infty} = at^b \tag{2.5}$$

where M_t/M_∞ is the fraction of astaxanthin release; a is a constant; t is the release time; b is the release exponent. Equation 2.5 is converted to a linear form, providing a linear fitting of the release data:

$$log\left(\frac{M_t}{M_\infty}\right) = log(a) + b \times log(t) \tag{2.6}$$

The release profile of astaxanthin from mPEG-PCL polymeric micelles was then modeled using the Michaelis-Menten model (equation 2.7):

$$\frac{M_t}{M_\infty} = \frac{t}{K+t} \tag{2.7}$$

where M_t/M_∞ is the fraction of astaxanthin release; K is the Michaelis-Menten constant; t is the release time. Equation 2.7 is then converted to its linear form:

$$\frac{M_\infty}{M_t} = \frac{K}{t} + 1 \tag{2.8}$$

The coefficient of correlation R^2 of the two models was compared to determine which model was more appropriate.

2.3.9 Effect of astaxanthin-encapsulated mPEG-PCL on proliferation of MSCs

MSCs were cultured with αMEM supplemented with 16.5% FBS, 1% penicillin-streptomycin and 2 mM L-glutamine. MSCs were inoculated on 6-well plates at 5.0×10^4 cells/cm^2 and incubated at 37°C in a 5% CO_2 incubator (Forma 310; Thermo Fisher Scientific, Waltham, MA, USA). Cellular uptake of mPEG-PCL polymeric micelles was evaluated by encapsulating 1 mg fluorescent rhodamine B. Free rhodamine B was removed by dialysis using Spectra/Por dialysis membrane tube (MW cutoff of 3.5 kD). EE and DL of rhodamine B by mPEG-PCL micelles was determined by measuring absorbance at 554 nm. MSCs were then treated with polymeric micelles loaded with rhodamine B for 4, 8, and 24 h. Phase contrast and fluorescent images were taken with a Leica DMi8 microscope equipped with Leica EC3 camera.

Astaxanthin-encapsulated mPEG-PCL micelles at 0, 0.25, 0.5 and 1 μg/mL were added separately to the MSC culture media for an 8-day period of cultivation; culture medium was replaced every 4 days. MSC culture with normal culture medium and MSC culture with the addition of mPEG-PCL micelles only were used as controls. The MSCs were harvested by treatment of 0.25% trypsin/EDTA, and the cell numbers were counted using a hemocytometer. The cell growth kinetics were determined to investigate the effect of astaxanthin-encapsulated mPEG-PCL micelles on the proliferation of MSCs.

2.3.10 Effect of astaxanthin-encapsulated mPEG-PCL on differentiation of MSCs

To evaluate the effect of astaxanthin-encapsulated mPEG-PCL micelles on MSC differentiation toward chondrogenic, adipogenic and osteogenic lineage, MSC differentiation were performed using differentiation medium kit according to manufacturer's instructions. MSCs were inoculated in 6-well plates with αMEM supplemented with 16.5% FBS, 1% penicillin-streptomycin and 2 mM L-glutamine at the seeding density of 20,000 cells/cm^2 for adipogenesis, 10,000 cells/cm^2 for osteogenesis and chondrogenesis. After 24 h, culture medium was replaced with the corresponding differentiation media supplemented with 20 ng/mL astaxanthin-encapsulated mPEG-PCL

micelles. Untreated MSC differentiation media and MSC differentiation media supplemented with non-encapsulated mPEG-PCL micelles were used as controls. All media were changed every 3 days by replacing half of media from each well with fresh media.

After 2 weeks of culture, chondrocytes were fixed with 4% paraformaldehyde and stained with Alcian Blue solution for overnight. Adipocytes were fixed with 4% paraformaldehyde stained with Oil Red O staining. Osteocytes were fixed with absolute methanol and stained with Alizarin red solution. Chondrogenic, adipogenic, and osteogenic differentiation were quantified by calculating blue, red, and black area respectively in at least 10 randomly selected microscopic fields using Image J (NIH, Bethesda, Maryland, USA). Adipogenic differentiation was quantified by counting stained adipocytes in at least 10 randomly selected microscopic fields. Osteogenic differentiation was quantified by calculating black area in at least 10 randomly selected microscopic fields using Image J.

2.3.11 Statistical Analysis

Statistical analyses were performed using Prism 8 software (Graphpad Software, San Diego, CA, USA). Data were presented as mean ± standard deviation from three independent experiments. For MSC proliferation and differentiation experiments, one-way analysis of variance, or ANOVA was performed followed by Tukey's post-hoc analysis for multiple comparisons between different groups including unmodified control, mPEG-PCL micelles, and astaxanthin-encapsulated polymeric micelles of various concentrations. $p < 0.05$ was considered statistically significant.

2.4 Results and discussion

2.4.1 Cultivation of *H. pluvialis* and induction of astaxanthin

Figure 2.1A shows the growth kinetics of *H. pluvialis* for an 8-day culture period under low light conditions, then followed by a two-day astaxanthin induction period under high light and high CO_2 stressful conditions. During the first 8 days, the cell density gradually increased from 10^5 to 1.07×10^6 cells/mL. However, after the inception of induction, the cell density slightly decreased from 1.07×10^6 to 9.61×10^5 cells/mL.

Figure 2.1B showed the color change of the microalgal cells before and after the induction stage. The color of the algae remained green during the first cultivation stage. The color of the cells turned from green (Figure 2.1B-i) to red (Figure 2.1B-ii) after two days of induction under stress conditions. After astaxanthin was extracted, the *H. pluvialis* turned colorless (Figure 2.1B-iii).
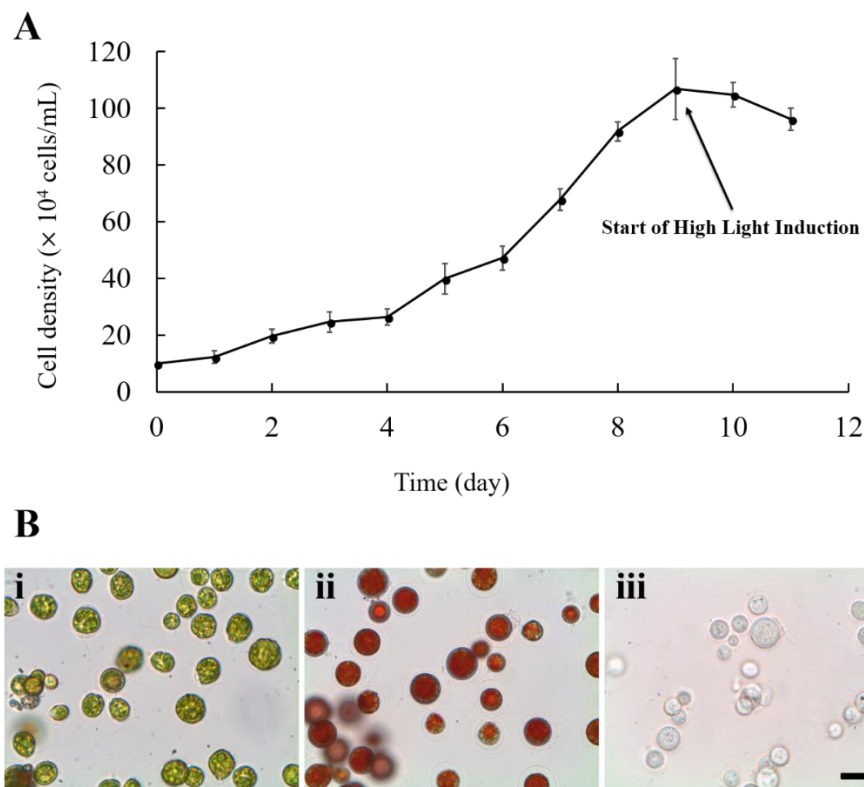
Figure 2.1. Growth kinetics and microscopic images of *H. pluvialis*. (A) Growth kinetics of *H. pluvialis* cultured at 80 µmol m^{-2}s^{-1} light intensity (0 – 8 days) and at 300 µmol m-2s-1 light intensity (9 – 10 days). Each value is expressed as the mean ± standard deviation (n = 3); (B) Microscopic images of *H. pluvialis* (i) at day 9 (before high light induction) (ii) day 10 (after high light induction) (iii) after astaxanthin has been extracted. Scale bar denotes 100 µm.

2.4.2 Extraction of astaxanthin from DMSO to ether

Although DMSO is good for storing astaxanthin at 4°C, it is difficult to remove DMSO by rotary evaporation due to its high boiling point of 189°C. Astaxanthin stored in DMSO was extracted to ether by adding a layer of ether on top of the DMSO, followed by shaking the mixture. Astaxanthin extracts in DMSO were mixed with different volume of water to make astaxanthin solutions in DMSO/water. The volume ratio of DMSO/water to ether was fixed at 1:1 to find out the optimal water volume ratio for

liquid-liquid extraction of astaxanthin. As shown in Figure 2.2A, the color of astaxanthin solution in DMSO/water was red (bottom layer), and the color of ether (top layer) was colorless before shaking. After shaking vigorously for about 10 s, the DMSO/water mixture turned from red to colorless, and the top layer turned from colorless to red/orange. This indicated most of the astaxanthin was successfully extracted from DMSO/water to ether layer. The absorbance spectra of astaxanthin in DMSO/water mixture were also measured before and after liquid-liquid extraction (Figure 2.2A). After extraction, the disappearance of absorbance peak at 492 nm also verified that astaxanthin was extracted from DMSO/water to ether.
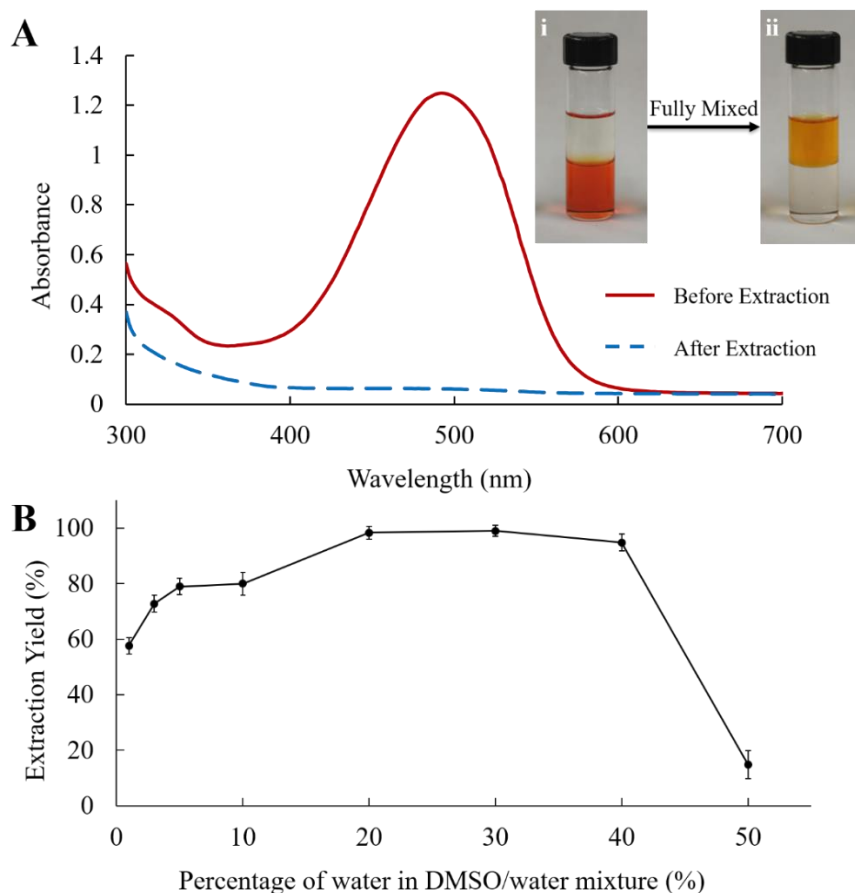
Figure 2.2. (A) 1 mL of ether was added on top of 1 mL of astaxanthin in DMSO containing 20% water (i); the mixture was fully mixed (ii). The color of astaxanthin in DMSO turned from red to colorless. The ether phase turned from colorless to orange. The absorption spectra of astaxanthin stored in DMSO before and after extraction to ether were depicted. (B) The effect of water percentage (v/v) on the extraction yield of astaxanthin from DMSO/water mixture to ether. Each value is expressed as the mean ± standard deviation (n = 3).

The absorbance readings at 492 nm were used to determine the concentrations of astaxanthin solutions. The extraction yield was then calculated by the equation 2.1 using the measured absorbance readings. Figure 2.2B depicts the extraction yield of astaxanthin plotted as a function of percentage of water in the DMSO/water mixture. About 98-99% of astaxanthin was extracted to ether when the volume of water was 20-40% (v/v). The extraction yield significantly dropped when the mixture contained 50% water (v/v). The optimal ratio of DMSO to water was 30%, giving an extraction yield of 99%.

2.4.3 Encapsulation of astaxanthin by mPEG-PCL polymeric micelles

Astaxanthin was encapsulated in mPEG-PCL micelles to overcome the problem of its poor water-solubility. Amphiphilic mPEG-PCL copolymer was produced, and polymeric micelle solution was prepared by self-assembly process. Figure 2.3A shows the average particle size of mPEG-PCL micelles and astaxanthin-encapsulated mPEG-PCL micelles. The average particle size of mPEG-PCL micelles was 87.1 ± 9.1 nm in diameter. The average size of the astaxanthin-encapsulated mPEG-PCL polymeric micelles increased to 112.3 ± 16.6 nm which is 28.9% increment of hydrophobic core volume, confirming the inclusion of hydrophobic astaxanthin in the core of polymeric micelles. The morphology of mPEG-PCL micelles before and after astaxanthin encapsulation was shown in TEM images (Figure 2.3A). The TEM images showed that the size of mPEG-PCL micelles slightly increased after encapsulation, probably due to expansion of the PLC core after encapsulation of astaxanthin. The encapsulation of astaxanthin was further confirmed by observing the absorption peak at 492 nm of astaxanthin-encapsulated micelles as well as the red color of the micelle solution (Figure 2.3B).
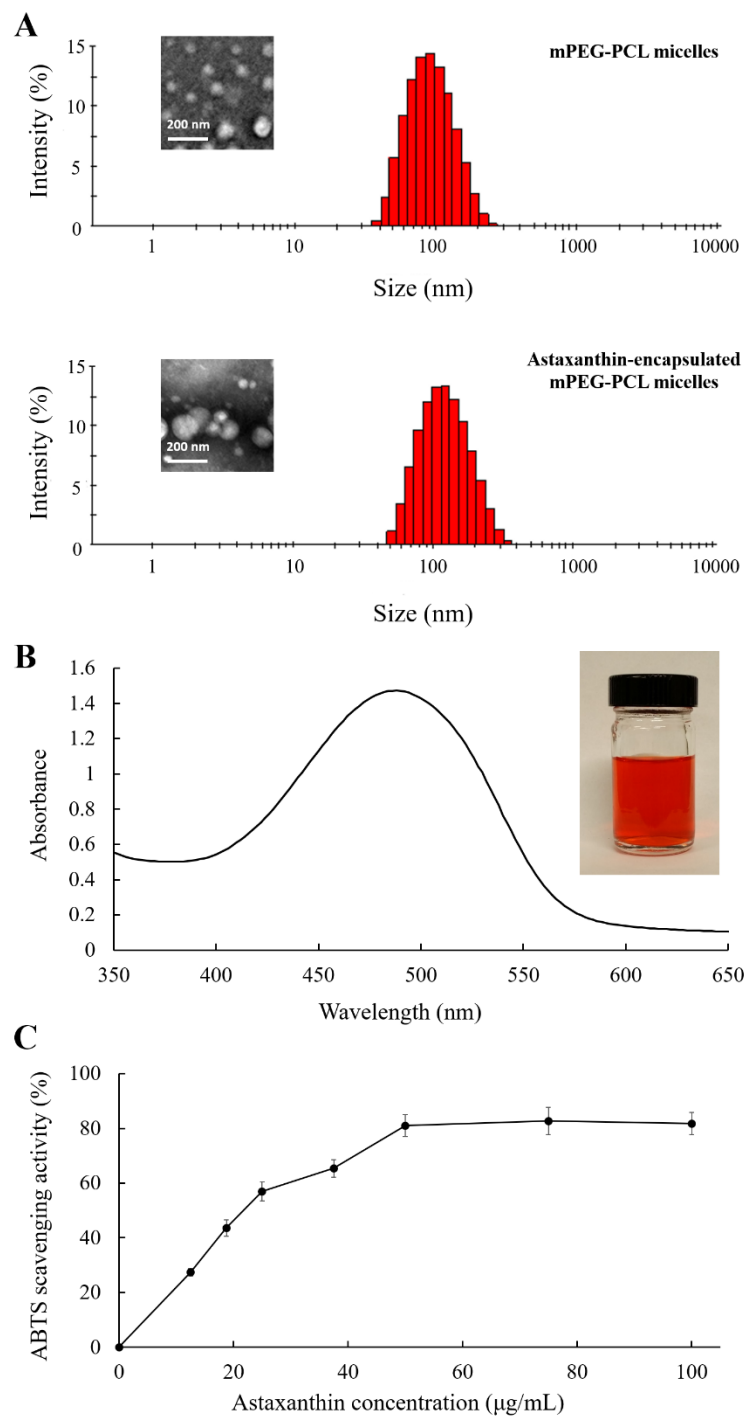
Figure 2.3. Characterization of astaxanthin encapsulated mPEG-PCL polymeric micelles. (A) Particle size distribution of mPEG-PCL polymeric micelles and astaxanthin-encapsulated mPEG-PCL polymeric micelles. The average size of mPEG-PCL polymeric micelles was 87.1 ± 9.1 nm; the average size of astaxanthin-encapsulated mPEG-PCL polymeric micelles was 112.3 ± 16.6 nm. Insets represent TEM images of corresponding micelles. Scale bar denotes 200 nm. (B) Absorption spectrum of astaxanthin-encapsulated mPEG-PCL polymeric micelles. The inserted image is the astaxanthin-encapsulated mPEG-PCL micelle solution. (C) The inhibition of absorbance at 734 nm as a function of astaxanthin concentration. Each value is expressed as the mean ± standard deviation (n = 3).

2.4.4 Astaxanthin loading and encapsulation efficiency by polymeric micelles

        To determine drug loading percentage of astaxanthin by mPEG-PCL, 5 mg of astaxanthin was encapsulated by 10 mg of mPEG-PCL copolymer. The absorbance of astaxanthin-encapsulated micelles was examined, and the amount of astaxanthin was calculated by the astaxanthin standard curve. As a result, 0.338 mg was the maximum amount of astaxanthin to be encapsulated by 10 mg of mPEG-PCL copolymer in 2 mL of acetone. Drug loading (DL) was 3.27%. The final concentration of astaxanthin-loaded mPEG-PCL micelle was 36.17 µg/mL, which is significantly higher than the reported 2 µg/mL concentration of astaxanthin-encapsulated Captisol® (sulfobutyl ether β-cyclodextrin) (Lockwood, O'Malley, and Mosher 2003). The encapsulation efficiency was determined by loading 0.3 mg of astaxanthin into 10 mg of mPEG-PCL copolymer, and the astaxanthin amount was quantified by UV/Vis spectroscopy. As a result, 0.29 mg of astaxanthin remained in the final solution of polymeric micelles, and the encapsulation efficiency was 96.67%.

2.4.5 ABTS radical scavenging

        The antioxidant activity of astaxanthin solution was determined by the inhibition of absorbance of ABTS radical cations. Figure 2.3C depicts the inhibition of absorbance at 734 nm plotted as a function of astaxanthin concentrations. Our results showed that a 50 µg/mL astaxanthin solution inhibited the absorbance at 734 nm by 82.2±4.1%. The astaxanthin collected from 10 mL of 50 µg/mL astaxanthin extracts was re-dissolved in 10 mL DMSO. The re-dissolved astaxanthin solution inhibited the absorbance at 734 nm by 79.5±3.3%, which is similar to the antioxidant activity of above-mentioned astaxanthin extracted by DMSO/water mixture. This indicates that the activity of astaxanthin was not affected by the liquid-liquid extraction method. After encapsulation by mPEG-PCL, a 64.7 µg/mL astaxanthin-encapsulated polymeric micelle solution was able to inhibit the absorbance at 734 nm by 81.6±5.4%. This indicated that the ABTS scavenging activity of astaxanthin was retained after encapsulation by mPEG-PCL polymeric micelles.

2.4.6 FT-IR spectrum of astaxanthin-encapsulated polymeric micelles

Figure 2.4 depicts the FT-IR spectra of astaxanthin, mPEG-PCL micelles, and astaxanthin-encapsulated mPEG-PCL micelles. In the spectrum of astaxanthin, the characteristic band appearing at 1649 cm^{-1} was due to the carbonyl group in astaxanthin. The peak at 1551 cm^{-1} was due to C=C in hexatomic ring (Yuan, Jin, and Xu 2012). The peak revealed at 963 cm^{-1} was due to C-H stretching. In the spectrum of mPEG-PCL micelles, the sharp peaks at 1722 cm^{-1} and 1168 cm^{-1} were due to the C=O and C-O-O stretching, respectively (Danafar et al. 2014). These two peaks indicated the formation of mPEG-PCL micelles was successful. The peak at 963 cm^{-1} for C-H stretching was also present in mPEG-PCL micelles. The sharp peak at 741 cm^{-1} was due to the aromatic C-H stretching in mPEG-PCL micelles. Comparing the spectrum of mPEG-PCL micelles and astaxanthin-encapsulated mPEG-PCL micelles, the peak appearing at 1551 cm^{-1} confirmed the encapsulation of astaxanthin. The characteristic peak for astaxanthin at 1551 cm^{-1} was weaker than that of commercial astaxanthin because the total amount of astaxanthin in the encapsulated micelles was low. The absorption peak for astaxanthin's carbonyl group shifted from 1649 cm^{-1} to 1722 cm^{-1}, probably because C=O stretching for mPEG-PCL micelles was much stronger than that of astaxanthin.
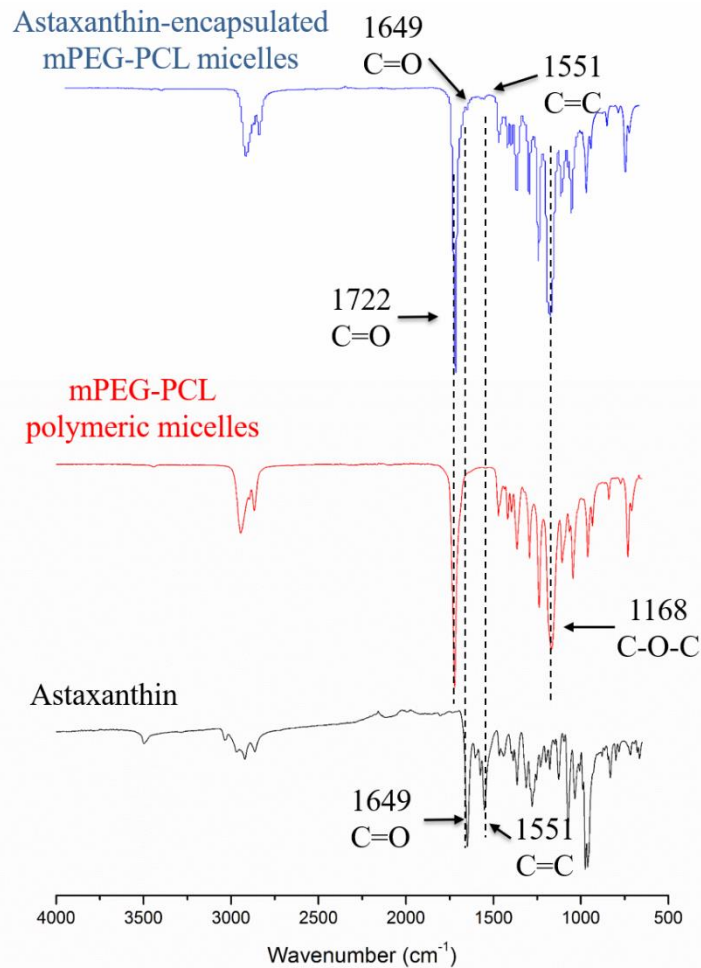
Figure 2.4. FT-IR spectra of astaxanthin, mPEG-PCL polymeric micelles, and astaxanthin-encapsulated mPEG-PCL polymeric micelles.

2.4.7 Release of astaxanthin from polymeric micelles

The release profile of astaxanthin from mPEG-PCL micelles in PBS at 25°C is shown in Figure 2.5. The release profile showed an initial burst release of astaxanthin for the first 8 h. In the initial burst release, the slope of the release profile was 14.23. Within 8 h, a total 71.85% of the encapsulated astaxanthin was released from mPEG-PCL micelles. After 8 h, the rate of astaxanthin release slowed down. A more sustained release pattern was observed from 8 to 48 h. The slope of the release profile decreased dramatically to 0.93 from 8 to 16 h. At the end of 48 h release, the cumulative release of astaxanthin from mPEG-PCL micelles was 87.31%. The slope decreased slight from 0.93 to 0.15 in the final stage.
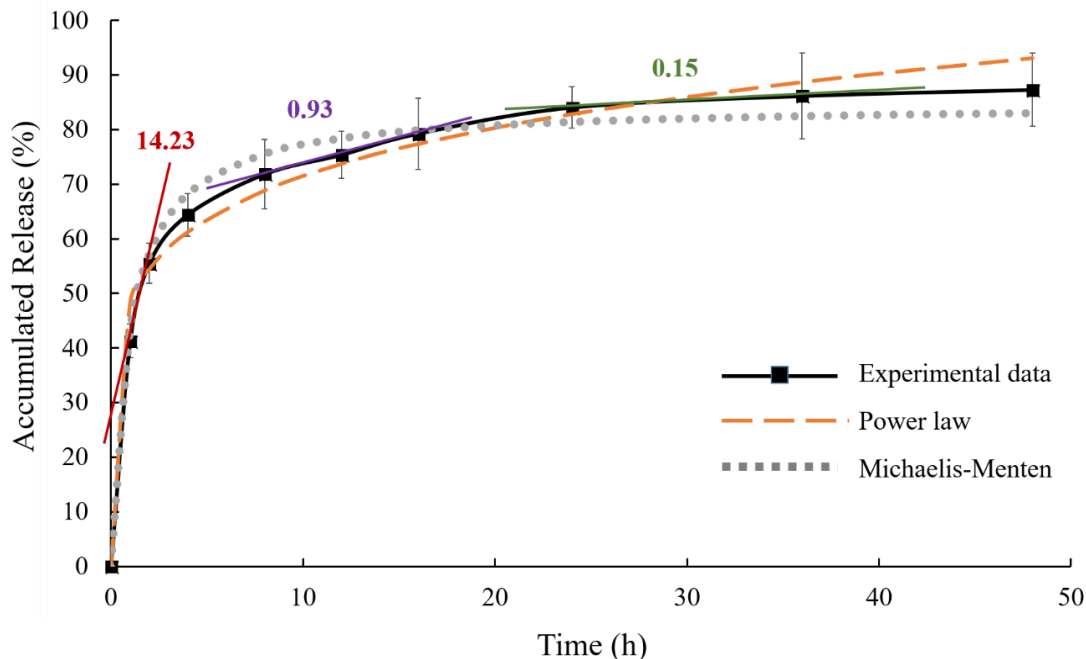
Figure 2.5. Astaxanthin release profile from mPEG-PCL polymeric micelles in PBS at 25°C (mean ± SD, n = 3). Plots generated from the power law and the Michaelis-Menten models were compared with the experimental data. K1, K2, K3 were the slopes of the in vitro release profile at different stages.

In the power law model, the constant a was equal to 48.53, and the calculated release exponent b was equal to 0.17 for astaxanthin-encapsulated mPEG-PCL micelles. In a diffusion controlled drug release mechanism, the release exponent b of a sphere with Fickian diffusion is 0.43 (Siepmann and Siepmann 2008). The release exponent of astaxanthin-encapsulated mPEG-PCL micelles is less than 0.43, indicating that the release of astaxanthin is due to not only diffusion, but also degradation and collapse of the micelles (Gou et al. 2009, Xue et al. 2012). The release kinetics of astaxanthin from mPEG-PCL micelles was also modeled using the Michaelis-Menten model. The calculated Michaelis-Menten constant K was equal to 0.97. The Michaelis-Menten model fitted the experimental data better than the power law model. In the late stage of the generated plots, the Michaelis-Menten curve showed a smoother pattern than the power law curve, which is closer to the experimental data. Moreover, curve fitting using the Michaelis-Menten model resulted in a higher correlation coefficient ($R^2 = 0.98$) than the power law model ($R^2 = 0.94$).

2.4.8 Effect of astaxanthin-encapsulated polymeric micelles on MSCs proliferation

Figure 2.6A reveals that, over the course of an 8-day culture, MSCs with mPEG-PCL micelles had the same growth kinetics profile as the ones without the treatment of polymeric micelles. After 8-day cultivation, the control group (i) had 1.77×10^5 cells/well, and non-encapsulated mPEG-PCL group (ii) had 1.79×10^5 cells/well. However, the number of MSCs treated with astaxanthin-encapsulated polymeric micelles was higher than the control groups on the 8th day post-inoculation: 1.98×10^5 cells/well for group (iii) and 2.28×10^5 cells/well for group (iv). Group (v) had 1.83×10^5 cells/well, which was close to the cell numbers of group (i) and (ii). The addition of 0.5 μg/mL astaxanthin-encapsulated polymeric micelles (group iv) led to a 26.3% increase of cell number compared to the control group. However, further increase of astaxanthin concentration to 1 μg/mL led to less proliferation than group (iii). Figure 2.6B shows the MSCs treated with polymeric micelles containing 0.5 μg/mL astaxanthin reached confluency after 8 days of cultivation, yet cell confluency was not observed for those receiving 1.0 μg/mL astaxanthin-encapsulated polymeric micelles. This observation is in line with the cell numbers presented in Figure 2.6A. Judging from the morphology of MSCs for all study groups, there was no notable morphological change of cells indicating both polymeric micelles and astaxanthin had no effect on cell morphology. Kim *et al.* reported ~67% increase of proliferation of neural stem cells when supplementing cells with 10 ng/mL astaxanthin (Kim et al. 2010). Similar decreasing trends of MSC proliferation with higher amount of antioxidant has been reported by Choi *et al.* [4]. They found that 250 μM ascorbic acid showed the highest MSC proliferation activity, but further increasing the concentration to 500 μM led to decrease of proliferation (Choi et al. 2008). It is noteworthy that the efficacy of enhancing MSC proliferation is similar for both astaxanthin and ascorbic acid treatment, yet 0.5 μg/mL astaxanthin (~0.84 μM) used in this study has much lower concentration than above-mentioned ascorbic acid. According to the release profile given in Figure 2.5, ~87% of astaxanthin was released. Thus, the concentration of astaxanthin in culture medium was about 0.73 μM. This is probably because antioxidant potency of astaxanthin is much higher than that of ascorbic acid. According to our findings, it is surmised that astaxanthin reduced ROS level in MSC culture, thereby promoting the proliferation of MSCs.
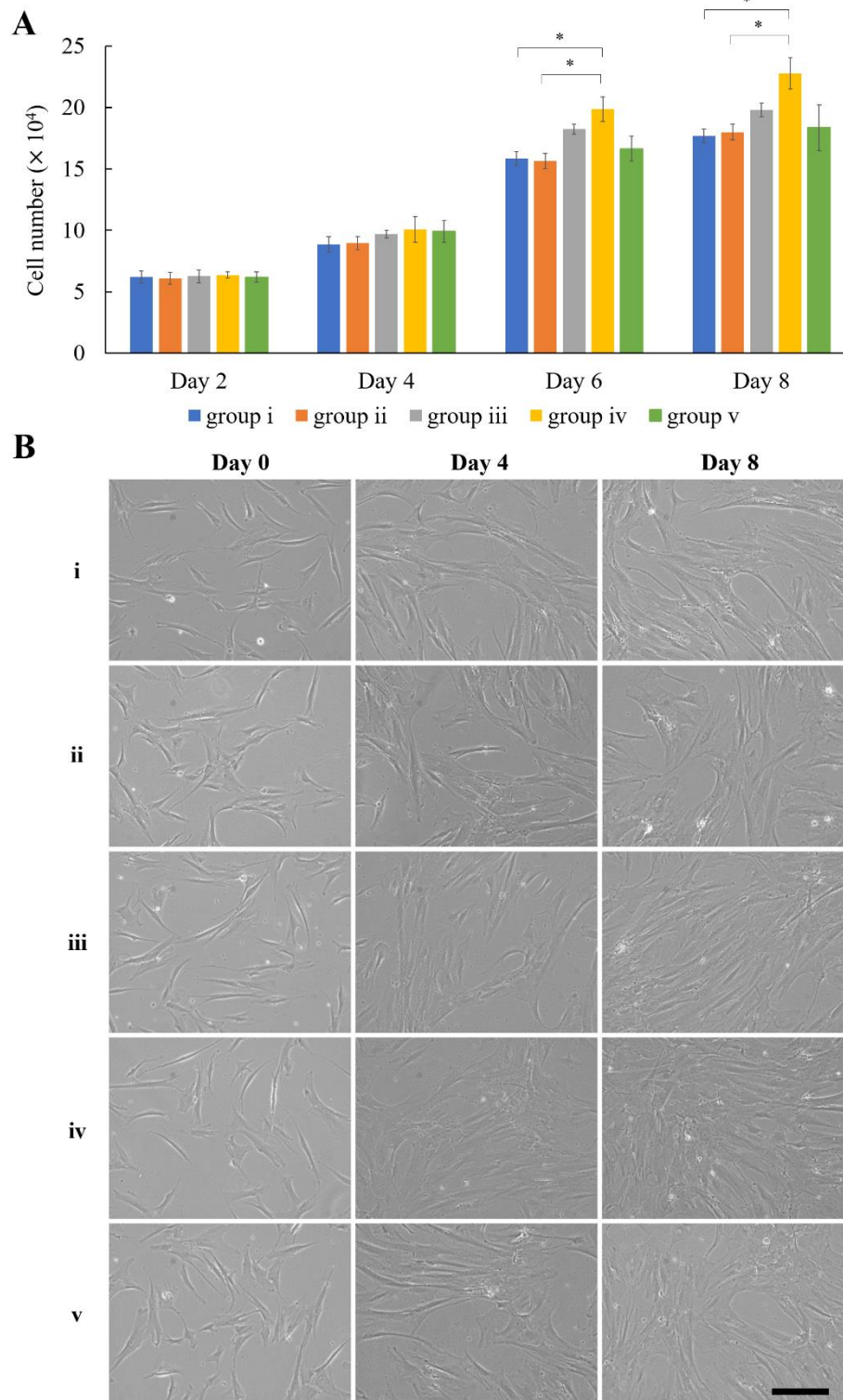
Figure 2.6. (A) Proliferation of MSCs control (group i) and MSCs treated with 0, 0.25, 0.5 and 1 μg/mL astaxanthin-encapsulated mPEG-PCL micelles (group ii – v). (B) Microscopic bright field images of MSCs at day 0, 4 and 8, respectively. Scale bar denotes 100 μm. Data were presented as mean ± standard deviation. One-way ANOVA with Tukey's post-hoc analysis was performed (n = 3). * denotes $p < 0.05$.

It should be noted that astaxanthin-encapsulated polymeric micelles could be ingested by MSCs, and therefore a portion of astaxanthin might be released intracellularly. To examine the endocytic process, MSCs were treated with rhodamine B encapsulated polymeric micelles. EE of rhodamine B by mPEG-PCL micelles was 62.5%. This was much lower than EE of astaxanthin (96.67%), probably due to less hydrophobicity of rhodamine B than astaxanthin. During encapsulation of rhodamine B, free rhodamine B in the aqueous solution was removed by dialysis, which was an extra step causing decreased EE. DL of rhodamine B by mPEG-PCL micelles was 3.03%, slightly lower than astaxanthin (3.27%). DL of rhodamine B was close to that of astaxanthin because the amount of mPEG-PCL polymer was significantly higher than the amount of encapsulated astaxanthin or rhodamine B, thereby only slight increasing in DL for astaxanthin. As shown in Figure 2.7, the fluorescent intensity of rhodamine B increased from 4 to 8 h post-treatment of polymeric micellar nanoparticles. The fluorescence intensity further increased from 8 to 24 h. This clearly showed that astaxanthin was gradually released from the polymeric micelles from extracellular to intracellular milieu, due to the internalization of micellular nanoparticles over the releasing period.
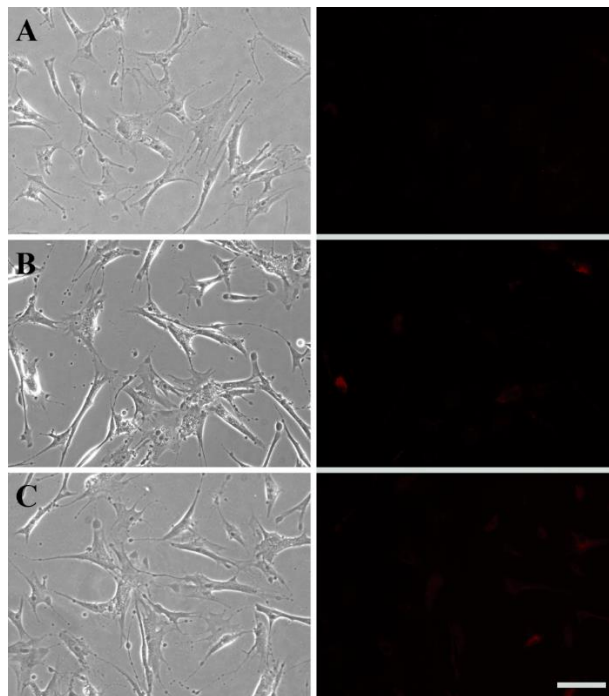
Figure 2.7. Human MSCs were treated with rhodamine B encapsulated mPEG-PCL micelles for (A) 4 h, (B) 8 h, and (C) 24 h. Scale bar denotes 100 μm.

2.4.9 The effect of astaxanthin-encapsulated mPEG-PCL on MSC differentiation

To determine the effect of astaxanthin on multipotency of MSCs, chondrogenic, adipogenic and osteogenic differentiation media supplemented with 20 ng/mL astaxanthin-encapsulated polymeric micelles were employed to induce MSC differentiation for 3 weeks. As shown in Figure 2.8A, chondrogenic, adipogenic and osteogenic differentiation of MSCs was achieved by using the media provided in the commercial kits without the addition of astaxanthin. MSCs treated with non-encapsulated mPEG-PCL micelles did not show any effect on MSC differentiation. MSCs treated with astaxanthin-supplemented differentiation media increased trilineage differentiation potency – chondrogenesis identified with sulfated proteoglycan stained by Alcian Blue (Figure 2.8A-i), adipogenesis demonstrated with lipid vacuole stained by Oil Red O (Figure 2.8A-ii), and osteogenesis visualized with calcium deposit stained by Alizarin Red (Figure 2.8A-iii). For chondrogenesis, measurements of the blue staining area indicated that astaxanthin led to 106% increase in chondrogenic differentiation of MSCs in 3 weeks compared to the control group (Fig 2.8B-i). For adipogenesis, astaxanthin-treated group showed moderate increase (52%) in formed red lipid vacuoles compared to the control group (Figure 2.8B-ii). For osteogenesis, astaxanthin-treated group showed 182% increase in black bone nodule formation compared to the control group (Figure 2.8B-iii).
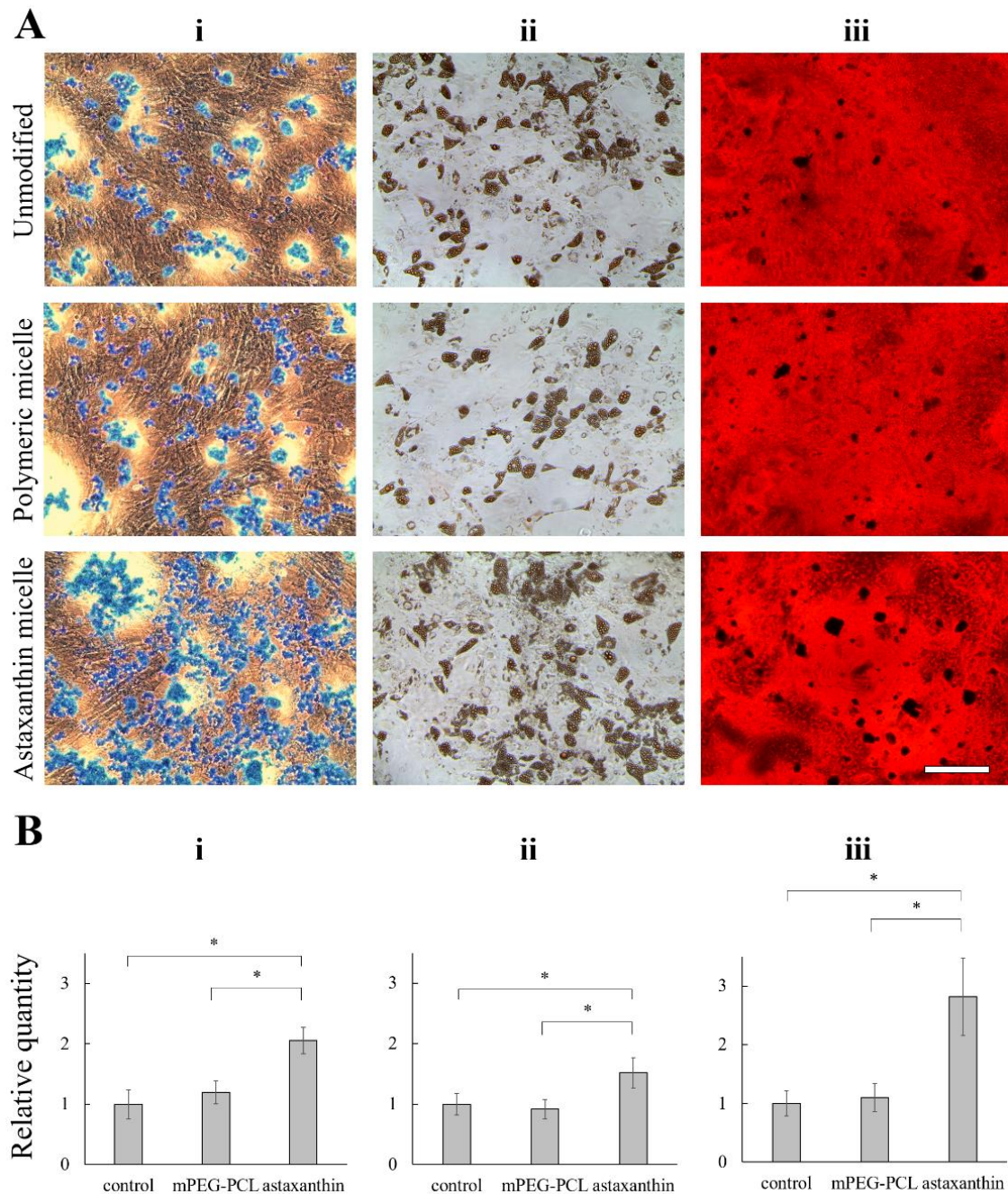
Figure 2.8. (A) The effect of 20 ng/mL astaxanthin-encapsulated mPEG-PCL micelles on (i) chondrogenesis (ii) adipogenesis and (iii) osteogenesis of MSCs. MSCs treated with unmodified differentiation media and MSCs treated with non-encapsulated mPEG-PCL micelles were used as control groups. Chondrocytes were stained with Alcian Blue. Adipocytes were stained with Oil Red O. Osteocytes were stained with Alizarin Red. Scale bar denotes 100 μm. (B) Stained area of chondrocytes, adipocytes and osteocytes were quantified using Image J. Data was presented as mean ± standard deviation and normalized to the controls. Data were presented as mean ± standard deviation. One-way ANOVA with Tukey's post-hoc analysis was performed (n = 3). * denotes $p < 0.05$.

2.5 Conclusions

In this study, astaxanthin was extracted from *H. pluvialis* by mechanical disruption in DMSO. A liquid-liquid extraction method was used to extract astaxanthin from a DMSO/water mixture to ether. Astaxanthin was collected by rotary evaporation. mPEG-PCL polymeric micelles were used to encapsulate astaxanthin to enhance its aqueous solubility. The antioxidant activity of astaxanthin was retained after encapsulation by mPEG-PCL polymeric micelles. The *in vitro* release profile showed that astaxanthin was released from mPEG-PCL micelles in a sustained manner with an initial burst release. The addition of 0.5 µg/mL astaxanthin-encapsulated mPEG-PCL micelles to MSC cultures enhanced the proliferation of MSCs. 20 ng/mL astaxanthin-encapsulated mPEG-PCL micelles enhanced the chondrogenic, adipogenic and osteogenic differentiation of MSCs.

2.6 References

Adams, M. L., A. Lavasanifar, and G. S. Kwon. 2003. "Amphiphilic block copolymers for drug delivery." *J. Pharm. Sci.* 92 (7):1343-1355.

Anarjan, N., I. A. Nehdi, H. M. Sbihi, S. I. Al-Resayes, H. J. Malmiri, and C. P. Tan. 2014. "Preparation of astaxanthin nanodispersions using gelatin-based stabilizer systems." *Molecules* 19 (9):14257-14265.

Boussiba, Sammy, Lu Fan, and Avigad Vonshak. 1992. "Enhancement and determination of astaxanthin accumulation in green alga *Haematococcus pluvialis*." In *Methods in Enzymology*, edited by Packer Lester, 386-391. Academic Press.

Boussiba, Sammy, and Avigad Vonshak. 1991. "Astaxanthin accumulation in the green alga *Haematococcus pluvialis*[1]." *Plant. Cell. Physiol.* 32 (7):1077-1082.

Choi, K. M., Y. K. Seo, H. H. Yoon, K. Y. Song, S. Y. Kwon, H. S. Lee, and J. K. Park. 2008. "Effect of ascorbic acid on bone marrow-derived mesenchymal stem cell proliferation and differentiation." *J. Biosci. Bioeng.* 105 (6):586-94.

Christian, David, Jun Zhang, Alicia J. Sawdon, and Ching-An Peng. 2018. "Enhanced astaxanthin accumulation in *Haematococcus pluvialis* using high carbon dioxide concentration and light illumination." *Bioresour. Technol.* 256:548-551.

Danafar, H., S. Davaran, K. Rostamizadeh, H. Valizadeh, and M. Hamidi. 2014. "Biodegradable m-PEG/PCL Core-Shell Micelles: Preparation and Characterization as a Sustained Release Formulation for Curcumin." *Adv. Pharm. Bull.* 4 (Suppl 2):501-510.

Denu, Ryan A., and Peiman Hematti. 2016. "Effects of Oxidative Stress on Mesenchymal Stem Cell Biology." *Oxid. Med. Cell. Longev.* 2016:2989076.

Fabregas, J., A. Otero, A. Maseda, and A. Dominguez. 2001. "Two-stage cultures for the production of astaxanthin from *Haematococcus pluvialis*." *J. Biotechnol.* 89 (1):65-71.

Fan, G., L. Wen, M. Li, C. Li, B. Luo, F. Wang, L. Zhou, and L. Liu. 2011. "Isolation of mouse mesenchymal stem cells with normal ploidy from bone marrows by reducing oxidative stress in combination with extracellular matrix." *BMC Cell. Biol.* 12:30.

Galvao, J., B. Davis, M. Tilley, E. Normando, M. R. Duchen, and M. F. Cordeiro. 2014. "Unexpected low-dose toxicity of the universal solvent DMSO." *Faseb J.* 28 (3):1317-30.

Gou, M., X. Zheng, K. Men, J. Zhang, B. Wang, L. Lv, X. Wang, Y. Zhao, F. Luo, L. Chen, X. Zhao, Y. Wei, and Z. Qian. 2009. "Self-assembled hydrophobic honokiol loaded MPEG-PCL diblock copolymer micelles." *Pharm. Res.* 26 (9):2164-2173.

Guerin, M., M. E. Huntley, and M. Olaizola. 2003. "*Haematococcus* astaxanthin: applications for human health and nutrition." *Trends Biotechnol.* 21 (5):210-216.

Hama, S., S. Uenishi, A. Yamada, T. Ohgita, H. Tsuchiya, E. Yamashita, and K. Kogure. 2012. "Scavenging of hydroxyl radicals in aqueous solution by astaxanthin encapsulated in liposomes." *Biol. Pharm. Bull.* 35 (12):2238-2242.

Higuera-Ciapara, I., L. Felix-Valenzuela, and F. M. Goycoolea. 2006. "Astaxanthin: a review of its chemistry and applications." *Crit. Rev. Food Sci. Nutr.* 46 (2):185-196.

Kim, J. H., S. W. Nam, B. W. Kim, W. J. Kim, and Y. H. Choi. 2010. "Astaxanthin improves the proliferative capacity as well as the osteogenic and adipogenic differentiation potential in neural stem cells." *Food Chem. Toxicol.* 48 (6):1741-5.

Kobayashi, M. 2000. "In vivo antioxidant role of astaxanthin under oxidative stress in the green alga *Haematococcus pluvialis*." *Appl. Microbiol. Biotechnol.* 54 (4):550-555.

Lockwood, S. F., S. O'Malley, and G. L. Mosher. 2003. "Improved aqueous solubility of crystalline astaxanthin (3,3'-dihydroxy-beta, beta-carotene-4,4'-dione) by Captisol (sulfobutyl ether beta-cyclodextrin)." *J. Pharm. Sci.* 92 (4):922-926.

Naguib, Y. M. 2000. "Antioxidant activities of astaxanthin and related carotenoids." *J. Agric. Food Chem.* 48 (4):1150-4.

Re, R., N. Pellegrini, A. Proteggente, A. Pannala, M. Yang, and C. Rice-Evans. 1999. "Antioxidant activity applying an improved ABTS radical cation decolorization assay." *Free Radic. Biol. Med.* 26 (9-10):1231-1237.

Sarugaser, Rahul, Lorraine Hanoun, Armand Keating, William L. Stanford, and John E. Davies. 2009. "Human Mesenchymal Stem Cells Self-Renew and Differentiate According to a Deterministic Hierarchy." *PLoS ONE* 4 (8):e6498.

Sawdon, A. J., and C. A. Peng. 2014. "Polymeric micelles for acyclovir drug delivery." *Colloids Surf. B Biointerfaces* 122:738-745.

Siepmann, J., and F. Siepmann. 2008. "Mathematical modeling of drug delivery." *Int. J. Pharm.* 364 (2):328-43.

Sun, Li-Yi, Cheng-Yoong Pang, Dian-Kun Li, Chia-Hsin Liao, Wei-Chao Huang, Chao-Chuan Wu, Yi-Yo Chou, Wei Wu Li, Shin-Yuan Chen, Hwan-Wun Liu, Yao-Jen Chang, and Ching-Feng Cheng. 2013. "Antioxidants cause rapid expansion of human adipose-derived mesenchymal stem cells via CDK and CDK inhibitor regulation." *Journal of Biomedical Science* 20 (1):53-53.

Tachaprutinun, A., T. Udomsup, C. Luadthong, and S. Wanichwecharungruang. 2009. "Preventing the thermal degradation of astaxanthin through nanoencapsulation." *Int. J. Pharm.* 374 (1-2):119-124.

Wang, Shihua, Xuebin Qu, and Robert Chunhua Zhao. 2012. "Clinical applications of mesenchymal stem cells." *J. of Hematol. Oncol.* 5:19-19.

Xue, B., Y. Wang, X. Tang, P. Xie, Y. Wang, F. Luo, C. Wu, and Z. Qian. 2012. "Biodegradable self-assembled MPEG-PCL micelles for hydrophobic oridonin delivery in vitro." *J. Biomed. Nanotechnol.* 8 (1):80-89.

Yang, Y., B. Kim, and J.Y. Lee. 2013. "Astaxanthin structure, metabolism, and health benefits." *J. Hum. Nutr. Food Sci.* 1:1003.

Yuan, C., L. Du, Z. Jin, and X. Xu. 2013. "Storage stability and antioxidant activity of complex of astaxanthin with hydroxypropyl-beta-cyclodextrin." *Carbohydr. Polym.* 91 (1):385-389.

Yuan, Chao, Zhengyu Jin, and Xueming Xu. 2012. "Inclusion complex of astaxanthin with hydroxypropyl-β-cyclodextrin: UV, FTIR, 1H NMR and molecular modeling studies." *Carbohydr. Polym.* 89 (2):492-496.

Chapter 3. Poly(N-isopropylacrylamide) Modified Polydopamine as Temperature-responsive Surface for Cultivation and Harvest of Mesenchymal Stem Cells

3.1 Abstract

A thermo-responsive surface was fabricated by depositing poly(*N*-isopropylacrylamide) (PNIPAAm) onto polydopamine coated cell culture substrata through free radical polymerization for the purpose of culturing and harvesting human mesenchymal stem cells (MSCs). Human MSCs were cultured onto PNIPAAm-*g*-polydopamine coated surface and harvested by changing from physiological to ambient temperature. The produced PNIPAAm-*g*-polydopamine surface was characterized by atomic force microscopy, Fourier transform infrared spectroscopy, nuclear magnetic resonance, water contact angle measurement, differential scanning calorimetry, and cell culture studies. Our results revealed that human MSCs could be detached from PNIPAAm-*g*-polydopamine surface within 60 min after switching temperature from 37ºC to room temperature. The detached human MSCs were able to proliferate on PNIPAAm-*g*-polydopamine coated surface for further growth and harvest.

3.2 Introduction

Poly(*N*-isopropylacrylamide) (PNIPAAm) is an extensively studied thermo-sensitive polymer with a lower critical solution temperature (LCST) of 32°C in aqueous solution. (Heskins and Guillet 1968). In the past, PNIPAAm modified surfaces have been used to harvest high-density cell sheets without disrupting the extracellular matrix proteins (Dalsin and Messersmith 2005). This is because PNIPAAm is hydrophobic in nature at temperatures higher than 32°C but becomes hydrophillic as the temperature falls. Cells attach more easily on hydrophobic surfaces than on hydrophilic, therefore, when the temperature of the PNIPAAm surface is lowered, the cells can easily detach.

Although using traditional proteolytic enzymes such as trypsin for cell harvesting is highly efficient, enzymatic treatment might cause disruption of the cell membrane and/or extracellular matrix (ECM) of the cells (Nakayama, Okano, and Winnik 2010), and make the mesenchymal stem cells lose their differentiated phenotypes (Yang et al. 2012). Cell harvesting from PNIPAAm-grafted surface can avoid damage of the ECM (Nagase, Kobayashi, and Okano 2009, Nakayama, Okano, and Winnik 2010). The intact ECM allows the cell sheets to be used directly for transplantation (Marion and Mao 2006). Mesenchymal stem cells (MSCs) have been extensively studied due to their self-renewal property and multi-differentiation potential for the field of tissue engineering and regenerative medicine (Caplan 2007). Due to tumor-tropic ability, MSCs have also been gaining importance in cancer therapy as cell carriers for delivering therapeutic agents (Shah 2012). Treating MSCs with trypsin for an extended time period and after multiple passages could harm MSCs and affect their proliferation. Yang et al. reported that MSCs harvested from PNIPAAm-modified surfaces have shown higher cell viability, better proliferation, and stronger differentiation than MSCs harvested by trypsinization after three cell passages (Yang et al. 2012).

Various techniques have been used to fabricate PNIPAAm-modified surfaces for cell and tissue engineering purposes. These methods include electron beam irradiation, plasma polymerization, UV irradiation, and spin coating (Yamada et al. 1990, Kim, Kanamori, and Shinbo 2002, Patel et al. 2012, Recum et al. 1997). Among all these methods, electron beam polymerization is the most employed method for producing PNIPAAm surfaces because the thickness of the polymer film can be carefully controlled to 15 – 20 nm, which is the optimized thickness for cell adhesion and temperature-controlled detachment (Nakayama, Okano, and Winnik 2010, Akiyama et al. 2004). In view of polydopamine film having been employed to serve as an excellent platform for further surface functionalization and biomolecule immobilization (Cui et al. 2012, Rivera and Messersmith 2012, Lee, Rho, and Messersmith 2009), this study intends to use polydopamine as the surface modification material to fabricate PNIPAAm surface by free radical polymerization for culturing and harvesting human MSCs. Polydopamine has recently drawn significant attention as a universal surface modification agent which can be prepared by simply immersing substrates into an aqueous dopamine solution under

alkaline conditions (Lee et al. 2007). The polydopamine film is ultrathin but robust, and it can be used to modify the surfaces of a vast range of materials.

Although polydopamine/PNIPAAm mixed films have been reported by mixing aminated PNIPAAm into the dopamine solution prior to the film deposition (Zhang et al. 2013), myoblast cells revealed less spreading feature than the pristine coatings after 24 h attachment. Moreover, no attempts were made to harvest cells with the fabricated polydopamine/PNIPAAm mixed films. In this study, a straightforward and cost-effective two-step method was used to produce PNIPAAm-*g*-polydopamine coated Petri dishes. Compared with other methods for producing PNIPAAm modified surfaces (Yamada et al. 1990, Kim, Kanamori, and Shinbo 2002, Patel et al. 2012, Recum et al. 1997), this facile two-step approach involves merely the deposition of biocompatible polydopamine film and free radical polymerization, without the need of any special instrument. In the first step, dopamine was first tagged with allyl groups by conjugating with itaconic anhydride (ITA). In the conjugation process, ITA reacted with the amine group of dopamine, and the anhydride ring was opened by nucleophilic attack (Figure 3.1). In the second step, the allyl-functionalized polydopamine film was then coated on the substratum by adding allylated dopamine into solution with slight basic pH. Through the allyl groups immobilized on the substratum, PNIPAAm was able to crosslink onto the surface by free radical polymerization.
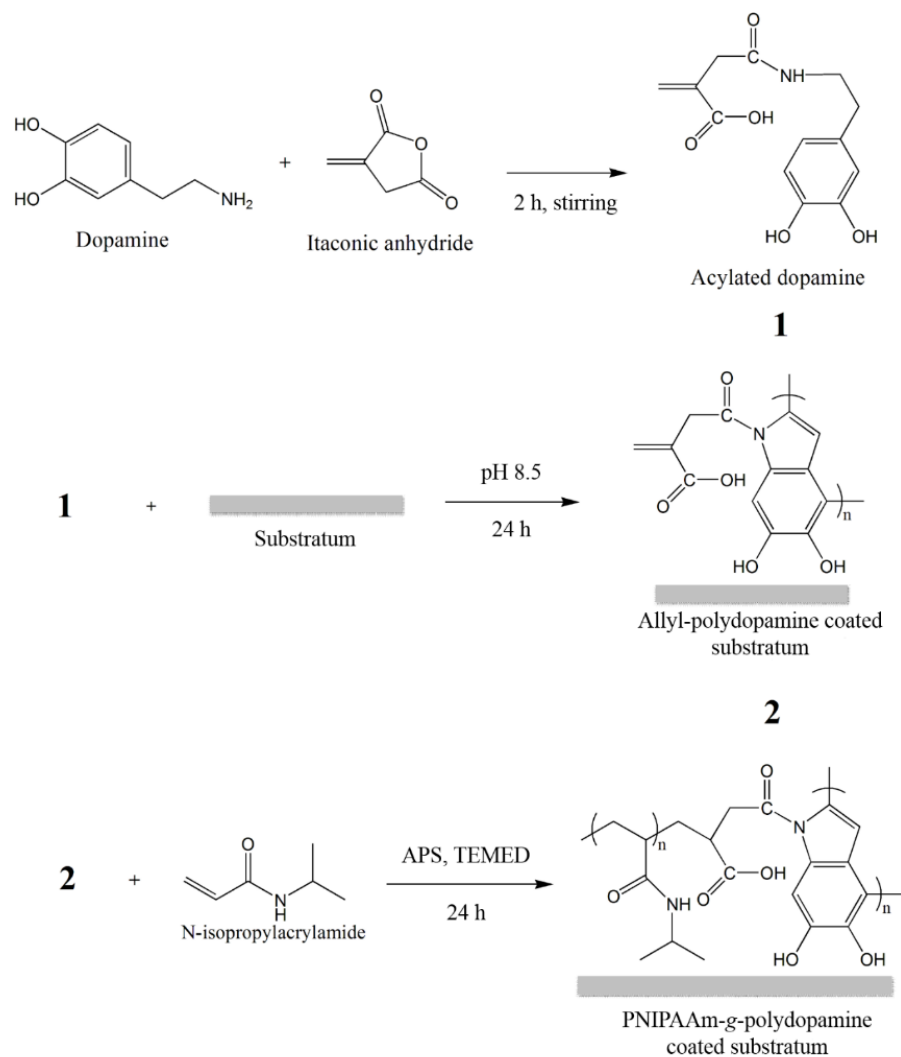
Figure 3.1. Reaction scheme for grafting PNIPAAm onto allyl functionalized polydopamine.

The fabricated PNIPAAm-*g*-polydopamine substrata after characterization were used to culture and harvest human MSCs. The morphology of cell shape, attachment, and spreading on the PNIPAAm-*g*-polydopamine surface was essentially the same as the ones observed on bare and polydopamine coated culture dishes. Our results showed that within 60 min, majority of cultured MSCs could be harvested from the PNIPAAm-*g*-polydopamine coated substrata by treating MSCs with culture medium at ambient temperature.

3.3 Materials and Methods

3.3.1. Materials

N-isopropylacrylamide (NIPAAm) was purchased from TCI (Tokyo, Japan). Dopamine hydrochloride, dimethyl sulfoxide-d6 (DMSO-d$_6$) and penicillin-streptomycin was purchased from Sigma-Aldrich (St. Louis, MO, USA). Tris (hydroxymethyl) aminomethane (Tris base), sodium hydroxide (NaOH), 0.25% trypsin/EDTA solution, Minimum Essential Medium Alpha Medium (αMEM), Dulbecco's Modified Eagle's Medium (DMEM) and L-glutamine were purchased from Fisher Scientific (Waltham, MA, USA). N-isopropylacrylamide (NIPAAm) was purchased from TCI America (Portland, OR, USA). Ammonium persulfate (APS) was purchased from J.T. Baker (Philipsburg, NJ, USA). Itaconic anhydride (ITA), and 99% N,N,N'N'-tetramethylethylenediamine (TEMED) were purchased from Alfa Aesar (Ward Hill, MA, USA). Fetal bovine serum (FBS) was purchased from Atlanta Biologicals (Lawrencevilla, GA, USA). Human mesenchymal stem cells were obtained from Texas A&M Health Science Center (College Station, TX, USA).

3.3.2. Preparation of PNIPAAm-g-polydopamine modified substratum

In order to modify the polydopamine film with allyl functional group, dopamine was first conjugated with itaconic anhydride (ITA) to form acylated dopamine before the polymerization process. Briefly, 0.04 g of dopamine and 0.04 g of ITA was dissolved in 20 mL of deionized (DI) water. The reaction mixture was stirred for 2 h. The pH of the solution was adjusted to 8.5 by adding Tris base to the solution. A 35-mm Petri dish was immersed in the mixture and secured at the bottom of the beaker. The beaker was then placed in an orbital incubator (MaxQ 4000; Thermo Fisher Scientific, Waltham, MA, USA) shaken at 100 rpm for overnight. The polydopamine modified substrate was cleaned by sonication in DI water for 10 min.

After the substrate surface was functionalized with allyl groups, PNIPAAm was deposited on the surface by free radical polymerization in the presence of APS and TEMED. Briefly, 15 mL of 0.5 M NIPAAm solution was prepared in DI water, and the polydopamine modified Petri dish was immersed in the NIPAAm solution. 0.3 g of APS and 10 µL of TEMED were added to the NIPAAm solution, and the mixture was stirred

at ambient temperature for 2 h. The PNIPAAm-*g*-polydopamine coated Petri dish was collected and repeatedly rinsed by DI water.

3.3.3. Characterization of PNIPAAm-*g*-polydopamine surface

To check whether PNIPAAm has been grafted onto the polydopamine surface, the surface topography of polydopamine and PNIPAAm-*g*-polydopamine films were compared. The tapping mode of atomic force microscopy (AFM) (Dimension 3000; Veeco Instruments, Plainview, NY, USA) was used, and both topographical and 3D images were acquired by Nanoscope software (Veeco Instruments). Sectional analysis was used to estimate the thickness of the film. The images were captured at a scan size of 5 μm.

The chemical structure of the polydopamine film and PNIPAAm-*g*-polydopamine film was characterized by Fourier transform infrared spectroscopy (FTIR) and nuclear magnetic resonance (NMR). FTIR spectrum was recorded by an ATR/FTIR Spectrometer (Spectrum One; Perkin Elmer, Waltham, MA, USA). ^{1}H NMR spectra were obtained by an NMR spectrometer (INOVA 400 MHz; Varian, Palo Alto, CA, USA). First, the PNIPAAm-*g*-polydopamine film was dissolved in 0.1 N NaOH. Then, 50 μL of the dissolved film was mixed with 550 μL DMSO-d_6 to obtain NMR spectrum.

The LCST of the dissolved PNIPAAm-*g*-polydopamine film was characterized by differential scanning calorimetry (DSC 2920; TA Instruments, New Castle, DE, USA). DSC thermogram was obtained with a heating rate of 10°C per min under N_2 purge. The cloud point temperature of the dissolved film, following the method described by (Jain et al. 2015), was determined by monitoring UV-Vis transmittance at 563 nm (Spectramax M2e microplate reader, Molecular Devices, Sunnyvale, CA, USA) in the temperature range of 25 to 37°C. The wettability of the PNIPAAm-*g*-polydopamine coated surface was characterized by water contact angle measurements on a goniometer (Krüss G10; KRÜSS GmbH, Hamburg, German). A clean bare Petri dish and a polydopamine coated petri dish were used as controls during the experiment. Here, a water droplet of 1 μL was dripped onto the control Petri dishes or the PNIPAAm-*g*-polydopamine coated Petri dish. The contact angles of the substrate surface were measured accordingly at ambient temperature and 40°C.

3.3.4. Culturing and harvesting MSCs on PNIPAAm-*g*-polydopamine surface

The PNIPAAm-*g*-polydopamine coated Petri dish was placed in a biological safety cabinet (1300 Series Class II, Thermo Fisher Scientific, Waltham, MA, USA) under UV irradiation for 1 h, and sterilized with 70% ethanol for 30 min. MSCs were inoculated onto the PNIPAAm modified Petri dish at 1.0 x 10^4 cells/cm^2 and incubated at 37°C in a 5% CO_2 incubator (Forma 310; Thermo Fisher Scientific, Waltham, MA, USA). The cells were cultured with αMEM supplemented with 16.5% FBS, 1% penicillin-streptomycin and 2 mM L-glutamine. Once the cells reached confluency, cells were harvested by lowering the temperature from 37°C to ambient temperature by replacing culture medium with αMEM kept in the room temperature. The cells were observed for 60 min after the temperature change, and phase contrast images were taken every 20 min with Leica DMi8 microscope equipped with Leica DFC360 FX camera (Leica Microsystems, Wetzlar, Germany). At 20, 40, and 60 min, MSCs were allowed to detach by giving the cells some gentle pipetting force. All images were processed by Leica Application Suite V3 software. Detached cells were counted using a hemocytometer. After 60 min, the cells not detached from the surface were harvested by treatment of 0.25% trypsin/EDTA, and the cell numbers were counted again. The numbers of cells detached by temperature switch and trypsin treatment were added up as the total cell number. The percentage of cell detachment was plotted against time from 0 to 60 min.

MSCs collected from PNIPAAm-*g*-polydopamine coated Petri dishes by temperature switch were centrifuged and resuspended in αMEM medium. The collected cells were inoculated on freshly prepared PNIPAAm-*g*-polydopamine coated Petri dishes at 10^3 cells/cm^2 and incubated at the aforementioned conditions. The cell numbers were counted every 3 days using a hemocytometer. Phase contrast images were taken with Leica DMi8 microscope equipped with Leica DFC360 FX camera.

3.4 Results and Discussion

3.4.1 Surface topography of PNIPAAm-*g*-polydopamine film

Thermo-responsive polymer PNIPAAm has been widely used in tissue and cell sheet engineering. Various methods have been developed to produce PNIPAAm surfaces

for culturing and harvesting human MSCs (Yang et al. 2012, Patel et al. 2012, Shi et al. 2010, Cho et al. 2004). Human MSCs cultivated and harvested from PNIPAAm surfaces have shown higher cell viability, and retaining their self-renewal and multipoietic activities after detaching from temperature-responsive surfaces, unlike trypsinized MSCs with ECM proteins being damaged (Marion and Mao 2006). PNIPAAm surface has been produced onto polydopamine coated surface using surface-initiated atom transfer radical polymerization (SI-ATRP) for making controlled release of fertilizers (Ma et al. 2013). Although the thickness of the PNIPAAm surface can be well controlled using SI-ATRP (Wei, Ji, and Shen 2008, Xu et al. 2006), the metal catalyst used in SI-ATRP is difficult to remove. This may cause cell toxicity problem during the cultivation of fastidious MSCs. The free radical polymerization approach used here for the formation of PNIPAAm-*g*-polydopamine has no concern of leaving toxic residues for MSC culture. Polydopamine/PNIPAAm mixed film was prepared by co-depositing polydopamine with amino-PNIPAAm (Zhang et al. 2013). The reactive quinones of the polydopamine react with nucleophilic amines via the Michael-type addition and/or Schiff base reaction. Generally, aliphatic amines favor the Schiff base reaction which could be affected by the chain length of the chemical incorporating the primary amine (Yang, Cohen Stuart, and Kamperman 2014). A longer chain leads to a decrease in the basicity of the primary amine, which results in a lower reaction rate (Yang, Cohen Stuart, and Kamperman 2014). The long aliphatic chain of the reported aminated PNIPAAm (MW of 2,500) (Zhang et al. 2013) probably decreased the coupling of amine-ended PNIPAAm with the quinone groups of polydopamine. This could lead to less detachment of the myoblast cells via the temperature switch. Unlike that, the polydopamine film reported here was modified with allyl groups through a simple anhydride ring-opening reaction. Our PNIPAAm film was deposited on the allyl-functionalized polydopamine surface via surface-initiated free radical polymerization. The synthesis of PNIPAAm from the pre-deposited allylated polydopamine assured the temperature-responsive PNIPAAm was on the top layer of the fabricated surface for efficient culture and harvest of MSCs.

The surface topography of the synthesized PNIPAAm-*g*-polydopamine surface was investigated by AFM. The surface of polydopamine coated Petri dish was fairly smooth (Figure 3.2A). During pH-induced polymerization of dopamine, dopamine self-

polymerized and formed nano-aggregates in the bulk solution, and those nanoparticles clustered randomly and were deposited onto the substrate surface (Jiang et al. 2011). Cross sectional analysis showed the deposition of a uniformly distributed polydopamine film onto the Petri dish. However, after grafting PNIPAAm by free radical polymerization, the PNIPAAm polymers were randomly deposited onto the substrate surface, with the height of the polymer aggregation from 50 to 100 nm. Although the height of the PNIPAAm-*g*-polydopamine polymer aggregate exceeded the optimum thickness (i.e., 15 - 20 nm) for temperature controlled cell harvesting (Nakayama, Okano, and Winnik 2010), MSCs were able to proliferate on the PNIPAAm-*g*-polydopamine modified Petri dish and be harvested through temperature switch.
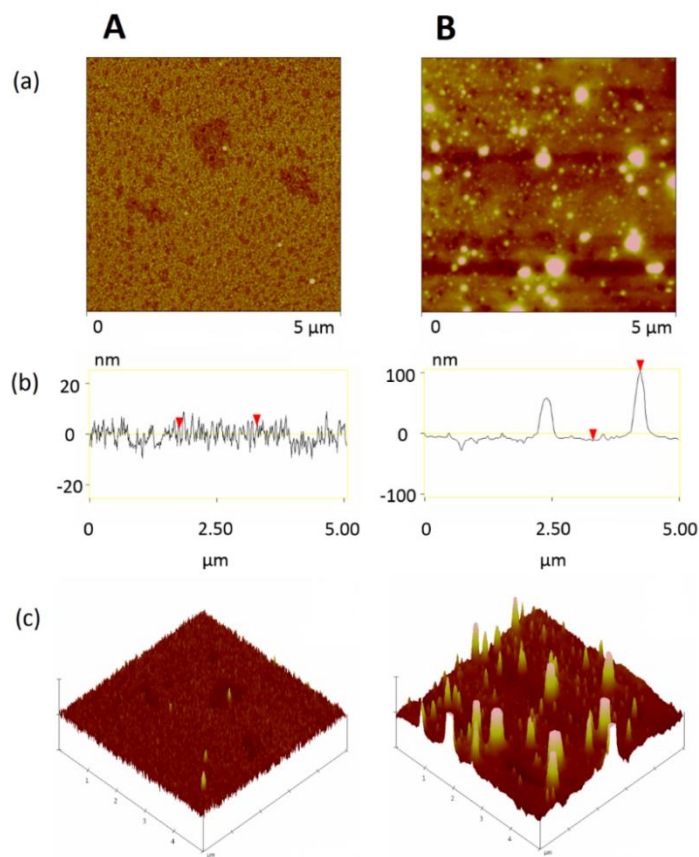
Figure 3.2. AFM analysis of (A) allyl-polydopamine coated and (B) PNIPAAm-*g*-polydopamine coated Petri dish. The experimental results were presented as (a) topographic image, (b) spectrum of sectional heights, and (c) 3D image.

3.4.2 Chemical structure of PNIPAAm-*g*-polydopamine film

The chemical structure of PNIPAAm-*g*-polydopamine film was characterized by FTIR spectroscopy. Figure 3.3 shows the FTIR spectra of PNIPAAm, polydopamine film and PNIPAAm-*g*-polydopamine film. In the spectrum of freeze-dried PNIPAAm powder, an absorption peak was observed at 3300 cm^{-1} due to the N-H stretching (Sun, Y., and Wu 2007). Also, three other absorption peaks at 2970, 2960, and 2900 cm^{-1} were observed next to the broad band. These peaks were due to the –CH$_3$ asymmetric stretching of PNIPAAm (Li et al. 2011). Three more absorption peaks were observed at 1620, 1550, and 1460 cm^{-1}. The peaks at 1620 and 1550 cm^{-1} were the typical amide I and amide II stretching from PNIPAAm (Sun, Y., and Wu 2007). The peak at 1460 cm^{-1} is the C-H stretching band. The characteristic peaks of PNIPAAm were all present in the spectrum of PNIPAAm-*g*-polydopamine. In the acquired spectrum of polydopamine film, a broad band was observed from 2500 to 3600 cm^{-1}, due to O-H stretching. Two distinctive peaks were observed at 1600 and 1500 cm^{-1}. These two peaks are the typical absorption peaks for indole structure (Dreyer et al. 2012). However, these two peaks did not show up in the spectrum of PNIPAAm-*g*-polydopamine, likely because the chemical composition of the PNIPAAm-*g*-polydopamine film consisted mainly of PNIPAAm. Finally, in the spectrum of PNIPAAm-*g*-polydopamine, a narrow absorption peak was observed at 3280 cm^{-1} owing to the N-H stretching. This was consistent with the N-H peak observed in freeze-dried PNIPAAm spectrum. The peaks at 2970, 2960, and 2900 cm^{-1} were consistent with the –CH$_3$ asymmetric stretching in the PNIPAAm spectrum. The absorption peaks observed at 1620, 1550, and 1460 cm^{-1} were the amide I and amide II peaks as well as C-H stretching peaks. The peaks of polydopamine were relatively weak compared to those of PNIPAAm because in PNIPAAm-*g*-polydopamine, the mass of PNIPAAm was much higher than the mass of polydopamine. In short, judging from the obtained FTIR spectra, it is confirmed that PNIPAAm film was established on the substrate surface via surface-initiated free radical polymerization from the surface pre-coated with polydopamine.
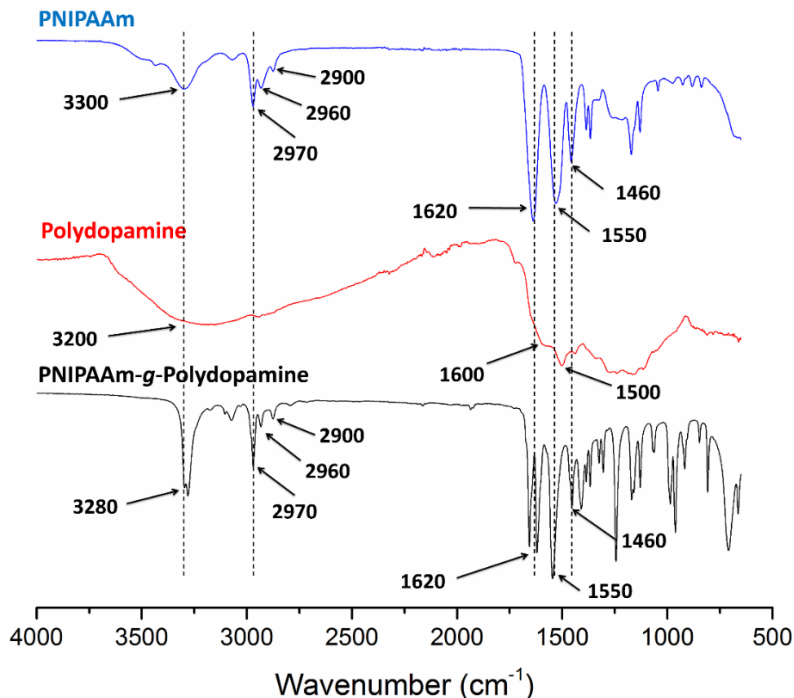
Figure 3.3. FTIR spectra of freeze-dried PNIPAAm, polydopamine, and PNIPAAm-*g*-polydopamine.

Figure 3.4 shows the ^{1}H NMR spectrum of PNIPAAm-*g*-polydopamine film. Chemical shifts at δ = 5.50 to 5.53 ppm, 5.99 to 6.17 ppm, 7.04 ppm and 7.97 ppm were assigned to protons in polydopamine. The structure of polydopamine film contains both 5,6-dihydroxyindole and 5,6-indolequinone (Zangmeister, Morris, and Tarlov 2013). Both structures have protons in the benzene ring and pyrrole ring. Multiple peaks observed at 6 to 6.2 ppm were due to the chemical shift of protons in the benzene ring. The protons of the pyrrole ring showed up at the chemical shift of 5.5 ppm. Characteristic peaks associated with PNIPAAm include δ = 1.03 ppm, 1.88 ppm, 2.20 ppm, 3.6 to 3.9 ppm. The peak present at 1 ppm was due to the protons of the methyl groups. The peaks at around 2 ppm were due to the methylene protons, and the peaks at 3.8 ppm were due to the protons of *N*-isopropyl groups. Finally, the chemical shift at 7.2 ppm was assigned to the amide protons. The peak intensity for PNIPAAm was much higher than those peaks for polydopamine, because the corresponding mass of PNIPAAm was much higher than polydopamine.
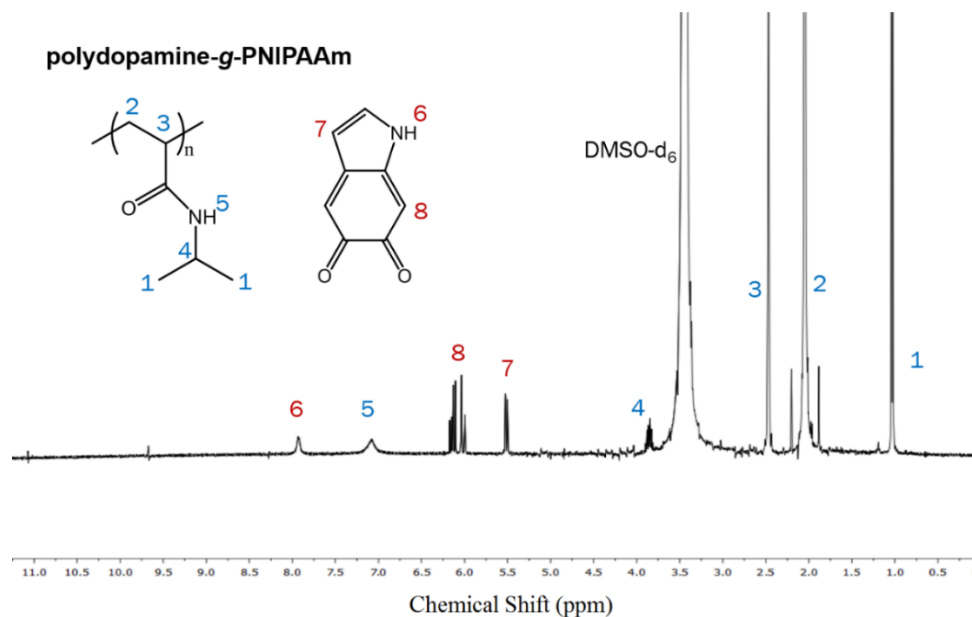
Figure 3.4. NMR spectrum of PNIPAAm-*g*-polydopamine.

3.4.3 Water contact angle and LCST of PNIPAAm-*g*-polydopamine film

The LCST for PNIPAAm-*g*-polydopamine polymer was determined by DSC thermogram. Figure 3.5A shows the enthalpy transition as a function of temperature for the PNIPAAm-*g*-polydopamine polymer film dissolved in 0.1 N NaOH. PNIPAAm-*g*-polydopamine showed an endothermic peak at 30.4°C which is lower than the reported LCST (i.e., 32°C) of PNIPAAm film (Heskins and Guillet 1968). It is speculated that the incorporation of a relatively hydrophobic copolymer to PNIPAAm led to the reduction of the LCST (Doorty et al. 2003, Kim et al. 2005). In fact, the higher the proportion of the copolymer, the lower the LCST (Doorty et al. 2003). Here, copolymerizing PNIPAAm film with polydopamine reduced the LCST from 32 to 30.4°C. The drop of LCST was not significant because the proportion of the polydopamine in the film is relatively small compared to PNIPAAm. Nevertheless, the enthalpy of transition confirmed the deposition of PNIPAAm onto polydopamine film. Moreover, the phase transition behavior of the PNIPAAm-*g*-polydopamine polymer film dissolved in 0.1 N NaOH was monitored by measuring the transmission of visible light at 563 nm, as a function of temperature. As shown in Figure 3.5B, the cloud point temperature was determined to be 30.5°C which is in line with the LCST detected by DSC thermogram.
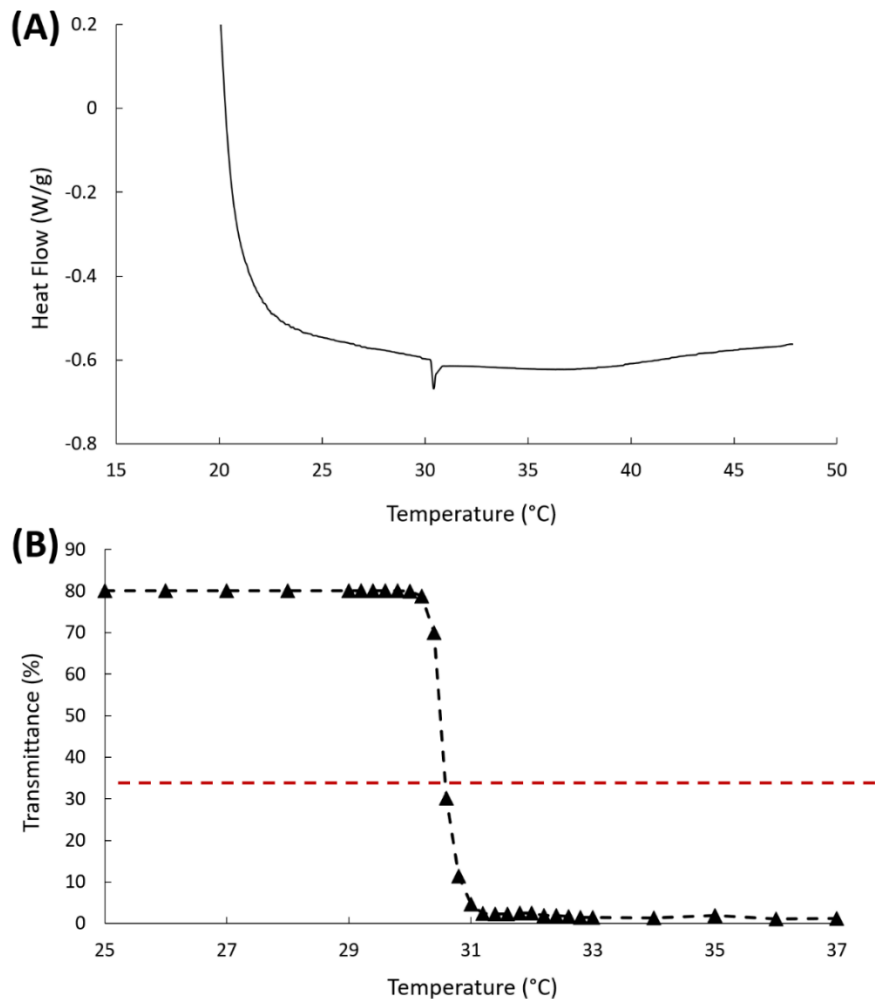
Figure 3.5. (A) DSC thermogram of PNIPAAm-*g*-polydopamine dissolved in 0.1 N NaOH. (B) UV-Vis transmittance at 563 nm of PNIPAAm-*g*-polydopamine film dissolved in 0.1 N NaOH as a function of temperature. The cloud point temperature (i.e., 30.5°C) corresponds to the transmittance which is 50% of the initial value.

In order to characterize the hydrophilicity/hydrophobicity change of the PNIPAAm-*g*-polydopamine surface, water contact angles of bare, polydopamine coated, and PNIPAAm-*g*-polydopamine coated Petri dishes were measured at ambient temperature and 40°C (Figure 3.6). The water contact angle of bare Petri dish at ambient temperature was 70.3°±1.8°. It slightly increased to 71.7°±0.5° when it was heated up to 40°C. The water contact angle of the polydopamine coated Petri dish was 48.9°±2.9° at ambient temperature and 49.8°±3.0° at 40°C. The polydopamine coating makes the Petri dish more hydrophilic, which was consistent with the findings of (Liu, Ai, and Lu 2014). The water contact angle of the produced PNIPAAm-*g*-polydopamine coating at the

ambient temperature was 36.1°±2.7°, indicating the produced PNIPAAm film was even more hydrophilic than the polydopamine film at ambient temperature. When heated up to 40°C, the contact angle on PNIPAAm-*g*-polydopamine coated Petri dish increased to 82.1°±4.2°. The results indicated that when the bare and polydopamine coated Petri dishes were heated up, the surfaces did not exhibit temperature-responsive hydrophobicity according to the measured contact angles. However, the dramatic increase of water contact angle on PNIPAAm-*g*-polydopamine indicated that the surface switched from hydrophilic to hydrophobic when it was heated up over its LCST.
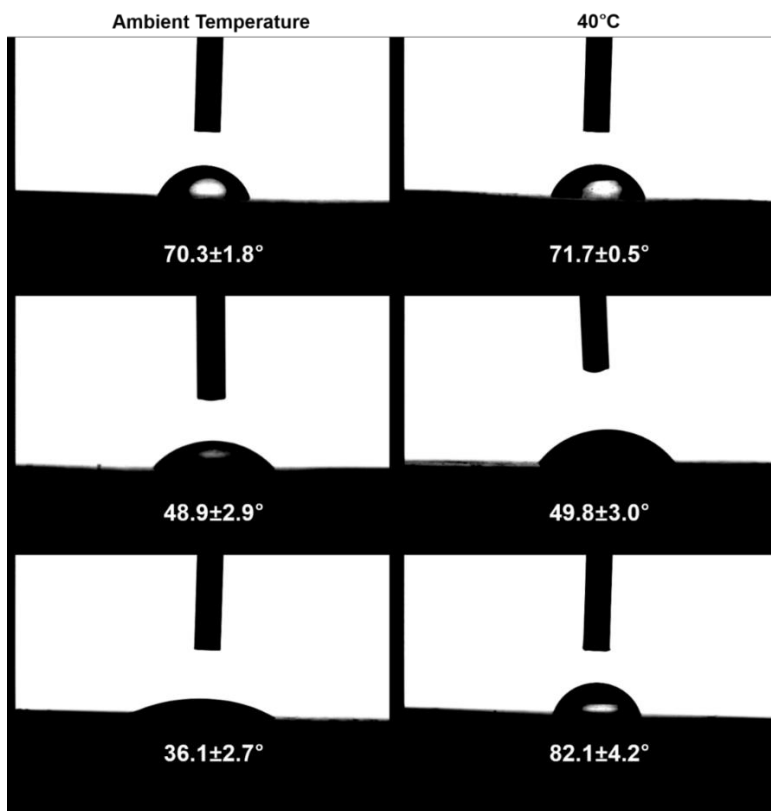
Figure 3.6. Water contact angles of (A) bare, (B) polydopamine coated, and (C) PNIPAAm-*g*-polydopamine coated Petri dish at ambient temperature and 40°C. Water contact angles were expressed as mean ± standard deviation (n=3). $p < 0.05$ is considered to be statistically significant.

3.4.4 Culture and Harvest of MSCs onPNIPAAm-*g*-polydopamine surface

In order to characterize the cell detachment behavior of PNIPAAm-*g*-polydopamine surface, MSCs were cultured onto bare, polydopamine coated, and PNIPAAm-*g*-polydopamine coated Petri dish. For detachment studies, the environment temperature of MSCs was reduced from 37°C to ambient temperature by replacing the

culture medium with 1 mL fresh αMEM. The MSCs grown on all three surfaces were given a mechanical disruption by a gentle pipetting force at 20, 40, and 60 min.

Our results showed that at temperature of 37°C (above the LCST), MSCs were able to attach to all three surfaces. After the treatment of cells with ambient temperature αMEM for 1 h, no significant cell detachment was observed on either bare or polydopamine controls (Figure 3.7A and 3.7B). A very small amount of cell detachment was observed from bare or polydopamine coated Petri dishes (Figure 3.8) 1 h after the temperature switch. As shown in Figure 3.8, only 3.1±0.2% of the cells detached from bare Petri dish, and 4.3±0.3% of the cells detached from the polydopamine coated Petri dish. On the other hand, the PNIPAAm film became expanded and hydrated, and MSCs started to detach from the surface. The MSCs grown on PNIPAAm-*g*-polydopamine surface showed changes in shape, from a stretched, spindle shape toward a circular shape over the span of 60 min (Figure 3.7C). Within 40 min, an average of 44.8±3.5% of the cells detached from the PNIPAAm-*g*-polydopamine surface after the temperature switch. At 60 min, 78.4±5.2% of the cells grown on the PNIPAAm-*g*-polydopamine Petri dish detached from the surface (Figure 3.8). It is noteworthy that cells having smaller size (i.e., human epithelial lung carcinoma A549 cells) rounded up faster than MSCs. According to our results (Figure 3.9), A549 cells started to round up at 20 min, and 90% of the A549 cells detached from the PNIPAAm-*g*-polydopamine surface at 40 min. The percentage of detached MSCs was not 100% probably because the PNIPAAm film was not uniformly deposited on the Petri dish surface (Figure 3.2A). In certain areas, the amount of deposited polymer was probably not enough to lift up all of the MSCs. This issue could be improved by the increment of PNIPAAm deposition with higher concentration of dopamine.
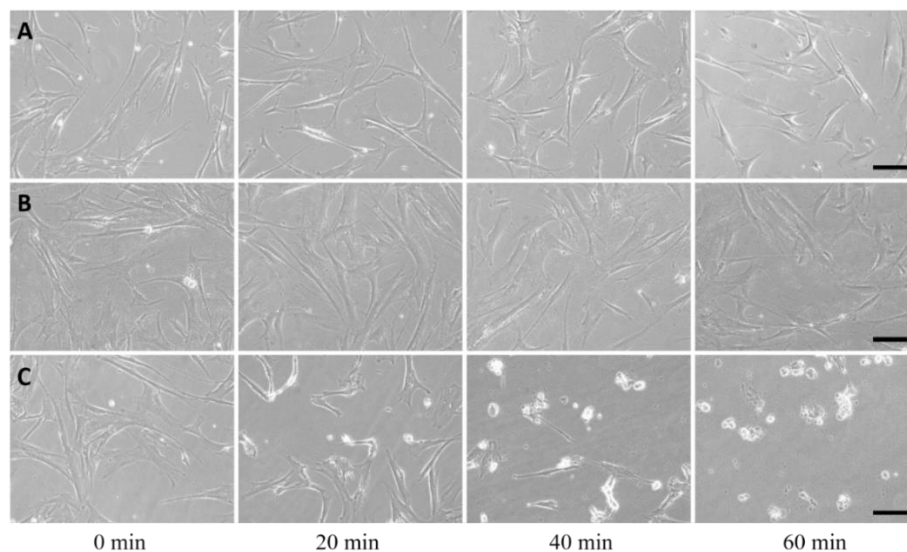
Figure 3.7. Phase contrast microscopic images of MSCs on (A) bare, (B) polydopamine coated, and (C) PNIPAAm-*g*-polydopamine coated Petri dish for 1 day. Then, the cells were taken out into ambient temperature, and phase contrast images were taken at 0, 20, 40, and 60 min, respectively. Scale bar denotes 100 μm.
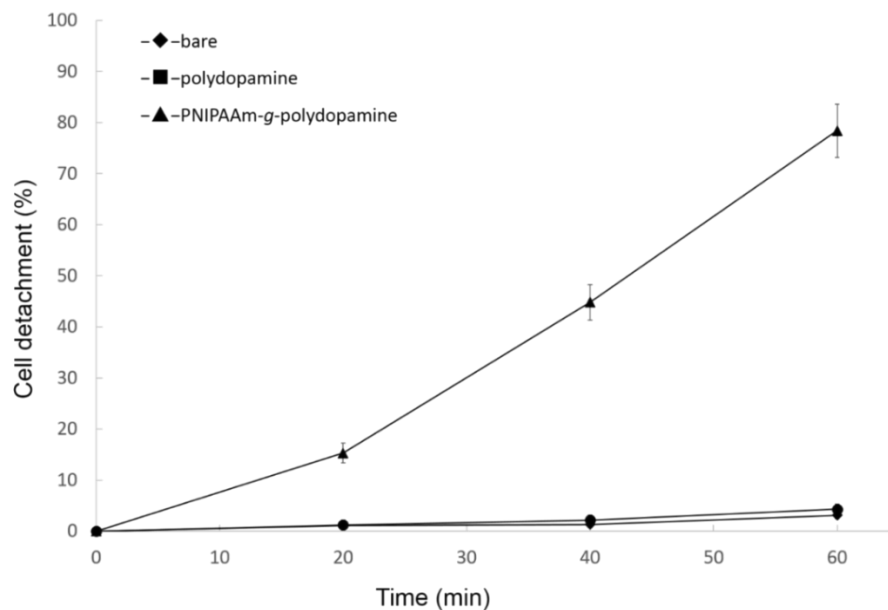
Figure 3.8. Percentage of MSCs detached from bare Petri dish (◆), polydopamine coated Petri dish (■), and PNIPAAm-*g*-polydopamine coated Petri dish (▲) due to the temperature switch. The numbers of detached cells were counted at 20, 40, and 60 min, respectively. Error bars indicate standard deviation (n=3). $p < 0.05$ is considered to be statistically significant.
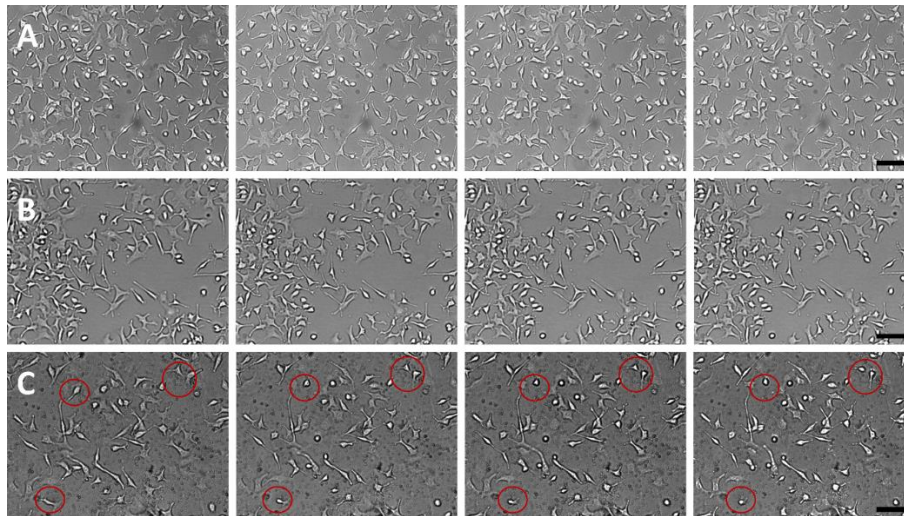
Figure 3.9. A549 cells were cultured on (A) bare, (B) polydopamine coated, and (C) PNIPAAm-*g*-polydopamine coated Petri dish. Then, the cells were taken right out into ambient temperature, and bright-field images were taken at 0, 20, 40, and 60 min, respectively. Circled A549 cells grown on PNIPAAm-*g*-polydopamine surface changed from stretched to rounded shape due to temperature switch. Scale bar denotes 100 μm.

The time for cells to detach from PNIPAAm and its copolymer surfaces typically ranges from 2 min to 2 h (Patel and Zhang 2013). Cell type has a remarkable effect on the detachment time from a PNIPAAm surface (Fukumori et al. 2009, Moran et al. 2007, Canavan et al. 2005). Our results showed that MSCs needed up to 60 min to detach from the PNIPAAm-*g*-polydopamine surface probably because MSCs need a larger force to detach themselves than cells smaller in size such as A549 and NIH 3T3 cells. The 30 min detachment time of A549 cells from PNIPAAm-*g*-polydopamine surface was comparable to the reported 30 min detachment time of retinal pigment epithelial cells from UV polymerized PNIPAAm surface (von Recum et al. 1999). From our results, we have demonstrated that PNIPAAm was successfully synthesized on the surface of Petri dish through polydopamine coating. Human MSCs were able to attach and proliferate onto PNIPAAm-*g*-polydopamine surface, and the cells can be harvested by reducing the temperature below LCST.

The detached MSCs from PNIPAAm-*g*-polydopamine coated Petri dishes were further inoculated on freshly prepared PNIPAAm-*g*-polydopamine coated dishes. The re-plated MSCs were able to attach, spread, and proliferate on PNIPAAm-*g*-polydopamine coated dishes. Figure 3.10 shows their growth kinetics. The plating density of 10^3

cells/cm^2 revealed 51-fold expansion after 12 days. It should be noted that over the course of culturing A549 cells using DMEM medium, the polydopamine film would collapse if the pH of the culture medium turned acidic after several days of culturing (Figure 3.11). This is probably because the pH change due to the production of lactic acid caused the deformation of the polydopamine film. Most cell growth occurs at an environment of neutral pH. The pH drops when lactic acid is produced as the by-products of cellular metabolism. According to our findings, the acidic environment led to the deformation of the polydopamine film, which is consistent with the reported finding (Wei et al. 2013). The deformed PNIPAAm-*g*-polydopamine film would be harvested along with the detached cells as unwanted by-products. Therefore, maintaining the pH of culture medium at a neutral level is of importance for cell harvest from the temperature-responsive surface reported here.
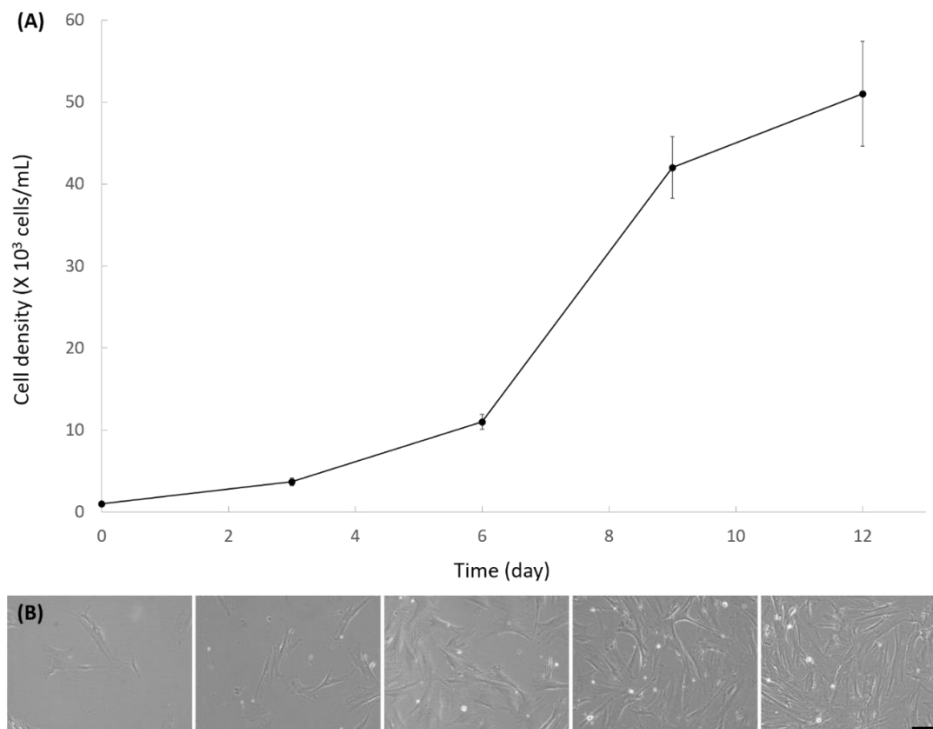
Figure 3.10. (A) Growth kinetics of MSCs detached from PNIPAAm-*g*-polydopamine coated Petri dishes and re-plated on new PNIPAAm-*g*-polydopamine coated Petri dishes. Inoculation density was 103 cells/cm2. Error bars indicate standard deviation (n=3). $p < 0.05$ is considered to be statistically significant. (B) Phase contrast images of MSCs re-seeded on new PNIPAAm-*g*-polydopamine coated Petri dish at day 0, 3, 6, 9, and 12. Scale bar denotes 100 μm.
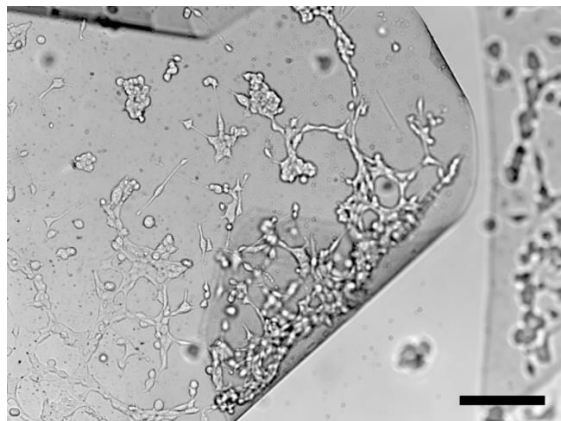
Figure 3.11. A549 cells were cultured on PNIPAAm-*g*-polydopamine coated Petri dish. After several days of culturing, the color of DMEM culture medium turned yellow, and PNIPAAm-*g*-polydopamine film collapsed. Scale bar denotes 100 μm.

3.5 Conclusions

In this study, free radical polymerization is combined with polydopamine chemistry to develop a straightforward and cost-effective way of preparing PNIPAAm surface for temperature-modulated cell harvesting. AFM images showed a layer of PNIPAAm film was grafted onto the allyl functionalized polydopamine coated substrata, with randomly distributed PNIPAAm polymer aggregates on the substrate surface. FTIR and NMR confirmed the formation of PNIPAAm-*g*-polydopamine polymer film on the surface. Water contact angle and DSC thermogram revealed the LCST of the PNIPAAm-*g*-polydopamine film at 30.4°C. After the environmental temperature changed from 37°C to ambient within 60 min, over 80% of cultured MSCs detached from the PNIPAAm-*g*-polydopamine surface. The detached MSCs after re-plating were able to spread and proliferate on newly prepared PNIPAAm-*g*-polydopamine coated dishes. In summary, polydopamine has provided a versatile platform for PNIPAAm grafting, and the fabricated PNIPAAm-*g*-polydopamine film can be used as temperature-responsive surface for cultivation and harvest of human mesenchymal stem cells.

3.6 References

Akiyama, Yoshikatsu, Akihiko Kikuchi, Masayuki Yamato, and Teruo Okano. 2004. "Ultrathin Poly(N-isopropylacrylamide) Grafted Layer on Polystyrene Surfaces for Cell Adhesion Detachment Control." *Langmuir* 20 (13):5506-5511.

Canavan, H. E., X. Cheng, D. J. Graham, B. D. Ratner, and D. G. Castner. 2005. "Cell sheet detachment affects the extracellular matrix: a surface science study comparing thermal liftoff, enzymatic, and mechanical methods." *J Biomed Mater Res A* 75 (1):1-13.

Caplan, A. I. 2007. "Adult mesenchymal stem cells for tissue engineering versus regenerative medicine." *J Cell Physiol* 213 (2):341-7.

Cho, J. H., S. H. Kim, K. D. Park, M. C. Jung, W. I. Yang, S. W. Han, J. Y. Noh, and J. W. Lee. 2004. "Chondrogenic differentiation of human mesenchymal stem cells using a thermosensitive poly(N-isopropylacrylamide) and water-soluble chitosan copolymer." *Biomaterials* 25 (26):5743-51.

Cui, J., Y. Yan, G. K. Such, K. Liang, C. J. Ochs, A. Postma, and F. Caruso. 2012. "Immobilization and intracellular delivery of an anticancer drug using mussel-inspired polydopamine capsules." *Biomacromolecules* 13 (8):2225-8.

Dalsin, Jeffrey L., and Phillip B. Messersmith. 2005. "Bioinspired antifouling polymers." *Materials Today* 8 (9):38-46.

Doorty, K. B., T. A. Golubeva, A. V. Gorelov, Y. A. Rochev, L. T. Allen, K. A. Dawson, W. M. Gallagher, and A. K. Keenan. 2003. "Poly(N-isopropylacrylamide) co-polymer films as potential vehicles for delivery of an antimitotic agent to vascular smooth muscle cells." *Cardiovasc Pathol* 12 (2):105-10.

Dreyer, D. R., D. J. Miller, B. D. Freeman, D. R. Paul, and C. W. Bielawski. 2012. "Elucidating the structure of poly(dopamine)." *Langmuir* 28 (15):6428-35.

Fukumori, K., Y. Akiyama, M. Yamato, J. Kobayashi, K. Sakai, and T. Okano. 2009. "Temperature-responsive glass coverslips with an ultrathin poly(N-isopropylacrylamide) layer." *Acta Biomater* 5 (1):470-6.

Heskins, M, and J. E Guillet. 1968. "Solution properties of poly(N-isopropylamide)." *J. E. Macromol. Sci. Chem. A* 2 (8):1441-1455.

Jain, Kamiya, Raman Vedarajan, Masaki Watanabe, Mamoru Ishikiriyama, and Noriyoshi Matsumi. 2015. "Tunable LCST behavior of poly(N-isopropylacrylamide/ionic liquid) copolymers." *Polymer Chemistry* 6 (38):6819-6825.

Jiang, J., L. Zhu, L. Zhu, B. Zhu, and Y. Xu. 2011. "Surface characteristics of a self-polymerized dopamine coating deposited on hydrophobic polymer films." *Langmuir* 27 (23):14180-7.

Kim, S., E. H. Chung, M. Gilbert, and K. E. Healy. 2005. "Synthetic MMP-13 degradable ECMs based on poly(N-isopropylacrylamide-co-acrylic acid) semi-interpenetrating polymer networks. I. Degradation and cell migration." *J Biomed Mater Res A* 75 (1):73-88.

Kim, So Yeon, Toshiyuki Kanamori, and Toshio Shinbo. 2002. "Preparation of thermal-responsive poly(propylene) membranes grafted withn-isopropylacrylamide by plasma-induced polymerization and their water permeation." *J Appl Polym Sci* 84 (6):1168-1177.

Lee, H., S. M. Dellatore, W. M. Miller, and P. B. Messersmith. 2007. "Mussel-inspired surface chemistry for multifunctional coatings." *Science* 318 (5849):426-30.

Lee, H., J. Rho, and P. B. Messersmith. 2009. "Facile Conjugation of Biomolecules onto Surfaces via Mussel Adhesive Protein Inspired Coatings." *Adv Mater* 21 (4):431-434.

Li, D., X. Zhang, J. Yao, G. P. Simon, and H. Wang. 2011. "Stimuli-responsive polymer hydrogels as a new class of draw agent for forward osmosis desalination." *Chem Commun (Camb)* 47 (6):1710-2.

Liu, Yanlan, Kelong Ai, and Lehui Lu. 2014. "Polydopamine and Its Derivative Materials: Synthesis and Promising Applications in Energy, Environmental, and Biomedical Fields." *Chemical Reviews* 114 (9):5057-5115.

Ma, Z., X. Jia, J. Hu, Z. Liu, H. Wang, and F. Zhou. 2013. "Mussel-inspired thermosensitive polydopamine-graft-poly(N-isopropylacrylamide) coating for controlled-release fertilizer." *J Agric Food Chem* 61 (50):12232-7.

Marion, N. W., and J. J. Mao. 2006. "Mesenchymal stem cells and tissue engineering." *Methods Enzymol* 420:339-61.

Moran, M. T., W. M. Carroll, I. Selezneva, A. Gorelov, and Y. Rochev. 2007. "Cell growth and detachment from protein-coated PNIPAAm-based copolymers." *J Biomed Mater Res A* 81 (4):870-6.

Nagase, K., J. Kobayashi, and T. Okano. 2009. "Temperature-responsive intelligent interfaces for biomolecular separation and cell sheet engineering." *J R Soc Interface* 6 Suppl 3:S293-309.

Nakayama, Masamichi, Teruo Okano, and Françoise M. Winnik. 2010. "Poly(N-isopropylacrylamide)-based Smart Surfaces for Cell Sheet Tissue Engineering." *Material Matters* 5 (3):56.

Patel, N. G., J. P. Cavicchia, G. Zhang, and B. M. Zhang Newby. 2012. "Rapid cell sheet detachment using spin-coated pNIPAAm films retained on surfaces by an aminopropyltriethoxysilane network." *Acta Biomater* 8 (7):2559-67.

Patel, N. G., and G. Zhang. 2013. "Responsive systems for cell sheet detachment." *Organogenesis* 9 (2):93-100.

Recum, H.A., S. W. Kim, A. Kikuchi, M. Okuhara, Y. Sakurai, and T. Okano. 1997. "Novel thermally reversible hydrogel as detachable cell culture substrate." *J Biomed Mater Res* 40 (4):631-639.

Rivera, J. G., and P. B. Messersmith. 2012. "Polydopamine-assisted immobilization of trypsin onto monolithic structures for protein digestion." *J Sep Sci* 35 (12):1514-20.

Shah, K. 2012. "Mesenchymal stem cells engineered for cancer therapy." *Adv. Drug Deliv. Rev.* 64 (8):739-48.

Shi, D., D. Ma, F. Dong, C. Zong, L. Liu, D. Shen, W. Yuan, X. Tong, H. Chen, and J. Wang. 2010. "Proliferation and multi-differentiation potentials of human mesenchymal stem cells on thermoresponsive PDMS surfaces grafted with PNIPAAm." *Biosci Rep* 30 (3):149-58.

Sun, B., Lin Y., and P. Wu. 2007. "Structure Analysis of Poly(N-isopropylacrylamide) Using Near- Infrared Spectroscopy and Generalized Two-Dimensional Correlation Infrared Spectroscopy." *Appl Spectrosc* 61 (7):765-71.

von Recum, H. A., T. Okano, S. W. Kim, and P. S. Bernstein. 1999. "Maintenance of retinoid metabolism in human retinal pigment epithelium cell culture." *Exp Eye Res* 69 (1):97-107.

Wei, H., J. Ren, B. Han, L. Xu, L. Han, and L. Jia. 2013. "Stability of polydopamine and poly(DOPA) melanin-like films on the surface of polymer membranes under strongly acidic and alkaline conditions." *Colloids Surf B Biointerfaces* 110:22-8.

Wei, Qingshan, Jian Ji, and Jiacong Shen. 2008. "Synthesis of Near-Infrared Responsive Gold Nanorod/PNIPAAm Core/Shell Nanohybrids via Surface Initiated ATRP for Smart Drug Delivery." *Macromolecular Rapid Communications* 29 (8):645-650.

Xu, F. J., S. P. Zhong, L. Y. Yung, Y. W. Tong, E. T. Kang, and K. G. Neoh. 2006. "Thermoresponsive comb-shaped copolymer-Si(100) hybrids for accelerated temperature-dependent cell detachment." *Biomaterials* 27 (8):1236-45.

Yamada, Noriko; , Teruo; Okano, Hideaki; Sakai, Fumiko; Karikusa, Yoshio; Sawasaki, and Yasuhisa. Sakurai. 1990. "Thermo-responsive polymeric surfaces; control of attachment and detachment of cultured cells." *Makromol. Chem., Rapid Commun.* 11 (11):571-576.

Yang, Juan, Martien A. Cohen Stuart, and Marleen Kamperman. 2014. "Jack of all trades: versatile catechol crosslinking mechanisms." *Chemical Society Reviews* 43 (24):8271-8298.

Yang, L., F. Cheng, T. Liu, J. R. Lu, K. Song, L. Jiang, S. Wu, and W. Guo. 2012. "Comparison of mesenchymal stem cells released from poly(N-isopropylacrylamide) copolymer film and by trypsinization." *Biomed Mater* 7 (3):035003.

Zangmeister, R. A., T. A. Morris, and M. J. Tarlov. 2013. "Characterization of polydopamine thin films deposited at short times by autoxidation of dopamine." *Langmuir* 29 (27):8619-28.

Zhang, Yan, Karthiga Panneerselvam, Ryosuke Ogaki, Leticia Hosta-Rigau, Rebecca van der Westen, Bettina E. B. Jensen, Boon M. Teo, Meifang Zhu, and Brigitte Städler. 2013. "Assembly of Poly(dopamine)/Poly(N-isopropylacrylamide) Mixed Films and Their Temperature-Dependent Interaction with Proteins, Liposomes, and Cells." *Langmuir* 29 (32):10213-10222.

Chapter 4. Migration of Mesenchymal Stem Cells Tethered with Carbon Nanotubes under a Chemotactic Gradient

"Migration of mesenchymal stem cells tethered with carbon nanotubes under a chemotactic gradient." *RSC Adv*, vol. 9, issue 13, 2019, pp. 7156-7164.

4.1 Abstract

Carbon nanotubes (CNTs) have been extensively studied for photothermal ablation of malignant cells due to their ability of absorbing near-infrared (NIR) laser light and converting it to thermal energy for the lysis of tumor cells. Functionalizing CNTs with tumor-targeting moieties can facilitate the delivery to tumor sites. Instead of using targeting moieties, mesenchymal stem cells (MSCs) have been considered as vehicles to deliver therapeutic agents to cancer cells. In this study, the effects of attaching CNTs to MSCs on cell migration in response to the chemotactic gradient were investigated. Multiwalled carbon nanotubes (MWCNTs) were functionalized with streptavidin-FITC (SA-FITC). The surface of human MSCs was biotinylated by culturing MSCs with biotin-lipid containing medium. CNTs were then attached on the outer cell membrane of biotinylated MSCs through SA-biotin binding. Fluorescence microscopy confirmed CNTs were located on the surface of MSCs. Various amounts of CNTs anchored on the membrane of MSCs were used to examine the effects of CNTs on MSC proliferation and migration. Our transwell migration assay showed that 4.26 ng CNT per cell is the threshold value that would not affect the migration speed of CNT-tagged MSCs toward the established gradient of chemoattractant SDF-1α.

4.2 Introduction

Carbon nanotubes (CNTs) have been well studied in cancer therapy and drug delivery due to their unique structures and properties such as high aspect ratio, large surface area, mechanical strength and thermal conductivity (Iijima 1991, Elhissi et al. 2012). In the field of cancer nanotechnology, CNTs have been demonstrated to be one of the potential photothermal absorbers for the ablation of malignant cells under near

infrared (NIR) laser exposure (Wang et al. 2011, Gannon et al. 2007, Zhou et al. 2009, Kam et al. 2005). In photothermal therapy, an engineered substance such as CNT absorbs NIR light and then converts it to thermal energy near tumor sites. The strong absorbance of CNTs in NIR region enables the optical stimulation of CNTs and the transmission of external heat inside body (Kam et al. 2005). Compared to traditional radio-chemotherapy, photothermal therapy has the advantage of low toxicity to body and less injuries to non-malignant cells and tissues (Peer et al. 2007, Son, Hong, and Lee 2016).

Due to their tendency to aggregate in aqueous solvents, CNTs have been chemically modified to enhance their aqueous solubility. For example, CNTs have been treated with strong acids to shorten the length and endow with carboxyl groups to increase their suspension in water (Liu et al. 1998, Saito, Matsushige, and Tanaka 2002). Amino acids and peptides have been used for enhanced CNT's aqueous solubility and biocompatibility (Bianco et al. 2005). CNTs have also been functionalized with poly(ethylene glycol) (Liu et al. 2008) and hyaluronic acid (Shi et al. 2013) for increased solubility and prolonged circulation time. In addition, functionalization of CNTs could enhance targeted delivery capabilities. For example, CNTs have been tethered with folic acid to target HeLa cells for the release of doxorubicin (Zhang et al. 2009). Magnetic nanoparticles incorporated CNTs were fabricated for cancer diagnosis and drug delivery (Wu et al. 2011, Peci, Dennis, and Baxendale 2015). CNTs have also been conjugated with monoclonal antibody CD133 for targeted delivery of CNTs to CD133$^+$ stem-like glioblastoma cells (Wang et al. 2011). However, efficient delivery of nanoparticles to tumor sites remains challenging such as ingesting by the reticuloendothelial system and eliciting inflammatory response. To circumvent the antecedent issues, mesenchymal stem cells (MSCs), due to their low immunogenicity and intrinsic tumor-tropism, have been considered as vehicles to deliver therapeutic agents to cancer cells (Lee et al. 2014, Kidd et al. 2009).

Mesenchymal stem cells (MSCs) are stromal cells which can be isolated from bone marrow and adipose tissue (Friedenstein et al. 1974). Their multipotency to differentiate into several mesenchymal lineages has great promise for regenerative medicine (Park et al. 2015) and their tumor homing capacity has initiated interest in using MSCs as cell carriers for cancer therapy (Kucerova et al. 2013, Roger et al. 2010). Using

MSCs as tumor-targeted delivery vehicles is associated with less risks for clinical complications (Santos et al. 2011). The migration of MSCs is mediated by homing factor and receptor pairs such as SDF-1/CXCR4, HGF/c-Met and VEGF/VEGFR (Park et al. 2017, Shah 2012), among which SDF1/CXCR4 plays the most critical role in migration and homing of MSCs (Moll and Ransohoff 2010, Myers et al. 2010). Recently, avidin attached nanodrug has been incorporated in MSCs by endocytosis as well as cell membrane anchoring (Yao et al. 2017). In that study, MSCs were first chemically modified with avidin, then treated with biotinylated DOX conjugates. The stemness and migration ability of nanodrug-loaded MSCs were both retained. Kang et al. used pH-sensitive gold nanoparticles (AuNPs) internalized MSCs in photothermal therapy for enhanced tumor-targeting efficiency (Kang et al. 2015). The use of MSC significantly increased tumor-targeting efficiency as well as local hyperthermia.

In the current study, CNTs were anchored on the outer membrane of human MSCs as a potential cancer photothermal therapy system. The surface of MSCs was first biotinylated by biotin-lipid treatment, and then MSCs were tethered with streptavidin (SA)-conjugated CNTs. Due to the rapid binding of biotin and SA, the anchorage of CNTs on the surface of MSCs occurred within 1 h in order to minimize the concern of particle internalization. A variety of weights of CNTs hitchhiking on MSC surface were harnessed to evaluate the effects of CNTs on MSC motility and proliferation. According to the transwell migration assay, 4.26 ng CNTs per cell is the threshold amount that would not affect the migration speed of CNT-tethered MSCs toward the established concentration gradient of chemoattractant SDF-1α. The growth kinetics of re-seeded CNT-tethered MSCs showed no cytotoxicity of CNTs treated MSCs.

4.3 Materials and Methods

4.3.1 Materials

Multiwalled carbon nanotube (MWCNT) was obtained from CNT Co., LTD (Incheon, Korea). Hydrogen peroxide (30%) and acetic acid were purchased from J.T. Baker (Philipsburg, NJ, USA). Succinic anhydride was purchased from Acros Organics (New Jersey, USA). Streptavidin-FITC (SA-FITC) was purchased from Invitrogen (Frederick, MD, USA). 1-ethyl-3-(3-dimethylaminopropyl) carbodiimide (EDC) and

collagen (bovine achilles tendon, Type I) were purchased from Sigma-Aldrich (St. Louis, MO, USA). N-hydroxysuccinimide (NHS) and paraformaldehyde were purchased from Alfa Aesar (Haverhill, MA, USA). Human bone marrow-derived mesenchymal stem cells were purchased from RoosterBio (Frederick, MD, USA). Minimum essential medium, alpha (αMEM), L-glutamine, 0.25% trypsin/EDTA, and methanol were purchased from Fisher Scientific (Waltham, MA, USA). Fetal bovine serum (FBS) was purchased from Gibco (Grand Island, NY, USA). 1,2-dipalmitoyl-sn-glycero-3-phosphoethanolamine-N-cap biotinyl (biotin-lipid) was purchased from Avanti (Alabaster, AL, USA). Trypan blue was purchased from BTC Beantown chemical (Hudson, NH, USA). 8-μm transwell inserts for 24-well plates were purchased from Corning Inc. (Kennebunk, ME, USA). SDF-1α was purchased from Tonbo Biosciences (San Diego, CA, USA). Hematoxylin was purchased from VWR (Radnor, PA, USA).

4.3.2 Cutting and functionalization of the MWCNTs

As schematically illustrated in Figure 4.1A, a series of chemical reactions were performed to conjugate SA-FITC with CNT. First, based on previously reported protocols (Weydemeyer, Sawdon, and Peng 2015) to produce CNT-OH from pristine CNTs, Briefly, 10 mg of CNTs were dissolved in 10 mL hydrogen peroxide (30%). The solution was autoclaved at 15 psi and 121°C for 3 h. The solution underwent sonication at 4 Watts for 4 h in an ice bath using a tip sonicator (Misonix XL-2000, Farmingdale, NY). Hydroxyl functionalized CNTs were collected by centrifugation. Secondly, the collected CNT-OH was re-dissolved in 50 mL of tetrahydrofuran (THF) in a 3-neck round bottom flask. 50 mg of succinic anhydride was added to the flask, and the solution was refluxed at 85°C under agitation for 48 h to form carboxylated CNTs. The CNT-COOH was collected by centrifugation, and then washed three times with deionized (DI) water. The CNT-COOH product was re-suspended in 10 mL of DI water for further treatment. Finally, 10 mg of EDC and 10 mg of NHS were added to the CNT-COOH solution. The solution was stirred with a magnetic stir bar for 2 h at room temperature. 50 μL of SA-FITC solution was added to the reaction mixture, and mixture was stirred at 4°C for overnight to obtain CNT-SA-FITC. The CNT-SA-FITC was collected by centrifugation at 10,000 $\times$ g for 10 min, and then washed three times with DI water to remove excess SA-

FITC. The washed CNT-SA-FITC was re-suspended in cell culture medium (see section below). The chemical analyses of pristine CNTs, CNT-COOH and CNT-SA-FITC were characterized by Fourier transform infrared spectroscopy (FT-IR). The FT-IR spectra were recorded by a Nicolet iS10 FT-IR Spectrometer (ThermoFisher Scientific, Waltham, MA, USA).
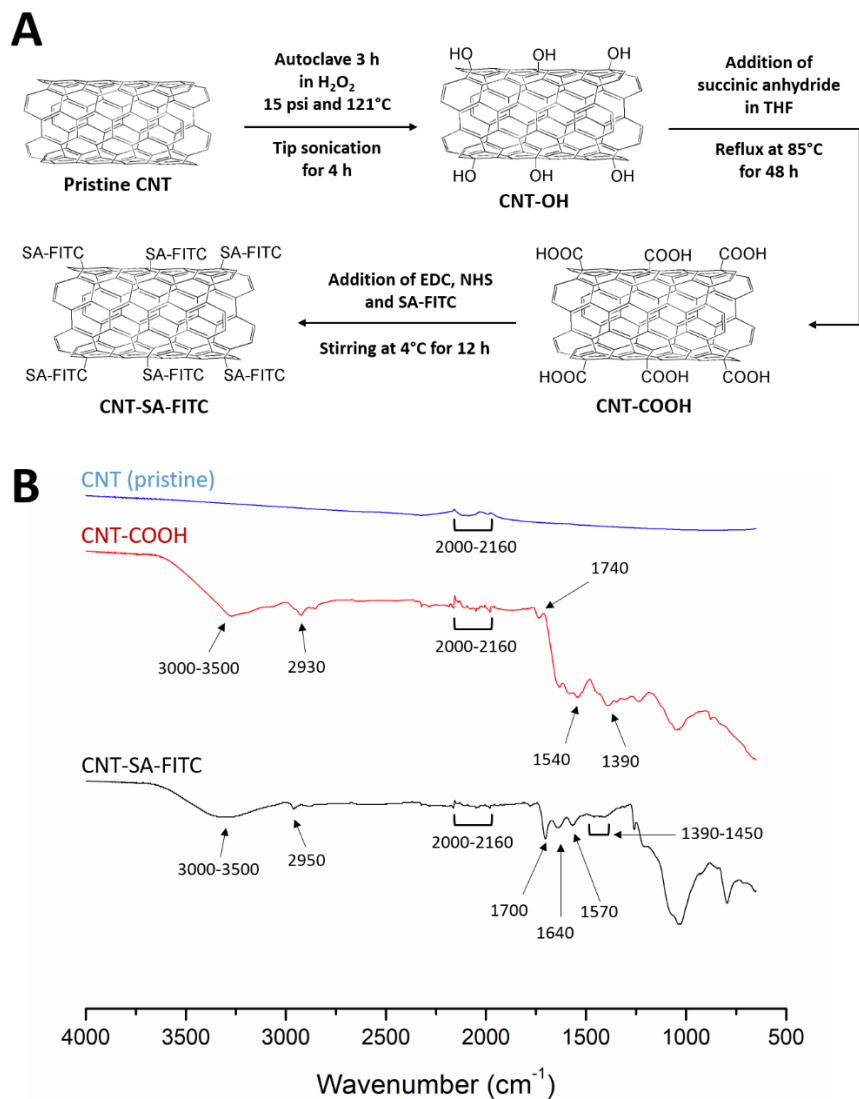
Figure 4.1. (A) A schematic diagram of a series of chemical reactions to produce the final product CNT-SA-FITC from pristine CNT. (B) FT-IR spectra of pristine CNTs, COOH-functionalized CNTs and SA-FITC-functionalized CNTs.

4.3.3 Surface biotinylation of MSCs

Human MSCs were cultivated at 37°C in 5% CO_2 balanced with humidified air. The MSCs were cultured with αMEM supplemented with 16.5% FBS, 1% penicillin-streptomycin and 2 mM L-glutamine. MSCs were incubated in culture medium containing 0.01 and 0.02 mg/mL biotin-lipid for different timings of up to 60 h in 24-well plates. Following biotinylating, MSCs were washed with 1x phosphate buffered saline (PBS). Biotinylated MSCs were treated with SA-FITC for 1 h for SA-biotin binding. After 1 h, unbound SA-FITC was discarded and each well was washed with 1× PBS for 3 times. The fluorescence intensity of MSCs at 525 nm emission with 485 nm excitation was measured by a SpectraMax M2e Microplate Reader (Molecular Devices, Sunnyvale, CA) to obtain a biotinylation standard curve. The MSC biotinylation standard curve was constructed by plotting fluorescence intensity versus time.

4.3.4 Preparation and characterization of CNT-tagged MSCs

To estimate the weight of CNTs attached on the surface of MSCs, MSCs cultured in T-25 flasks were treated with 0.01 mg/mL biotin-lipid for different timings up to 48 h. Non-treated MSCs were used as control. Each biotinylated MSC well was then treated with culture medium containing 20 μg/mL CNT-SA-FITC for 1 h. After 1 h, the culture medium was discarded, and the CNT-MSCs were washed three times with 1× PBS. Phase contrast and fluorescence images of CNT-MSCs were taken with Leica DMi8 microscope equipped with Leica EC3 camera (Leica Microsystems, Wetzlar, Germany). To assess the degree of anchored CNTs internalized by MSCs, FITC-CNT-MSCs were imaged at right after tethering CNT-SA-FITC on biotinylated MSC surface. The cultures were maintained for additional 12 and 24 h and then quenched by 0.01 mg/ml trypan blue, respectively. Phase contrast and fluorescence images were taken accordingly.

A variety of weights of CNTs anchored on MSCs were determined by the following approach. MSCs and CNT-MSCs were suspended by treating the cells with 0.25% trypsin/EDTA, and the cell numbers were counted using a hemocytometer. The cells were collected by centrifugation at 400 x g for 8 min. The pellet was washed with 1× PBS, and the cells were centrifuged again to collect cell pellets. The cell pellets were taken up by a pipettor and transferred to a microbalance (XS3DU, Mettler Toledo,

Columbus, OH). The weight of control MSCs and CNT-MSCs was divided by the cell number to obtain an estimated weight of MSCs and CNT-MSCs. The weight of CNTs on MSCs was estimated by subtracting the weight of control MSCs from CNT-MSCs. All of the experiments were performed in triplicate.

After CNT-SA-FITC attached to the MSC surface, the excess CNTs were washed away, and cells were suspended by treating the cells with 0.25% trypsin/EDTA. The MSCs were re-seeded on 24-well plates at the seeding density of 3,000 cells/cm^2. The cells were allowed to grow for 8 days, and the cell numbers were counted every 2 days using a hemocytometer. Phase contrast images were taken with a Leica DMi8 microscope equipped with Leica EC3 camera (Leica Microsystems, Wetzlar, Germany).

4.3.5 Migration of CNT-MSCs

The migration capacity of CNT-MSCs was assessed using transwell plates with 8-μm pore size inserts (Corning Incorporated, Corning, NY). The transwell inserts were immersed in 10 μg/mL collagen solution at 4°C for 6 to 8 h. The inserts were then rinsed with 1× PBS. 2 x 10^5 CNT-MSCs were suspended in 200 μL serum-free αMEM and added to the top chamber of each transwell inserts. The lower chamber was loaded with 600 μL αMEM containing 10% FBS and 200 ng/mL chemoattractant SDF-1α. CNT-MSCs were allowed to migrate for 24 h at 37°C in a 5% CO_2-balanced and humid culture chamber. The CNT-MSCs that migrated to the bottom of the insert were fixed with 4% paraformaldehyde at room temperature for 15 min. The cells were then stained with hematoxylin at room temperature for 20 min. Cells in the top chamber were removed with a cotton swab. Cells in lower chamber were counted manually by phase contrast microscopy.

4.4 Results and Discussion

4.4.1 FT-IR of Functionalized MWCNTs

Figure 4.1B shows the FT-IR spectra of pristine CNTs, CNT-COOH, and CNT-SA-FITC. The FT-IR spectra of both pristine CNTs and functionalized CNTs exhibited bending vibrations from 2000 to 2160 cm^{-1}. This bending vibration was due to the C=C of the cyclic carbons in the CNTs. In the spectrum of COOH-functionalized CNTs, the

broad peak from 3000 to 3500 cm^{-1} was due to O-H stretching from the carboxyl group. The peak at 2930 cm^{-1} was from C-H stretching of the carboxyl group. The peak at 1740 cm^{-1} was due to the carboxylic C=O stretching. The peak at 1540 cm^{-1} was probably due to C=C stretching of the CNTs. The C-O stretching was observed at 1390 cm^{-1}. These peaks confirmed the functionalization of COOH on CNTs. In the spectrum of CNTs functionalized with SA-FITC, the peaks at 1700 and 1570 cm^{-1} were related to the stretching vibration of C=O and bending vibration of N-H caused by the formation of amide linkage via the EDC crosslinking of amines of SA with COOH of CNT. The peak at 1640 cm^{-1} was due to the unreacted amines on SA showing N-H bending vibration. It should be noted that the characteristic peaks of FITC were not clearly observed because they were merged with peaks of CNT and SA. For example, the N=C=S peak at 2100-2150 cm^{-1}, O-H peak at 3000-3500 cm^{-1}, and aromatic keto group around 1715 cm^{-1}. However, the weak peaks at 1390-1450 cm^{-1} associated with the stretching vibration of the FITC aromatic ring were observed. Through the FT-IR analysis, the functionalization of SA-FITC on CNTs is confirmed.

4.4.2 Surface biotinylation of MSCs

Instead of using conjugating chemicals (e.g., Sulfo-NHS-LC-biotin) to biotinylated MSCs, an alternative mild approach was employed by having MSCs pre-fed with biotinylated lipid. MSCs were treated with culture medium containing 0.01 and 0.02 mg/mL biotin-lipid followed by SA-FITC treatment. It has been reported using 0.02 mg/mL biotin-lipid containing culture medium to biotinylate the surface of Vero cells (Huang et al. 2012). In that study, biotinylated Vero cells were able to proliferate without obvious cell toxicity. However, in the present study, treating human MSCs with 0.02 mg/mL biotin-lipid followed by SA-FITC caused an uneven distribution of SA-FITC on MSC cell surfaces as well as some cell morphology change (Figure 4.2A). This is probably because MSCs are more sensitive to biotin-lipid than Vero cells and high concentration of biotin-lipid lead to uneven distribution of biotin on MSC surface. Decreasing the concentration of biotin-lipid to 0.01 mg/mL resulted in a more uniform distribution of biotin on the cell surfaces (Figure 4.2B). In any case, 0.01 mg/mL biotin-lipid was chosen to biotinylate the surface of MSCs. Figure 4.3C shows the MSC

biotinylation standard curve where fluorescence intensity was plotted against time. From 0 to 24 h, the fluorescent intensity showed an initial burst increase, and the intensity then slowly increased from 24 to 60 h.
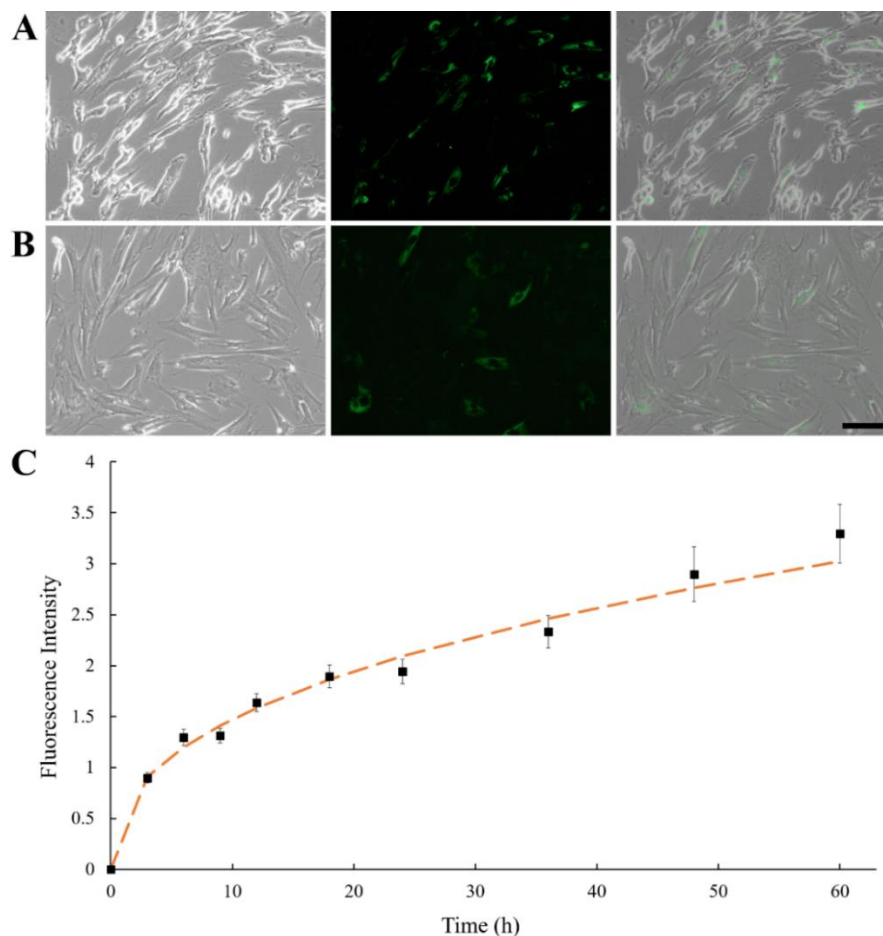
Figure 4.2. Phase contrast, fluorescence and overlay images of human MSCs treated with (A) 0.02 mg/mL biotin-lipid and (B) 0.01 mg/mL biotin-lipid for 48 h, followed by SA-FITC treatment. Scale bar denotes 100 μm. (C) MSCs were treated with 0.01 mg/mL biotin-lipid for different time, up to 60 h. MSCs were treated with SA-FITC, and fluorescence intensity was plotted against time. Error bars indicate standard deviation (n = 3).

4.4.3 Verification of CNT-Loaded MSCs

In Figure 4.3A, fluorescence microscopy confirmed that CNTs were attached to MSCs. In order to minimize cytotoxicity and cellular interference (e.g., migration and proliferation), keeping CNTs external to MSCs could be a better option than being internalized. However, nanoparticles are prone to be endocytosed when located in the vicinity of cell membrane, hence CNTs might not anchor long enough on the surface of

MSCs. To test whether CNTs were internalized by MSCs, fluorescence on CNT-MSCs were quenched by treating the cells with trypan blue solution. In Figure 4.3B, fully quenching of FITC fluorescence indicated the CNTs were indeed located on the surfaces of the MSCs via the strong affinity of biotin-SA. The cells were imaged 12 and 24 h respectively after CNT anchored on MSC surface. As shown in Figure 4.3C and 4.3D, the fluorescence intensity observed was extremely low indicating just a few of CNTs were internalized by MSCs and majority of CNTs remained tethered on the outer membrane of MSCs, and therefore their labeled FITC fluorescence was quenched by trypan blue. According to published accounts, internalization of CNTs depends on various factors such as size, aspect ratio and concentration of CNTs (Maruyama et al. 2015). Since a substantial amount of CNTs were still anchored on the outer cell membrane over 24 h (the time of used for the transwell migration study), it is conjectured that the reduced endocytosis of CNTs into MSCs was due to their large aspect ratios compared to spherical nanoparticles. Moreover, Chen et al. prepared glycopolymer-coated CNTs and anchored CNTs to Chinese hamster ovary cell surface via crosslinking agent *Helix pomatia* agglutinin (HPA) (Chen et al. 2006). They found that at low CNT concentration in the bulk solution, CNTs efficiently bound cell surface; however, when the bulk concentration was high, cellular internalization of CNTs were observed. In the current study, few CNTs on cell surface were internalized by MSCs probably because the concentration of CNTs on cell surface was low.

Yao et al. have used Sulfo-NHS-LC-biotin to chemically conjugate the surface of MSCs, and then treated MSCs with an avidin solution (Yao et al. 2017). The avidinylated MSCs were then treated with biotinylated DOX conjugates, and nanodrugs were observed on both cell surface and cytoplasm. In this study, the approach is through the incorporation of biotin-lipid into lipid membrane of MSCs which is much mild than the chemical conjugation method via N-hydroxysuccimide. Moreover, the steps involved in anchoring nanomaterials are much less than the ones reported by (Yao et al. 2017).
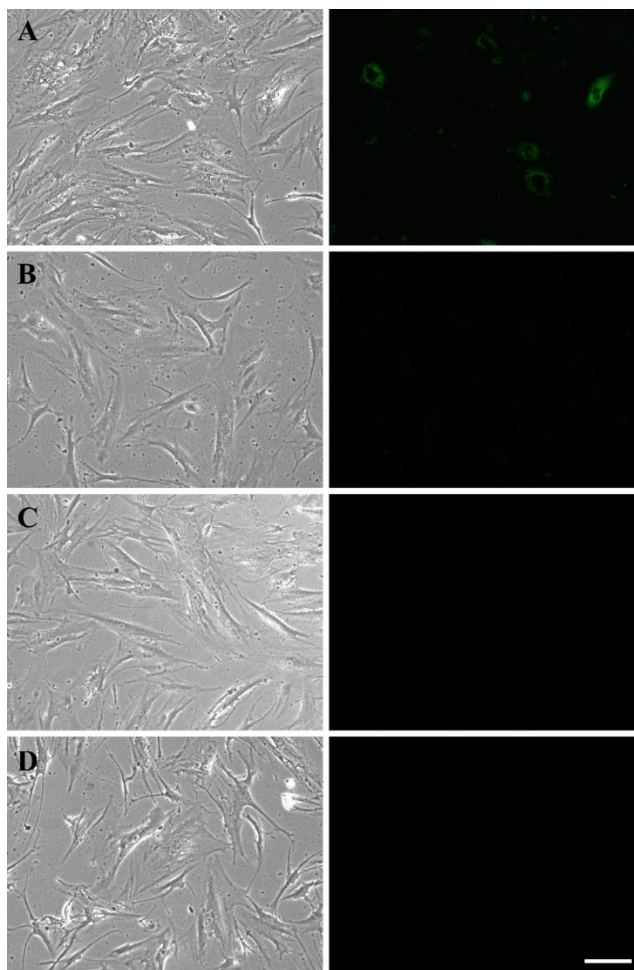
Figure 4.3. MSCs were biotinylated by treating cells with 0.01 mg/mL biotin-lipid for 48 h. Biotinylated MSCs were then treated with CNT-SA-FITC for 1 h. Cells were washed with 1× PBS for 3 times. (A) Phase contrast (left) and fluorescent (right) images were taken after washing with PBS. (B-D) After anchoring of CNTs on MSCs, fluorescence was quenched by treating cells with 0.01 mg/mL trypan blue at different timing (0, 12 and 24 h). Scale bar denotes 100 μm.

Cytotoxicity is one of the major concerns when nanoparticles such as AuNPs or CNTs were internalized by MSCs for 24 h or longer (Ahmadi et al. 2017, Lara-Martínez et al. 2017). A previous study showed that culture medium containing over 32 μg/mL CNTs causes toxicity to MSCs after 6 days of culture, while reducing concentration to 6.4 μg/mL showed lower toxicity effect (Mooney et al. 2008). Another study showed that cellular uptake of AuNPs can cause a dose-dependent cytotoxicity to MSCs (Schaeublin et al. 2011). MSCs treated with 500 μg/mL AuNPs could lead to decreased cell viability (Kang et al. 2015). In the present study, due to the rapid attachment of CNT-SA to biotinylated MSCs (less than 1 h), fewer CNTs had the chance of getting internalized by

MSCs. The CNT-MSCs were re-seeded on 24-well plates at the seeding density of 3,000 cells/cm^2. After re-seeding, MSCs were able to proliferate to confluency (Figure 4.4). The amount of CNTs observed on cell surfaces decreased over the course of cultivation.
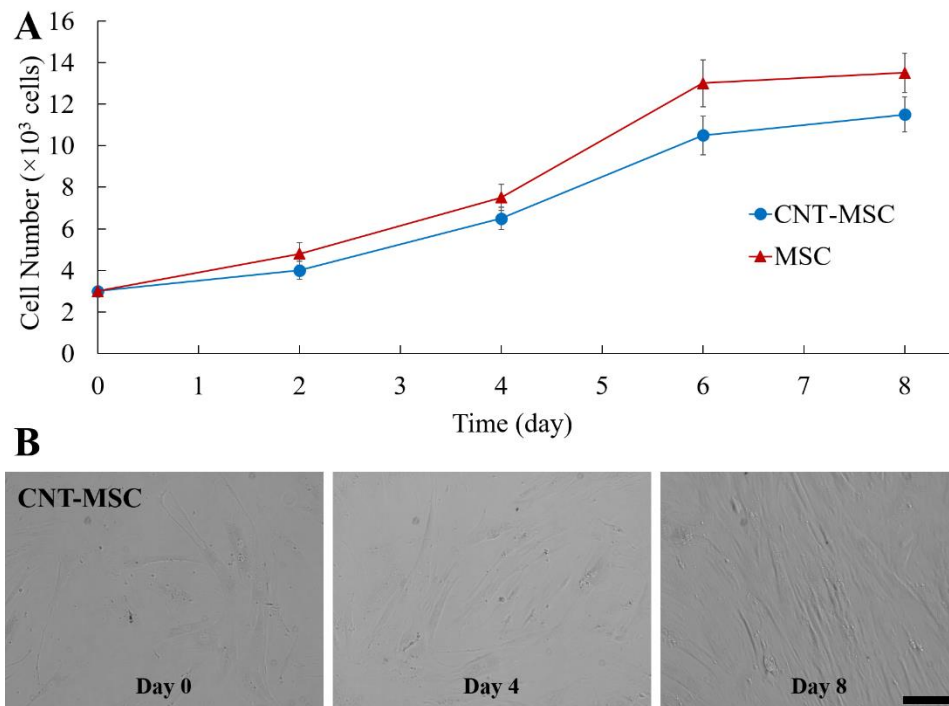
Figure 4.4. (a) Growth kinetics of MSCs from the control group and CNT-MSC re-seeded on 24-well plates at the seeding density of 3000 cells/cm2. (b) Re-seeded CNT-MSCs at day 0, 4 and 8. Scale bar denotes 100 μm. Error bars indicate standard deviation (n = 3).

4.4.4 Effect of CNTs on MSC migration toward chemoattractant SDF-1

The weights of CNTs on MSCs was estimated by a microbalance. The amount of CNT attached on the MSC increased with duration of cell surface biotinylation up to 48 h. The average weight of individual MSC used in the control group was 17.65 ± 0.75 ng. When MSC were treated with biotin-lipid for 12, 24, 36, and 48 h, the estimated weight of CNT on MSCs was 2.47±0.53, 4.26 ± 0.62, 7.71 ± 1.97 and 7.96 ± 2.29 ng per cell, respectively. The effect of CNT amount on the migration capacity of MSCs was evaluated by *in vitro* transwell migration assay. With respect to the transwell migration assay, our results demonstrated that SDF-1α induced migration of CNT-MSCs depends on the amount of CNTs on the MSC surfaces. The cell number of migrated control MSCs toward 200 ng/mL SDF-1α was 48.9 ± 9.5 cells per microscopic field. The higher rate of migration was observed with MSCs treated with 0.01 mg/mL biotin-lipid for 12 h and 24

h (Figure 4.5A). The average observed cell number was 52.4 ± 10.6 and 46.2 ± 7.4 cells per field, respectively (Figure 4.5B). When time of biotinylation was increased to 36 h or longer, the rate of migration toward the chemoattractant decreased significantly. The average observed cell number was 18.7 ± 5.5 and 16.3 ± 4.3 cells per field for 36 h and 48 h of biotin treatment time, respectively. It is speculated that the weight of CNTs on MSCs over the threshold of 4.26 ng/cell hindered the migration of the cells. Nold et al. reported that the migration capacity of MSCs was retained when MSCs were exposed to 10 nM AuNPs (Nold et al. 2017). However, when the concentration was increased to 25 nM or above, the migration capacity of MSCs significantly decreased. Therefore, finding an optimized nanoparticle concentration is crucial for MSCs to retain their proliferation and migration capacity. In the present study, prolonged biotinylation time resulted in more CNT anchoring on MSC surfaces. The migration ability of MSCs was significantly decreased with more than 4.26 ng CNTs per cell anchored on the surface of MSCs. The reason that MSCs could not retain their motility toward the established chemotactic gradient is speculated to be 1) CNT amount over the threshold that a cell could move with normal speed, and/or 2) CNTs loaded on cell surface increasing the friction force for cells to pass through the 8-μm membrane pores of transwell inserts.
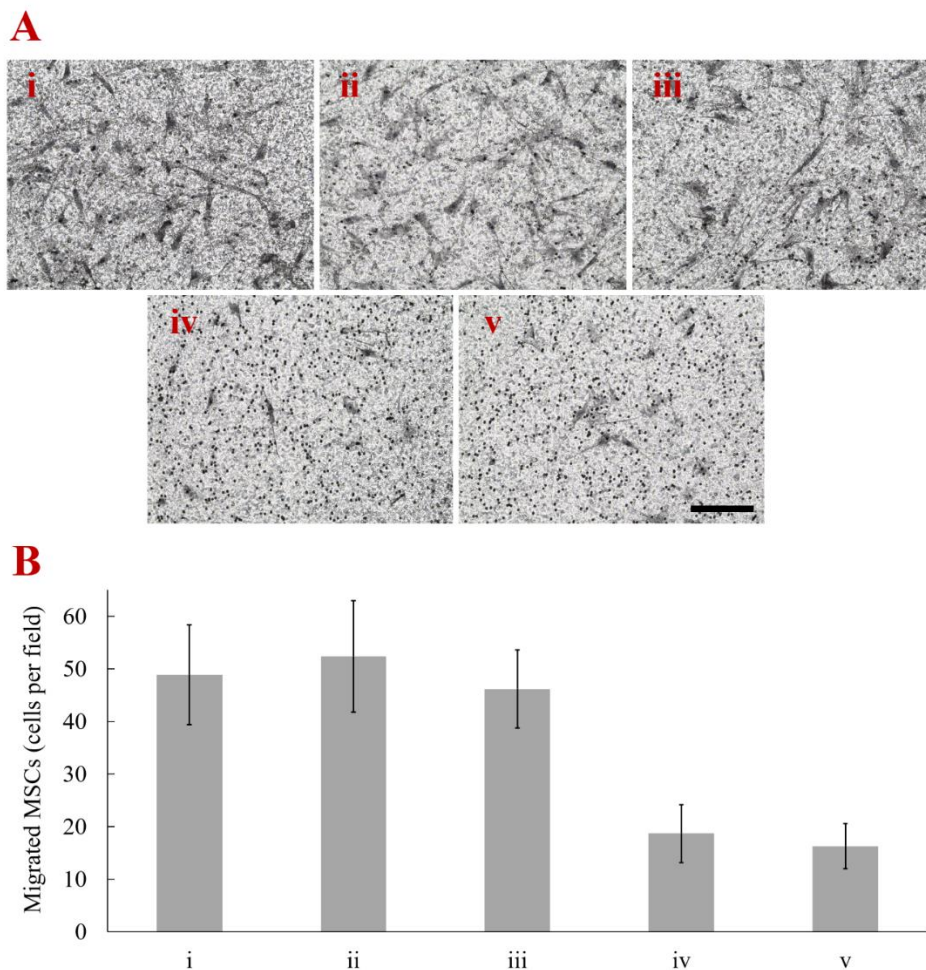
Figure 4.5. (a) Representative images of transwell migration assay of (i) control MSCs (ii - v) CNT-MSCs with 12, 24, 36, 48 h biotinylation time toward 200 ng/mL SDF-1α over 24-hr exposure. Cell were fixed and stained with hematoxylin. Scale bar denotes 100 μm. (b) Transwell migration results showed a decreased number per microscopic field of MSCs migrating toward SDF-1α when MSCs were treated with biotin-lipid for 48 h. Error bars indicate standard deviation (n = 3).

4.5 Conclusion

In this study, we demonstrated that CNT-hitchhiking MSC can be manufactured while retaining cell viability and their tumor-tropic property. When triggered by the chemotactic concentration gradient established by SDF-1α, MSCs could loaded up to ~ 4.26 ng of CNT per cell without decreasing their migration capability. The MSCs tethered with CNTs reported here can be considered for future applications in tumor-targeted photothermal therapy.

4.6 References

Ahmadi, Homa, Mohammad Ramezani, Rezvan Yazdian-Robati, Behzad Behnam, Kamal Razavi Azarkhiavi, Azadeh Hashem Nia, Ahad Mokhtarzadeh, Maryam Matbou Riahi, Bibi Marjan Razavi, and Khalil Abnous. 2017. "Acute toxicity of functionalized single wall carbon nanotubes: A biochemical, histopathologic and proteomics approach." *Chem.-Biol. Interact.* 275:196-209.

Bianco, Alberto, Kostas Kostarelos, Charalambos D. Partidos, and Maurizio Prato. 2005. "Biomedical applications of functionalised carbon nanotubes." *Chem. Comm.* (5):571-577.

Chen, Xing, Un Chong Tam, Jennifer L. Czlapinski, Goo Soo Lee, David Rabuka, Alex Zettl, and Carolyn R. Bertozzi. 2006. "Interfacing Carbon Nanotubes with Living Cells." *J. Am. Chem. Soc.* 128 (19):6292-6293.

Elhissi, Abdelbary M. A., Waqar Ahmed, Israr Ul Hassan, Vinod R. Dhanak, and Antony D'Emanuele. 2012. "Carbon Nanotubes in Cancer Therapy and Drug Delivery." *J. Drug Deliv.* 2012:837327.

Friedenstein, A. J., R. K. Chailakhyan, N. V. Latsinik, A. F. Panasyuk, and I. V. Keiliss-Borok. 1974. "Stromal cells responsible for transferring the microenvironment of the hemopoietic tissues. Cloning in vitro and retransplantation in vivo." *Transplantation* 17 (4):331-40.

Gannon, C. J., P. Cherukuri, B. I. Yakobson, L. Cognet, J. S. Kanzius, C. Kittrell, R. B. Weisman, M. Pasquali, H. K. Schmidt, R. E. Smalley, and S. A. Curley. 2007. "Carbon nanotube-enhanced thermal destruction of cancer cells in a noninvasive radiofrequency field." *Cancer* 110 (12):2654-65.

Huang, Bi-Hai, Yi Lin, Zhi-Ling Zhang, Fangfang Zhuan, An-An Liu, Min Xie, Zhi-Quan Tian, Zhenfeng Zhang, Hanzhong Wang, and Dai-Wen Pang. 2012. "Surface Labeling of Enveloped Viruses Assisted by Host Cells." *ACS Chem. Biol.* 7 (4):683-688.

Iijima, Sumio. 1991. "Helical microtubules of graphitic carbon." *Nature* 354:56.

Kam, N. W., M. O'Connell, J. A. Wisdom, and H. Dai. 2005. "Carbon nanotubes as multifunctional biological transporters and near-infrared agents for selective cancer cell destruction." *Proc. Natl. Acad. Sci. U S A* 102 (33):11600-5.

Kang, S., S. H. Bhang, S. Hwang, J. K. Yoon, J. Song, H. K. Jang, S. Kim, and B. S. Kim. 2015. "Mesenchymal Stem Cells Aggregate and Deliver Gold Nanoparticles to Tumors for Photothermal Therapy." *ACS Nano* 9 (10):9678-90.

Kidd, S., E. Spaeth, J. L. Dembinski, M. Dietrich, K. Watson, A. Klopp, V. L. Battula, M. Weil, M. Andreeff, and F. C. Marini. 2009. "Direct evidence of mesenchymal stem cell tropism for tumor and wounding microenvironments using in vivo bioluminescent imaging." *Stem Cells* 27 (10):2614-23.

Kucerova, L., S. Skolekova, M. Matuskova, M. Bohac, and Z. Kozovska. 2013. "Altered features and increased chemosensitivity of human breast cancer cells mediated by adipose tissue-derived mesenchymal stromal cells." *BMC Cancer* 13:535.

Lara-Martínez, Luis A., Felipe Massó, Eduardo Palacios González, Isabel García-Peláez, Alejandra Contreras–Ramos, Mahara Valverde, Emilio Rojas, Felipe Cervantes-Sodi, and Salomón Hernández-Gutiérrez. 2017. "Evaluating the biological risk of functionalized multiwalled carbon nanotubes and functionalized oxygen-doped multiwalled carbon nanotubes as possible toxic, carcinogenic, and embryotoxic agents." *Int. J. Nanomedicine* 12:7695-7707.

Lee, Miyoung, Sang Young Jeong, Jueun Ha, Miyeon Kim, Hye Jin Jin, Soon-Jae Kwon, Jong Wook Chang, Soo Jin Choi, Wonil Oh, Yoon Sun Yang, Jae-Sung Kim, and Hong Bae Jeon. 2014. "Low immunogenicity of allogeneic human umbilical cord blood-derived mesenchymal stem cells in vitro and in vivo." *Biochem. Biophys. Res. Commun.* 446 (4):983-989.

Liu, J., A. G. Rinzler, H. Dai, J. H. Hafner, R. K. Bradley, P. J. Boul, A. Lu, T. Iverson, K. Shelimov, C. B. Huffman, F. Rodriguez-Macias, Y. S. Shon, T. R. Lee, D. T. Colbert, and R. E. Smalley. 1998. "Fullerene pipes." *Science* 280 (5367):1253-6.

Liu, Zhuang, Corrine Davis, Weibo Cai, Lina He, Xiaoyuan Chen, and Hongjie Dai. 2008. "Circulation and long-term fate of functionalized, biocompatible single-walled carbon nanotubes in mice probed by Raman spectroscopy." *Proc Natl Acad Sci* 105 (5):1410-1415.

Maruyama, Kayo, Hisao Haniu, Naoto Saito, Yoshikazu Matsuda, Tamotsu Tsukahara, Shinsuke Kobayashi, Manabu Tanaka, Kaoru Aoki, Seiji Takanashi, Masanori Okamoto, and Hiroyuki Kato. 2015. "Endocytosis of Multiwalled Carbon Nanotubes in Bronchial Epithelial and Mesothelial Cells." *Biomed. Res. Int.* 2015:9.

Moll, N. M., and R. M. Ransohoff. 2010. "CXCL12 and CXCR4 in bone marrow physiology." *Expert Rev. Hematol.* 3 (3):315-22.

Mooney, E., P. Dockery, U. Greiser, M. Murphy, and V. Barron. 2008. "Carbon nanotubes and mesenchymal stem cells: biocompatibility, proliferation and differentiation." *Nano Lett* 8 (8):2137-43.

Myers, T. J., F. Granero-Molto, L. Longobardi, T. Li, Y. Yan, and A. Spagnoli. 2010. "Mesenchymal stem cells at the intersection of cell and gene therapy." *Expert Opin. Biol. Ther.* 10 (12):1663-79.

Nold, Philipp, Raimo Hartmann, Neus Feliu, Karsten Kantner, Mahmoud Gamal, Beatriz Pelaz, Jonas Hühn, Xing Sun, Philipp Jungebluth, Pablo del Pino, Holger Hackstein, Paolo Macchiarini, Wolfgang J. Parak, and Cornelia Brendel. 2017. "Optimizing conditions for labeling of mesenchymal stromal cells (MSCs) with gold nanoparticles: a prerequisite for in vivo tracking of MSCs." *J. Nanobiotechnology* 15 (1):24.

Park, J. S., S. Suryaprakash, Y. H. Lao, and K. W. Leong. 2015. "Engineering mesenchymal stem cells for regenerative medicine and drug delivery." *Methods* 84:3-16.

Park, Siwan, Hwanseok Jang, Byung Soo Kim, Changmo Hwang, Gi Seok Jeong, and Yongdoo Park. 2017. "Directional migration of mesenchymal stem cells under an SDF-1α gradient on a microfluidic device." *PLOS ONE* 12 (9):e0184595.

Peci, Taze, T. John S. Dennis, and Mark Baxendale. 2015. "Iron-filled multiwalled carbon nanotubes surface-functionalized with paramagnetic Gd (III): A candidate dual-functioning MRI contrast agent and magnetic hyperthermia structure." *Carbon* 87:226-232.

Peer, Dan, Jeffrey M. Karp, Seungpyo Hong, Omid C. Farokhzad, Rimona Margalit, and Robert Langer. 2007. "Nanocarriers as an emerging platform for cancer therapy." *Nat. Nanotech.* 2:751.

Roger, M., A. Clavreul, M. C. Venier-Julienne, C. Passirani, L. Sindji, P. Schiller, C. Montero-Menei, and P. Menei. 2010. "Mesenchymal stem cells as cellular vehicles for delivery of nanoparticles to brain tumors." *Biomaterials* 31 (32):8393-401.

Saito, T., K. Matsushige, and K. Tanaka. 2002. "Chemical treatment and modification of multi-walled carbon nanotubes." *Physica B Condens. Matter.* 323 (1):280-283.

Santos, J. L., D. Pandita, J. Rodrigues, A. P. Pego, P. L. Granja, and H. Tomas. 2011. "Non-viral gene delivery to mesenchymal stem cells: methods, strategies and application in bone tissue engineering and regeneration." *Curr Gene Ther* 11 (1):46-57.

Schaeublin, Nicole M., Laura K. Braydich-Stolle, Amanda M. Schrand, John M. Miller, Jim Hutchison, John J. Schlager, and Saber M. Hussain. 2011. "Surface charge of gold nanoparticles mediates mechanism of toxicity." *Nanoscale* 3 (2):410-420.

Shah, K. 2012. "Mesenchymal stem cells engineered for cancer therapy." *Adv. Drug Deliv. Rev.* 64 (8):739-48.

Shi, J., R. Ma, L. Wang, J. Zhang, R. Liu, L. Li, Y. Liu, L. Hou, X. Yu, J. Gao, and Z. Zhang. 2013. "The application of hyaluronic acid-derivatized carbon nanotubes in hematoporphyrin monomethyl ether-based photodynamic therapy for in vivo and in vitro cancer treatment." *Int. J. Nanomedicine* 8:2361-73.

Son, Kuk Hui, Jeong Hee Hong, and Jin Woo Lee. 2016. "Carbon nanotubes as cancer therapeutic carriers and mediators." *Int. J. Nanomedicine* 11:5163-5185.

Wang, C. H., S. H. Chiou, C. P. Chou, Y. C. Chen, Y. J. Huang, and C. A. Peng. 2011. "Photothermolysis of glioblastoma stem-like cells targeted by carbon nanotubes conjugated with CD133 monoclonal antibody." *Nanomedicine: NBM* 7 (1):69-79.

Weydemeyer, Ethan J., Alicia J. Sawdon, and Ching-An Peng. 2015. "Controlled cutting and hydroxyl functionalization of carbon nanotubes through autoclaving and sonication in hydrogen peroxide." *Chem. Comm.* 51 (27):5939-5942.

Wu, Huixia, Gang Liu, Xue Wang, Jiamin Zhang, Yu Chen, Jianlin Shi, Hong Yang, He Hu, and Shiping Yang. 2011. "Solvothermal synthesis of cobalt ferrite nanoparticles loaded on multiwalled carbon nanotubes for magnetic resonance imaging and drug delivery." *Acta Biomaterialia* 7 (9):3496-3504.

Yao, Sen, Xuqian Li, Jingxuan Liu, Yuqing Sun, Zhuanhe Wang, and Yanyan Jiang. 2017. "Maximized nanodrug-loaded mesenchymal stem cells by a dual drug-loaded mode

for the systemic treatment of metastatic lung cancer." *Drug Deliv* 24 (1):1372-1383.

Zhang, Xiaoke, Lingjie Meng, Qinghua Lu, Zhaofu Fei, and Paul J. Dyson. 2009. "Targeted delivery and controlled release of doxorubicin to cancer cells using modified single wall carbon nanotubes." *Biomaterials* 30 (30):6041-6047.

Zhou, F., D. Xing, Z. Ou, B. Wu, D. E. Resasco, and W. R. Chen. 2009. "Cancer photothermal therapy in the near-infrared region by using single-walled carbon nanotubes." *J. Biomed. Opt.* 14 (2):021009.

Chapter 5. Diminution of Phagocytosed Micro/Nanoparticles by Tethering with Immunoregulatory CD200 Protein

5.1 Abstract

CD200, known as an anti-inflammatory transmembrane glycoprotein in the immunoglobin superfamily, interacts with its receptor CD200R which is expressed on the surface of myeloid cells such as macrophages and neutrophils. Such interaction has known to reduce macrophage activation and chronic inflammation. To harness the immunomodulatory property of CD200 for surface modification, CD200-streptavidin fusion protein was expressed from bacteria transformed with pET20b plasmid recombinant with CD200 extracellular domain and core streptavidin. The purified CD200-SA protein was bound to biotin-coated fluorescent particles of various sizes ranging from 0.15 to 3 µm. THP-1 macrophages were cultivated with CD200-modified micro/nanoparticles in comparison with untreated ones. Our results showed that both nano- and micro-sized particles decorated with CD200 decreased phagocytosis activities of THP-1 macrophages. Such diminution of phagocytosis was examined to be associated with downregulation of Toll-like receptor 4 (TLR4) expression on the surface of macrophages. Moreover, THP-1 macrophages treated with CD200-coated particles decreased the secretion of interleukin-6 and tumor necrosis factor-α.

5.2 Introduction

Macrophage is a phagocyte of the immune system that engulfs foreign microbes and cellular debris (Elhelu 1983). Macrophage clearance is a major challenge for therapeutic application of nanoparticles is limited because nanoparticles are cleaned up by macrophage clearance (Oh and Park 2014, Rattan et al. 2017, Yoo, Chambers, and Mitragotri 2010). The surfaces of particles have been modified by various materials to reduce phagocytic clearance by macrophages. For example, modification with polyethylene glycol (PEG) chains reduces the uptake of nanoparticles by macrophages and thus prolonging their circulation time (Bartlett et al. 2007, Gabizon, Barenholz, and Bialer 1993). Although surface modification with PEG achieves longer circulation time in the blood, PEGylation may have some drawbacks such as attenuated delivery efficiency,

immunological responses and non-biodegradability (Hatakeyama, Akita, and Harashima 2013, Knop et al. 2010, Remaut et al. 2007). Surface modification with CD47 is an alternative approach to avoid phagocytic clearance by macrophages. CD47 is a "marker of self" protein that reduces phagocytic activity by the interaction with its receptor SIRPα (signal-regulatory protein α) on the macrophage surface (Oldenborg et al. 2000). Particles coated with CD47 protein have the ability to prolong the blood circulation, thereby promoting drug delivery to tumors by diminishing macrophage-mediated phagocytic clearance via CD47-SIRPα interaction (Rodriguez et al. 2013, Qie et al. 2016). CD47-modified zymosan microparticles also showed reduced phagocytic activities of J774A.1 macrophages (Salehi and Peng 2016).

CD200, another broadly expressed self-protein like CD47, is an anti-inflammatory transmembrane glycoprotein in the immunoglobin superfamily. CD200 is expressed in a myriad of cells such as myeloid cells (macrophages, dendritic cells), lymphoid cells (T, B cells), neurons, cardiomyocytes, keratinocytes, and endothelial cells (Barclay et al. 2002, McMaster and Williams 1979, Dick et al. 2001). CD200R known as CD200 cognate receptor is expressed on the surface myeloid cells such as macrophages, neutrophils, and microglia (Hoek et al. 2000, Wright et al. 2000). Hoek et al. found that CD200-CD200R interaction elicits an inhibitory signal that downregulates macrophage activity (Hoek et al. 2000). In cancer stem cell (CSC) immunology, the expression of CD200 on CSCs allows the CSCs to evade or suppress the immune system (Kawasaki and Farrar 2008). Several other studies also supported the inhibitory role of CD200-CD200R signal in the activation of macrophages and dendritic cells (Rosenblum et al. 2004, Gorczynski et al. 1999, Taylor et al. 2005, Gorczynski, Yu, and Clark 2000). Most functional findings of CD200-CD200R interaction have focused on dampening proinflammatory cytokine secretion of myeloid cells. More recently, its involvement in reducing phagocytosis has been reported. For example, *in vivo* CD200-Fc administration facilitated white matter recovery by suppressing phagocytosis of susceptible oligodendrocyte precursors (Hayakawa et al. 2016). The absence of CD200-CD200R interaction increased engulfment of FITC-labelled amyloid-β or fluorescently labelled 1-μm latex beads cultured with microglial cells isolated from CD200^{-/-} mice. Moreover, increased phagocytosis was observed in microglial cells isolated from CD200-deficient mice (Lyons et al. 2017). On the contrary, a study indicated that

CD200 coating of 7 μm fluorescein-containing poly(lactic-co-glycolic acid) (PLGA) microparticles enhanced their phagocytosis by both mouse macrophages and human monocytes (Chen et al. 2017). Judging from the inconsistence of CD200-CD200R engagement on the ingestion of CD200-coated particles by phagocytes, this topic warrants further investigation.

In the present study, the surfaces of particles with size ranging from nano- to micro-meters were coated with CD200 to evaluate the effect of CD200 on macrophage phagocytosis. The CD200 protein used here is tagged with streptavidin (SA) by recombinant DNA approach. The expressed and purified CD200-SA fusion protein was bound to biotinylated fluorescent particles due to the high affinity of SA with biotin. THP-1 macrophages were treated with uncoated particles and CD200-coated particles. The antiphagocytic efficacy of CD200 was evaluated. Our results showed that both nano- and micro-sized particles decorated with CD200 decreased phagocytosis activities of THP-1 macrophages. Moreover, THP-1 macrophages treated with CD200-coated 0.56 μm particles showed 26.9% and 26.1% decrease in interleukin-6 (IL-6) and tumor necrosis factor-α (TNF-α) secretion, respectively.

5.3 Materials and Methods

5.3.1 Materials

Plasmid encoding human CD200 DNA was acquired from DNASU Plasmid Repository of Arizona State University (plasmid ID No: HsCD00620970; Tempe, Arizona, USA). Phusion DNA polymerase and Quick-Load® Purple 2-Log DNA Ladder were purchased from New England Biolabs (Ipswich, MA, USA). FastDigest restriction enzymes (XhoI, EcoRI, BamHI and EcoRV), T4 DNA ligase, subcloning efficiency DH5α competent cells, glycerol, B-PER bacterial protein extraction reagent, Halt protease inhibitor, lysozyme, DNase I, HisPur Ni-NTA Resin, disposable polystyrene columns, Coomassie brilliant blue R 250, Pierce ECL Western blotting substrate, Tween-20, BCA protein assay kit and RPMI 1640 Medium, human IL-6 ELISA kit and human TNF-α ELISA kit were purchased from Thermo Fisher Scientific (Waltham, MA, USA). Plasmid Maxi Kit was purchased from QIAGEN (Valencia, CA, USA). Ampicillin, Isopropyl β-D-1-thiogalactopyranoside (IPTG), penicillin-streptomycin, phorbol 12-myristate 13-acetate

(PMA), fluorescein isothiocyanate (FITC), biotin-FITC, 1-ethyl-3-(3-dimethylaminopropyl)carbodiimide (EDC), Zymosan A from *Saccharomyces cerevisiae* and sodium bicarbonate were purchased from Sigma-Aldrich (St. Louis, MO, USA). Rosetta™(DE3) competent cells were purchased from Merck Millipore (Darmstadt, Germany). Acetic acid was purchased from J.T. Baker (Philipsburg, NJ, USA). Imidazole, sodium chloride (NaCl) was purchased from ACROS (Fair Lawn, NJ, USA). Laemmli sample buffer was purchased from Bio-Rad (Hercules, CA, USA). Methanol was purchased from Avantor Performance Materials (Center Valley, PA, USA). Polyvinylidene difluoride (PVDF) membrane was purchased from Pall Life Science (Port Washington, NY, USA). Human/mouse CD200 antibody and mouse IgG HRP-conjugated antibody were purchased from R&D Systems (Minneapolis, MN, USA). Rabbit anti-streptavidin antibody, goat anti-rabbit IgG horseradish peroxidase conjugate were purchased from GenScript (Piscataway, NJ, USA). Bovine serum albumin (BSA) was purchased from Rockland Immunochemicals Inc (Limerick, PA, USA). THP-1 cell line (catalog number TIB-202) was purchased from ATCC (Manassas, VA, USA). J774A.1 macrophage cell line was kindly provided by Dr. Tanya Miura, University of Idaho. Fetal bovine serum (FBS) was purchased from Atlanta Biologicals (Lawrencevilla, GA, USA). 0.15 (yellow), 0.56 (Nile red), 0.84 (pink), 2 µm (pink) biotin-coated fluorescent polystyrene particles were purchased from Spherotech (Lake Forest, IL, USA). 2-mercaptoethanol was purchased from Gibco (Grand Island, NY, USA). 2-(N-morpholino)ethanesulfonic acid (MES) was purchased from TCI (Portland, OR, USA). Trypan blue was purchased from BTC Beantown chemical (Hudson, NH, USA). Anti-human CD200 receptor monoclonal antibody with PE label was purchased from BioLegend (San Diego, CA, USA). Human TLR4 antibody (HTA125) with FITC label was purchased from Santa Cruz Biotechnology (Dallas, Texas, USA).

5.3.2 Construction of CD200-SA encoding plasmid

The extracellular domain of CD200 was amplified from full-length human CD200 by polymerase chain reaction (PCR) with sense primer 5'-TAAGTCGATATCGGTCATGGCAGCAGTGGT-3' and antisense primer 5'-TAAGCAGGATCCCACCTGGCAGATCACCTC-3'. CD200 PCR reactions were

performed with Phusion DNA polymerase in a thermocycler (Bio-Rad, Hercules, CA, USA) with initial denaturation at 98°C for 30 s, and then 30 cycles of denaturation at 98°C for 10 s, annealing at 62°C for 30 s, and extension at 72°C for 15 s. Final extension was performed at 72°C for 5 min. CoreSA DNA was amplified by PCR from pSTE2-215 (yol) plasmid (Dubel et al. 1995) using sense Primer: 5'-ACTGGAATTCGCTGAAGCAGGTATCACC-3' and antisense primer: 5'-ATCGCTCGAGGATGGGATAGATCTTCTTCTG-3'. CoreSA PCR reactions were performed with Phusion DNA polymerase in a thermocycler (Bio-Rad, Hercules, CA, USA) with initial denaturation at 98°C for 30 s, and then 30 cycles of denaturation at 98°C for 10 s, annealing at 60°C for 30 s, and extension at 72°C for 15 s. Final extension was performed at 72°C for 5 min. The PCR products of CD200 and coreSA were analyzed by 1% agarose gel electrophoresis. pET20b plasmid (vector) and coreSA DNA (insert) were cut with restriction enzymes XhoI and EcoRI. The digested pET20b and coreSA were ligated by T4 DNA ligase to get PMZ005 plasmid. The ligation product PMZ005 was amplified by transformation with subcloning efficiency DH5α competent cells, and purified by QIAGEN Plasmid Maxi Kit. The PMZ005 plasmid (vector) and CD200 DNA (insert) were cut with restriction enzymes BamHI and EcoRV. The digested PMS005 and CD200 products were ligated by Blunt/TA Ligase Master Mix to get PMZ006 plasmid. The PMZ006 ligation product was again amplified by transformation with subcloning efficiency DH5α competent cells, and purified by QIAGEN Plasmid Maxi Kit.

5.3.3 Expression and purification of CD200-SA fusion protein

Rosetta™(DE3) competent cells were transformed with CD200-SA encoding plasmid PMZ006 and plated on agar plates containing 50 μg mL^{-1} ampicillin. A single colony was picked up and grown in 5 mL of lysogeny broth (LB) medium supplemented with 10% (v/v) glycerol and 50 μg mL^{-1} ampicillin at 225 rpm, at 37°C in a shaker incubator for overnight. The start culture was then diluted 1:20 with LB containing 10% (v/v) glycerol and 50 μg mL^{-1} ampicillin, and grown in a shaker incubator at 225 rpm, 37°C. The optical density (OD) at 600 nm was monitored by a Spectramax M2e microplate reader (Molecular Devices, Sunnyvale, CA, USA). When OD 600 nm reached 0.6 to 0.8, IPTG was added to the culture to the final concentration of 0.05, 0.2, 0.5, and 1 mM to induce the protein expression. The culture was grown in a shaker incubator at 225 rpm at 37°C for

3 h and room temperature for 6 h, respectively. The cells were harvested by centrifugation at 4,500 rpm for 5 min at 4°C. The cell pellet was washed with cold 1× phosphate buffer saline (PBS), and harvested at 4,500 rpm for 5 min at 4°C.

The cell pellet from 50 mL bacterial culture was resuspended in 5 mL of B-PER bacterial protein extraction reagent supplemented with 1× Halt protease inhibitor, 1 mg mL^{-1} lysozyme, and 2 µL mL^{-1} DNase I. Cell lysis was performed according to manufacturer's instruction to collect the clear protein lysate. 1 mL of protein lysate was mixed with 1 mL of binding buffer (50 mM Na$_2$HPO$_4$, 300 mM NaCl, pH 7.4), and then applied to an IMAC column filled with 1 mL of HisPur Ni-NTA resin. The resin was then washed with one resin-bed volume (1 mL) of wash buffer (10 mM imidazole, 50 mM Na$_2$HPO$_4$, 300 mM NaCl, pH 7.4) 5 times or until the absorbance at 280 nm reached baseline. CD200-SA fusion protein was eluted with 5 resin-bed volumes of elution buffer (250 mM imidazole, 50 mM Na$_2$HPO$_4$, 500 mM NaCl, pH 7.4). Protein elution was monitored by measuring absorbance at 280 nm. To determine the concentration of purified CD200-SA protein, BCA protein assay kit was used according to the manufacturer's instructions. Briefly, 2 mg mL^{-1} BSA standard was serially diluted and used as protein standards. 50 parts of BCA reagent A was mixed with 1 part of BCA reagent B and the mixture was used as working reagent. 10 µL of purified protein was mixed with 200 µL of working reagent and incubated at 37°C for 30 min. The absorbance at 562 nm was measured by a Spectramax M2e microplate reader.

5.3.4 SDS-PAGE and Western blot analysis

The CD200-SA crude protein lysate and purified CD200-SA protein was characterized by SDS-PAGE. The protein lysate was mixed with same volume Laemmli sample buffer, and loaded on a 12% polyacrylamide gel made by Mini-PROTEAN Tetra handcast systems (Bio-Rad, Hercules, CA, USA). SDS-PAGE was performed at 200 V for 40 min. The gel was stained with 0.006% (w/v) Coomassie brilliant blue R 250 solution with 10% (v/v) acetic acid and 40% (v/v) methanol. The gel was destained in a fast destaining solution containing 10% (v/v) acetic acid and 40% (v/v) methanol for 1 h, and a slow destaining solution containing 10% (v/v) acetic acid and 10% (v/v) methanol for overnight.

For western blot analysis, purified CD200-SA protein on the 12% polyacrylamide gel was transferred to a PVDF membrane using a Trans-Blot SD Semi-Dry Transfer Cell (Bio-Rad, Hercules, CA, USA) at 18V for 1 h. The membrane was washed with 1X Tris buffered saline (TBS) at room temperature for 10 min, and then blocked with blocking buffer (5% (w/v) BSA in TBS with 0.1% Tween-20) at room temperature for 1 h with mild shaking. The membrane was then immersed in 1:500 diluted Human/mouse CD200 antibody solution in blocking buffer, and incubated on a mini rocker (Hercules, CA, USA) at 4°C for overnight. The membrane was washed with TBST for 10 min, three times at room temperature, and then incubated with 1:1,000 diluted mouse IgG HRP-conjugated antibody for 1 h at room temperature. The membrane was washed with TBST for 10 min, three times. The CD200 protein was characterized by detecting horseradish peroxidase activity using ECL substrate via Syngene PXi chemiluminescence imager (Syngene, Cambridge, UK). Similarly, coreSA was detected by rabbit anti-streptavidin antibody as the primary antibody and goat anti-rabbit IgG horseradish peroxidase conjugate as the secondary antibody.

5.3.5 Preparation of CD200 coated fluorescent particles

Biotin coated fluorescent polystyrene particles of various sizes (0.15, 0.56, 0.84 and 2 µm) were dissolved in CD200-SA protein purified in previous section. The particles were gently shaken at 4°C for 30 min, and particles were collected by centrifugation at 8,000× g for 5 min, followed by three times wash with 1× PBS. CD200 modified 0.56 µm particles were characterized by dot blot analysis. Briefly, 2 µL of CD200-modified and 2 µL of unmodified particles were added to a PVDF membrane. The membrane was blocked with blocking buffer (5% (w/v) BSA in TBS with 0.1% Tween-20) at room temperature for 1 h with mild shaking. The membrane was blocked with blocking buffer at room temperature for 1 h with mild shaking. The membrane was then incubated in primary antibody (human/mouse CD200 monoclonal antibody) and secondary antibody (mouse IgG HRP-conjugated antibody) solutions same as described in previous section. The membrane was also treated with ECL substrate and imaged by chemiluminescence imager same as described in previous section.

To quantify CD200-SA coated on 0.56 µm polystyrene particles, 200 µL of 0.56 µm biotinylated polystyrene particles (0.1% w/v) was dissolved in 1 mL purified CD200-SA protein and mildly shaken for 30 min. The particles were collected by centrifugation at 8,000× g for 5 min, followed by washing with 1× PBS for three times. CD200-SA coated particles were then re-suspended in a solution containing biotin-FITC and gently shaken for 30 min. After biotin-FITC bound CD200-SA coated particles, the particles were washed and re-suspended in 100 µL 1× PBS. The FITC intensity (λ_{ex}= 485 nm, λ_{em}=525 nm) was measured by a Spectramax M2e microplate reader. The molar concentration of CD200 was quantified using the standard calibration curve of FITC. The amount of CD200 on particles was expressed as molecules μm^{-2}.

Fluorescent zymosan particles (size ~3 µm) were also prepared to test the effect of CD200 on macrophage phagocytosis. The preparation of fluorescent zymosan particles were previously described (Salehi and Peng 2016). 10 mg of zymosan suspended in 10 mL 0.3 M sodium bicarbonate buffer (pH 9.2). The particles were centrifuged and re-suspended to 5 mL MES buffer (pH 7.4). The particles were then tip-sonicated 30 sec for three times. 50 µL of 1 mg/mL FITC was added to the zymosan particles and incubated for overnight. The excess FITC was washed by 1× PBS for three times. 10 mg biotin and 10 mg EDC were dissolved in 10 mL MES buffer (pH 7.4) and stirred for 15 min. The FITC-labeled zymosan particles were added to the biotin-EDC mixture and stirred for 3 h at room temperature. The zymosan-biotin-FITC particles were collected by centrifugation and washed by 1× PBS for three times.

5.3.6 Phagocytosis study of THP-1 induced macrophages

THP-1 macrophages were cultured with RPMI 1640 medium supplemented with 10% FBS, 1% penicillin-streptomycin and 0.05 mM 2-mercaptoethanol. The differentiation of THP-1 cells to macrophages was induced by supplementing the culture medium with 1.6×10^{-7} M PMA for 2 days. The seeding density was 5×10^4 cells cm^{-2} on 6-well plates. After 2 days, medium was discarded and cells were washed with 1× PBS for three times.

The expression of CD200R on THP-1 macrophage surface was quantified by FACS study. THP-1 macrophages were detached from culture flasks by gentle scraping. Cells

were collected by centrifugation at 400× g for 5 min, followed by washing with 1× PBS. Cells were incubated in 1× PBS with 3% BSA containing human CD200R antibody with PE label for 30 min. Cells were washed three times by centrifugation at 400× g for 5 min. The cells were analyzed by BD Accuri C6 flow cytometer (BD Biosciences, San Jose, CA, USA), and data was processed by BD Accuri C6 Plus software. The effect of CD200-coated particles on the expression of TLR4 on macrophage surface was also evaluated by FACS. THP-1 macrophages were allowed to engulf unmodified and CD200-coated 0.56 μm particles (Nile red) for 2 h. The cells were detached from the culture flasks by gentle scraping. Cells were collected by centrifugation at 400× g for 5 min, followed by washing with 1× PBS. Cells were incubated in 1× PBS with 3% BSA containing human TLR4 monoclonal antibody (HTA125) with FITC label for 30 min. Cells were washed three times by centrifugation at 400× g for 5 min. The cells were analyzed the same as described above.

To assess the effect of CD200 on macrophage phagocytosis, THP-1 macrophages were treated with CD200-coated and unmodified fluorescent particles of various sizes for 2, 5, and 10 h. The amount of particles added to the plate wells was 1, 4, 10 and 64 μg cm^{-2} for 0.15, 0.56, 0.84 and 2 μm, respectively. At each time point, the particles not taken up by macrophages were gently washed away with 1× PBS for three times. 0.56 μm particles were also modified with SA (pMZ005) to compare with the effect of CD200 (pMZ006) on macrophage phagocytosis. After each time point, the fluorescence was quenched by treating cells with 0.01 mg/ml trypan blue. Bright field and fluorescent images were taken with Leica DMi8 microscope equipped with Leica EC3 camera (Leica Microsystems, Wetzlar, Germany). The fluorescence intensity was measured by a Spectramax M2e microplate reader. The excitation and emission wavelength was λ_{ex}= 485 nm, λ_{em}=525 nm for yellow and green fluorescence, and λ_{ex}= 552 nm, λ_{em}=636 nm for Nile red and pink fluorescence.

5.3.7 The effect of CD200-coated on IL-6 and TNF-α secretion from THP-1 macrophages.

THP-1 macrophages were seeded on 6-well plates at 5×10^4 cells cm^{-2}. THP-1 macrophages were treated with unmodified and CD200-coated 0.56 μm polystyrene particles (Nile red) for 18 h. The level of IL-6 and TNF-α in culture media was quantified by commercial ELISA kits according to manufacturer's instructions. Briefly, 100 μL coating buffer containing IL-6 and TNF-α capture antibody was added to each well of the ELISA 96 well plate and incubated overnight at 4°C. After overnight, coating buffer was removed and the wells were washed three times with washing buffer (1× PBS with 0.05% Tween-20). 200 μL 1× ELISPOT diluent was added to each well and incubated at room temperature for 1 h. The wells were washed three times with washing buffer. 100 μL of the culture medium collected above, IL-6 standards and TNF-α standards were added to each well and incubated at room temperature for 2 h. After that, samples and standards were removed, and the wells were washed three times with washing buffer. 100 μL of 1× ELISPOT diluent containing IL-6 and TNF-α detection antibody was added to each well and incubated at room temperature for 1 h. After 1 h, detection antibody solutions were removed, and the wells were washed three times with wash buffer. 100 μL of 1× ELISPOT diluent containing streptavidin-HRP was then added to each well and incubated at room temperature for 30 min. Streptavidin-HRP solution was removed, and the wells were washed five times with wash buffer. 100 μL of 1× TMB solution was added to each well and incubated at room temperature for 15 min. The reaction was stopped with by adding 50 μL of 1 M phosphoric acid to each well, and absorbance was measured at 450 nm with a SpectraMax M2e microplate reader. The concentrations of IL-6 and TNF-α in the culture medium were quantified using standard curves.

5.3.8 Statistical analysis.

To assess the effect of CD200 coating on macrophage phagocytosis and inflammatory cytokine secretion, unpaired t-test was used to compare unmodified particles and CD200-coated particles treated groups. $p < 0.05$ was considered statistically significant.

5.4 Results and Discussion

5.4.1 Expression of CD200-SA fusion protein

The CD200-SA encoding recombinant plasmid (PMZ006) was constructed by inserting the gene sequences of CD200 extracellular domain (CD200ECD) and core streptavidin (coreSA) into plasmid vector pET20b (Figure 5.1a). The gene sequences encoding CD200ECD and coreSA from pMZ006 cloned by PCR were verified by DNA gel electrophoresis with ~0.6 kb for CD200ECD and ~0.5 kb for coreSA (shown in Figure 5.1b). Given the sequence of CD200ECD (amino acids 31-232, Gln-Gly, being 600 bp (~22.2 kDa), the gap (from EcoRI to BamHI) being 6 bp (~0.22 kDa), and coreSA sequence being 424 bp (~15.5 kDa, Glu-Ser), CD200-SA fusion protein has an estimated molecular weight around 38 kDa. As shown in Figure 5.2, SDS-PAGE analysis of cell lysates indicated that the enhanced protein bands with MW of 38-40 kDa were observed for transformed bacteria with IPTG induction. To confirm the insertion of CD200ECD and coreSA into pET20b, the gene sequences of hCD200 and coreSA from PMZ006 were amplified by PCR, and the PCR products were characterized by DNA gel electrophoresis (Figure 5.1b). The CD200ECD PCR product showed the size of ~0.6 kb, and coreSA PCR product showed the size of ~0.5 kb on agarose gel, confirming both gene sequences were present in pMZ006. The crude protein lysates on SDS-PAGE gel was stained with Coomassie blue (Figure 5.2). Among all IPTG-induced protein expression, the one obtained from transformed Rosetta™(DE3) competent cells treated with 0.05 mM IPTG at room temperature for 6 h (see lane 7 in Figure 5.2) showed the most prominent protein band. Thus, 0.05 mM IPTG induction at room temperature for 6 h was chosen as the expression condition for pMZ006.

Figure 5.1. (A) The circular map showing multiple cloning sites for CD200-SA fusion gene. CoreSA was inserted between XhoI and EcoRI; the extracellular domain of human CD200 was inserted between BamHI and EcoRV. (B) DNA gel electrophoresis of DNA ladder (lane 1), extracellular domain of human CD200 (0.6 kb) and core streptavidin (CoreSA).

Figure 5.2. Effects of IPTG concentration and induction time on human CD200-SA expression using Rosetta competent E. coli cells. (1) All blue protein standard, (2) non-induced E. coli control, (3-6) Induction 0.05, 0.2, 0.5 and 1 mM IPTG at 37°C for 3 h, (7-10) Induction 0.05, 0.2, 0.5 and 1 mM IPTG at room temperature for 6 h.

To purify CD200-SA fusion protein tagged with His6x from bacterial lysate, immobilized metal affinity chromatography (IMAC) columns with Ni-NTA resin was used. It was observed that the binding of His6x-tag and Ni-NTA resin was not strong. After binding the crude protein lysate to the resin, washing the column with 25 mM imidazole wash buffer would wash off the target protein. Thus, the imidazole concentration in binding and wash buffer was kept lower than 10 mM. The target protein was eluted with 250 mM imidazole elution buffer, and the elution profile showed that the target CD200-SA protein was eluted mostly in the second fraction (i.e., fraction #9 in Figure 5.3a). The concentration of this eluted fraction was detected to be 187.2 ± 16.8 µg mL^{-1} (mean $\pm$ standard deviation, n = 3) by the BCA assay.
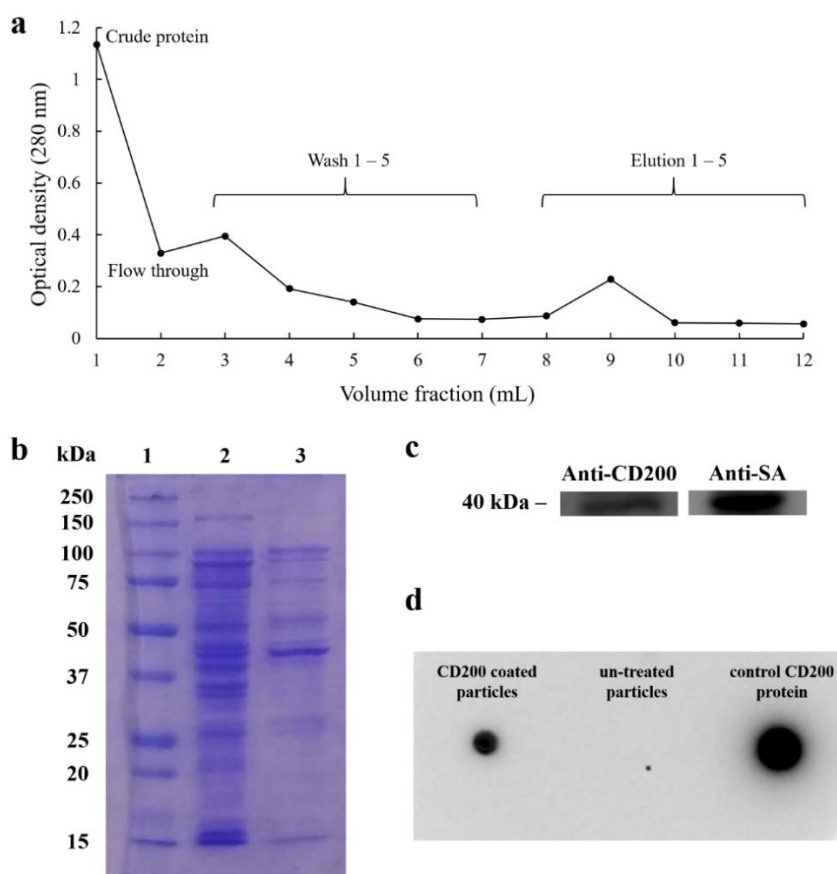
Figure 5.3. (a) Elution profile of CD200-SA fusion protein purified by Ni-NTA resin. Wash buffer contains 10 mM imidazole and elution buffer contains 250 mM imidazole. (b) Purification of human CD200-SA protein using HisPur Ni-NTA resin. (1) All blue protein standard. (2) crude protein lysate of human CD200-SA using Rosetta competent E. coli cells, induced by 0.05 mM IPTG at room temperature for 6 h. (3) purified human CD200-SA protein. (c) Western blot of purified protein human CD200-SA with human/mouse CD200 antibody (left) and rabbit anti-streptavidin antibody (right). (d) Dot blot analysis of CD200 coated 0.56 µm particles (left), unmodified 0.56 µm particles (middle) and control CD200 protein (right) using human/mouse CD200 antibody as primary antibody.

The purified CD200-SA protein was characterized by SDS-PAGE along with the crude protein lysate induced at 0.05 mM IPTG for 6 h at room temperature. The eluted protein band at ~40 kDa (shown in lane 3 of Figure 5.3b) was close to the estimated size of CD200-SA fusion protein. The purified CD200-SA protein was further examined by Western blot analysis. As shown in Figure 5.3c, the purified fusion protein was detected by both human/mouse CD200 antibody and anti-streptavidin antibody against coreSA of CD200-SA protein. It should be noted that bovine serum albumin (BSA) was chosen to make the blocking buffer because non-fat dry milk contains biotin and it interfered with the detection of coreSA protein. Furthermore, CD200-coated particles (size = 0.56 μm) were characterized by dot blot analysis, with unmodified particles as negative control and CD200 protein as positive control (Figure 5.3d). Dot blot analysis using human/mouse CD200 antibody confirmed the attachment of CD200 protein on biotin coated particles. The dot for CD200-coated particles was a little smaller than that for control CD200 protein probably because the diffusion of nanoparticles on PVDF membrane was not as fast as the soluble protein.

5.4.2 The effect of CD200 on phagocytosis of THP-1 macrophages

First, the level of CD200R expression on THP-1 macrophages was analyzed by flow cytometry (FACS). The mean fluorescence intensity (MFI) slightly increased from 531 to 736 compared to the background control (i.e., no binding with anti-CD200R-PE) after THP-1 macrophages were treated with anti-CD200R-PE (Figure 5.4a). Our results indicated that the expression level of CD200R on THP-1 macrophages is low, which is similar to the findings of (Byrareddy et al. 2015). To assess the effect of CD200 on macrophage phagocytosis, THP-1 macrophages were treated with unmodified and CD200-coated fluorescent particles, ranging from 0.15 to 2 μm for 5 h (Figure 5.5a). As shown in Figure 5.5a, the fluorescent intensities of uncoated polystyrene particles for all four different sizes ingested by macrophages were significantly higher than the ones of CD200-coated counterparts. From the bar charts presented in Figure 5.5b, the unmodified particles had already been taken up by the THP-1 macrophages at 2 h. The fluorescence intensity did not increase much after 5 and 10 h, indicating most of the particles had been taken up by the macrophages within 2 h. For CD200-coated particles with all four sizes, CD200

acting through CD200R did suppress the phagocytic process of macrophages. The phagocytosis-resistant efficacy of CD200 retained up to 10 h. It was noticed that 2 μm microparticles were taken up much slower than the other three types of particles. They were not engulfed by the cells until 5-10 h. This was probably because the large size of microparticles delayed the phagocytosis.
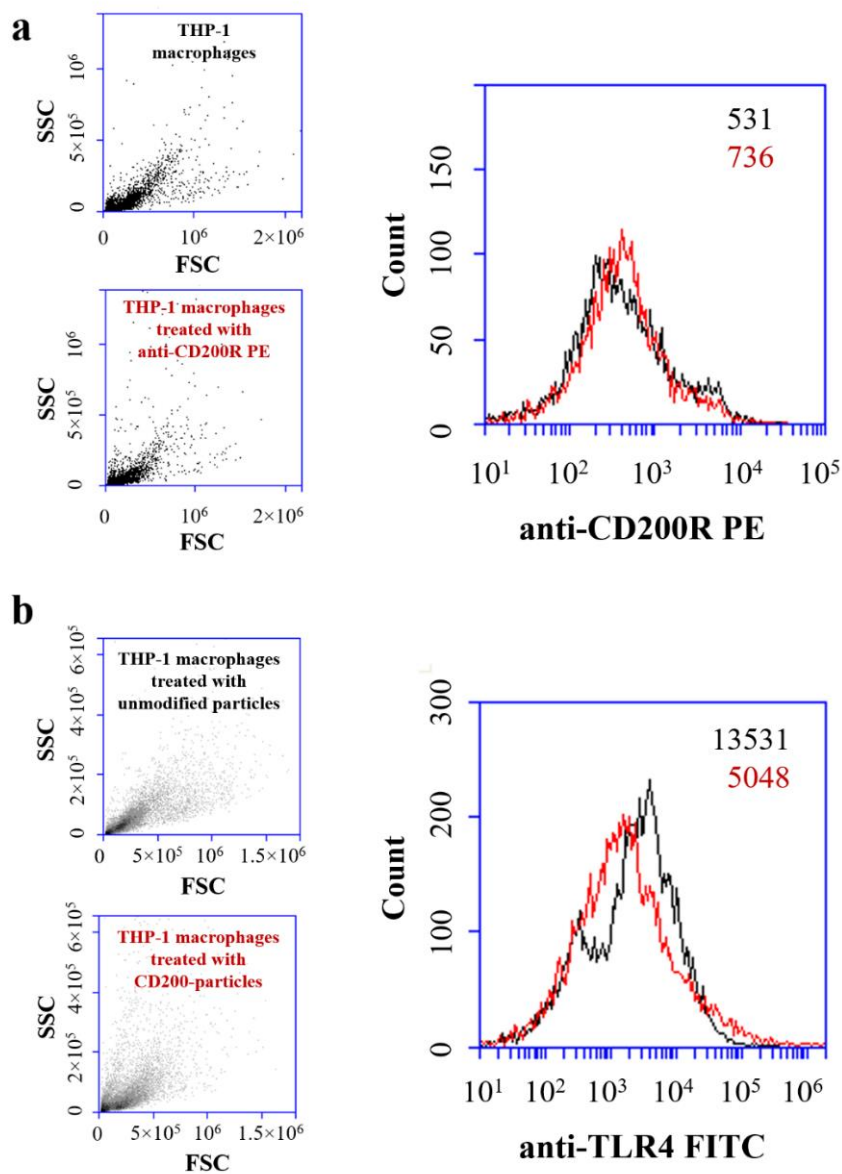
Figure 5.4 (a) The expression level of CD200R on THP-1 macrophages was analyzed by FACS. THP-1 macrophages were treated with anti-human CD200R with PE label. Non-treated macrophages were used as control. (b) FACS analysis of THP-1 macrophages engulfing control and CD200 coated 0.56 μm polystyrene particles for 2 h. FACS analysis showed that CD200 coated particles decreased TLR4 expression on THP-1 macrophages.
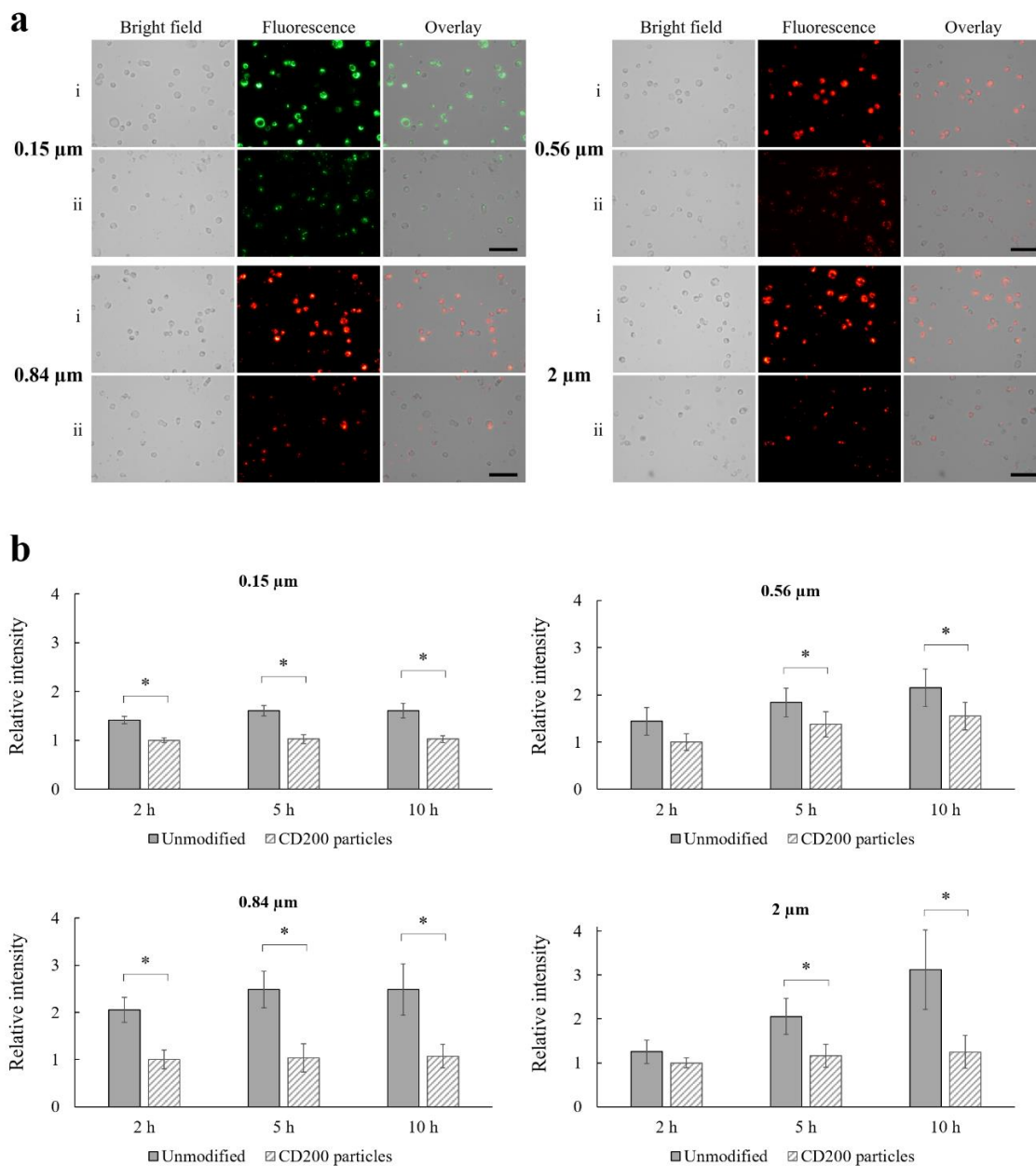
Figure 5.5. (a) Bright field, fluorescence and overlay images of THP-1 macrophages engulfing (i) unmodified and (ii) CD200-coated fluorescent polystyrene particles. Cells were incubated with 0.15, 0.56, 0.84 μm and 2 μm polystyrene particles for 5 h. Scale bar denotes 100 μm. (b) Relative fluorescence intensity of THP-1 macrophages engulfing unmodified and CD200-coated fluorescent polystyrene particles for 2, 5 and 10 h. Data were presented as mean ± standard deviation (n = 3). * denotes $p < 0.05$.

To further confirm the anti-phagocytosis effect was caused solely by CD200 (rather than partial effect from the fused SA section), THP-1 macrophages were treated with control, SA-coated, and CD200-SA coated 0.56 µm polystyrene particles. After 5 h, most unmodified and SA-coated particles were taken up by THP-1 macrophages (Figure 5.6a and b). Quantification of the fluorescence intensity showed the amount of SA-coated particles taken up by macrophages was 16.4% lower than unmodified particles. For particles coated with CD200-SA, the amount of particles taken up by macrophages was decreased by 44.7% (Figure 5.6c). The results indicated that the diminished phagocytosis of particles was indeed attributed to CD200 which was engaged with CD200R to inhibit the activation of macrophage phagocytosis.
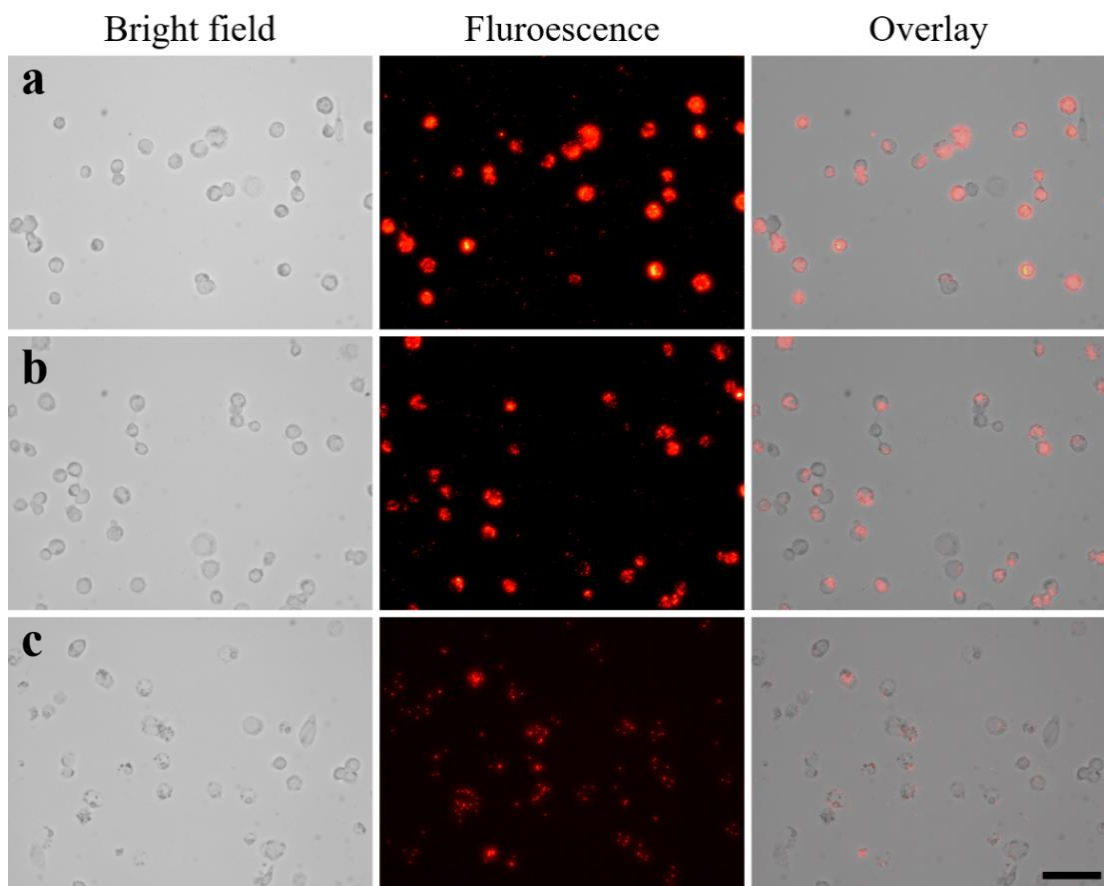

Figure 5.6. THP-1 macrophages were allowed to engulf (A) unmodified (B) SA coated (C) CD200-SA coated 0.56 µm polystyrene particles for 5 h. Scale bar denotes 100 µm.

In a previous study, CD200-deficient mice showed accelerated macrophage activation due to the absence of CD200-CD200R interaction (Hoek et al. 2000). Increased phagocytosis was also reported for microglial cells isolated from CD200-deficient mice in another study (Lyons et al. 2017). On the contrary, administration of soluble CD200-Fc fusion protein restrained phagocytosis of oligodendrocyte precursor cells by peritoneal macrophages (Hayakawa et al. 2016). These studies all suggest that CD200-CD200R engagement plays an inhibitory role in macrophage phagocytosis. One possible explanation for this functional finding is that CD200 deficiency increases expression of toll-like receptor 4 (TLR4) on microglia (Lyons et al. 2017), which can result in enhanced phagocytosis; however, soluble CD200 downregulates TLR4 expression on macrophage, leading to reduced phagocytosis. In the present study, to check whether CD200 regulates TLR4 expression on THP-1 macrophages, FACS analysis was performed on cells engulfing control particles and CD200-coated particles. As shown in Figure 5.4b, a higher MFI was observed on THP-1 macrophages challenged with untreated particles (MFI = 13,531). When THP-1 macrophages were treated with CD200-coated particles, the MFI dropped to 5,048, indicating that CD200 coating decreased TLR4 expression on THP-1 macrophages. Our results were consistent with the finding by Hayakawa et al.; when macrophages (isolated from rat peritoneal cavity) were treated with soluble CD200-Fc, surface levels of TLR4 were downregulated (Hayakawa et al. 2016).

We further examined if the material used to make the particles would affect the observed anti-phagocytic feature of CD200-coated latex particles. Zymosan particles comprised of yeast wall were selected for this study. Generally, macrophage cell lines express TLRs such as TLR2, TLR4, TLR6 on their surfaces (Ljunggren, Wallin, and Applequist 2002, Medzhitov, Preston-Hurlburt, and Janeway 1997). Macrophage phagocytosis activities can be stimulated by zymosan through TLR2-mediated signaling (Underhill et al. 1999). This will upregulate the expression of TLR2 and lead to increased secretion of inflammatory cytokines such as TNF-α and interleukin-8 (IL-8) (Sanguedolce et al. 1992). As shown in Figure 5.7, THP-1 macrophages challenged with CD200-coated FITC-zymosan particles (average size of 3 μm) exhibited much less phagocytosis than the ones treated with control FITC-zymosan particles up to 5 h. This result implied that the signal elicited by CD200-CD200R engagement could down-regulate TLR4 but also

attenuated phagocytosis stimulated by TLR2 involved with zymosan. It should be noted that after 2-h treatment, the amount of unmodified zymosan particles (3 μm) engulfed by THP-1 macrophages was much higher than the unmodified 2 μm polystyrene particles. By comparing these two types of particles with similar sizes, our results showed that zymosan particles stimulated the phagocytic activity of THP-1 macrophages within 2 h of incubation.
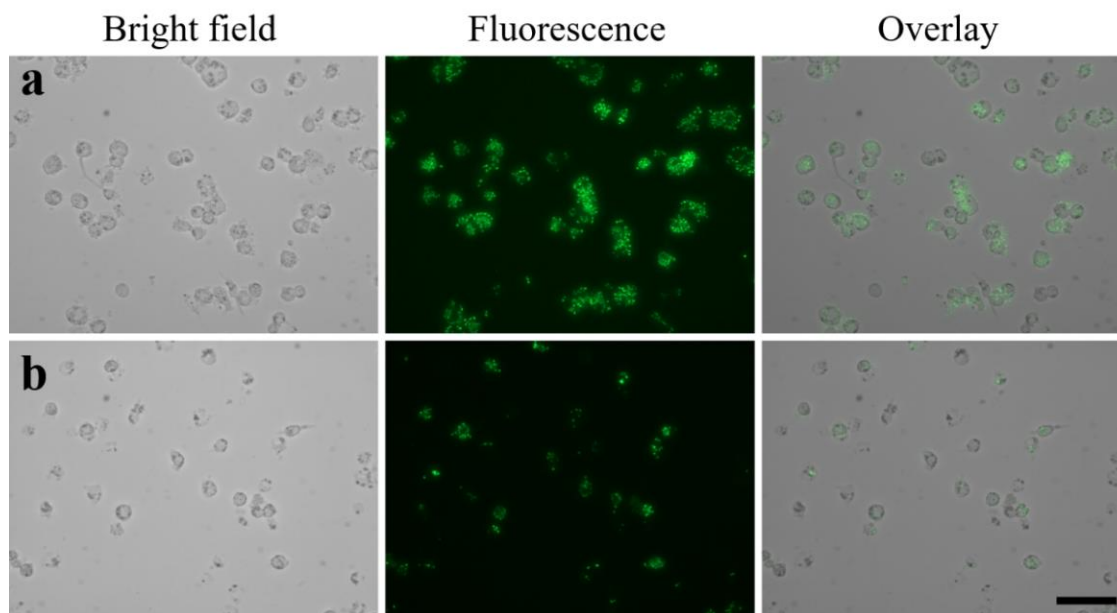
Figure 5.7. Bright field, fluorescence and overlay image of THP-1 macrophages engulfing (a) FITC-zymosan particles and (b) CD200-coated FITC-zymosan particles for 5 h. Scale bar denotes 100 μm.

Our findings and other aforementioned studies from other research groups suggest that the presence of interaction between CD200 and CD200R diminishes the engulfment capability of phagocytes. However, Chen et al. coated micro-sized poly(lactic-co-glycolic acid) (PLGA) with CD200 and found that CD200 enhanced phagocytosis of PLGA particles (average size of 7 μm) by human monocytes and murine macrophages (Chen et al. 2017). The PLGA microparticles were synthesized and conjugated with CD200-PE by that group. As noted in their study, high heterogeneity of CD200 conjugation was observed varying from particle to particle. With their determined average density of 30 molecules $μm^{-2}$, the heterogeneous distribution of CD200 on 7-μm microparticles might lead to extremely low number of molecules encountering CD200R expressed on macrophages and monocytes used in the study, and thereby not triggering antiphagocytic potency from the

engagement of CD200-CD200R. Macrophages generally engulf particles with size less than 12 µm (Kanke, Sniecinski, and Deluca 1983). However, the phagocytic activity of macrophages decreases when particle size increases (Simon and Schmid-Schonbein 1988). PLGA particles with average size of 7 µm most likely could render less phagocytosis activities than particles of smaller sizes. Indeed, Chen et al. reported that only 8% of cells phagocytosed control PLGA microparticles and 15% of cells engulfed CD200-PLGA particles after 12-h incubation. Due to extremely low phagocytic rate, the claim of 2-fold increment of phagocytosis of CD200-coated PLGA microparticles could be a concern. It has been reported that microparticles with size 2-3 µm are optimal for macrophage phagocytosis (Champion, Walker, and Mitragotri 2008, Tabata and Ikada 1988). Furthermore, nanoparticles are generally easier to be delivered to a greater portion of a macrophage population (Pacheco, White, and Sulchek 2013). In this study, the sizes of control particles (including polystyrene and zymosan) ranged from 0.15 to 3 µm. According to Figure 5.5a and Figure 5.7, the percentage of cells phagocytosed untreated micro/nanoparticles was in the range of 70-90%. With such high rate of phagocytosis, the antiphagocytic effect attributed to CD200-CD200R interaction could be firmly determined. Since the biotinylated fluorescent polystyrene particles used in this study were purchased from a vendor with uniform distribution of fluorescence and biotin, there was no concern of heterogeneity of CD200 in contact with CD200R on macrophages. Taking the 0.56 µm polystyrene particle as an example, the surface density of CD200 coated on it was calculated to be 564 ± 86 molecules μm^{-2}, which should be sufficient over the threshold value to engage with CD200R and lead to reduced phagocytosis.

5.4.3. The effect of CD200 on IL-6 and TNF-α secretion from THP-1 macrophages.

Macrophages can generally be activated by treating cells with lipopolysaccharide (LPS) or interferon-gamma (IFN-γ). However, in this study, THP-1 macrophages were not activated to simplify the experiment. The effect of CD200 coating on level of proinflammatory cytokine IL-6 and TNF-α secretion was shown in Figure 5.8a. Macrophages treated with CD200-coated 0.56 µm nanoparticles secreted 26.1% less TNF-α than unmodified nanoparticles (Figure 5.7a). The level of TNF-α detected in the present study was much higher than IL-6 detected. Although THP-1 macrophages treated with

CD200-coated nanoparticles secreted 26.9% less IL-6 than unmodified nanoparticles, the IL-6 secretion level of was low to start with (~30 pg mL^{-1}) (Figure 5.7b). In this study, the inhibition of IL-6 and TNF-α secretion level was not as dramatic as previously reported by (Kim et al. 2014), probably because the THP-1 macrophages in the study were not activated. The level of proinflammatory cytokines, especially IL-6, was low to start with. Compared to literature, Pietila et al. reported 1763.5 pg mL^{-1} TNF-α secreted from unactivated THP-1 macrophages, and it increased to 5002.3 and 2510.3 pg mL^{-1} after activation by LPS and IFN-γ, respectively (Pietilä et al. 2012). Li et al. reported low production of IL-6 from THP-1 macrophages (~50 pg mL^{-1}) (Li et al. 2014), which was similar to the findings of this study. In short, our findings indicated that coating of CD200 on nanoparticles decreased the level of TNF-α and IL-6 secretion from THP-1 macrophages.
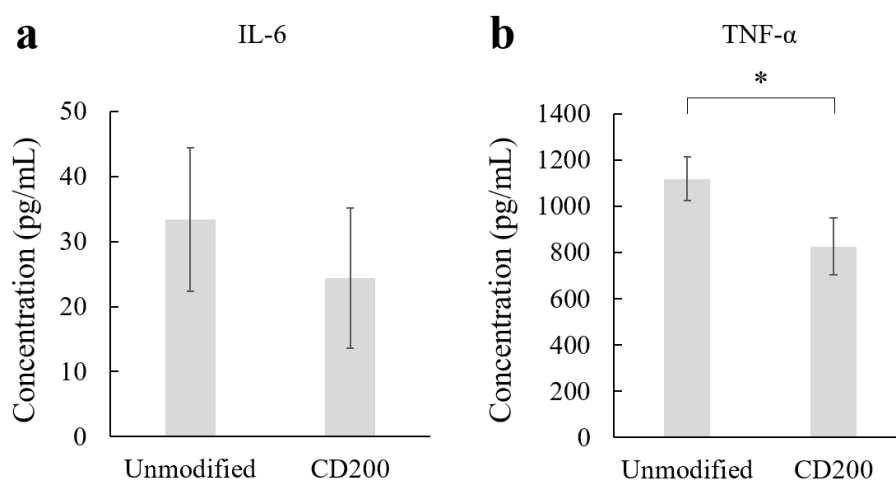
Figure 5.8. THP-1 macrophages were allowed to engulf unmodified and CD200 coated 0.56 μm polystyrene particles for 18 h. After 18 h, culture media were collected and concentrations of (a) IL-6 and (b) TNF-α were measured by commercial ELISA kits. Data were presented as mean ± standard deviation (n = 3). * denotes $p = 0.006$.

5.5 Conclusion

A plasmid encoding CD200 extracellular domain and coreSA was constructed. CD200-SA fusion protein was expressed by bacterial transformation and IPTG induction. Surface modification of CD200 reduced macrophage phagocytosis of polystyrene particles ranging from 0.15 to 2 μm and zymosan particles with size of 3 μm. The expression of

TLR-4 on THP-1 macrophages was down-regulated after treating cells with CD200-coated particles. Secretion of IL-6 and TNF-α from THP-1 macrophages was decreased when cells were treated with CD200-coated particles compared to unmodified particles. All in all, surface modification of micro/nanoparticles with CD200 can potentially be used in therapeutic particle delivery in order to evade immune surveillance and enhance delivery efficiency.

5.6 References

Barclay, A. Neil, Gavin J. Wright, Gary Brooke, and Marion H. Brown. 2002. "CD200 and membrane protein interactions in the control of myeloid cells." *Trends in Immunology* 23 (6):285-290.

Bartlett, D. W., H. Su, I. J. Hildebrandt, W. A. Weber, and M. E. Davis. 2007. "Impact of tumor-specific targeting on the biodistribution and efficacy of siRNA nanoparticles measured by multimodality in vivo imaging." *Proc. Natl. Acad. Sci. U. S. A.* 104 (39):15549-54.

Byrareddy, S. N., D. Little, A. E. Mayne, F. Villinger, and A. A. Ansari. 2015. "Phenotypic and Functional Characterization of Monoclonal Antibodies with Specificity for Rhesus Macaque CD200, CD200R and Mincle." *PLoS One* 10 (10):e0140689.

Champion, Julie A., Amanda Walker, and Samir Mitragotri. 2008. "Role of particle size in phagocytosis of polymeric microspheres." *Pharmaceutical research* 25 (8):1815-1821.

Chen, Esther Y., Shu-Hui Chu, Lanny Gov, Yoon Kyung Kim, Melissa B. Lodoen, Andrea J. Tenner, and Wendy F. Liu. 2017. "CD200 modulates macrophage cytokine secretion and phagocytosis in response to poly(lactic-co-glycolic acid) microparticles and films." *J. Mater. Chem. B* 5 (8):1574-1584.

Dick, A. D., C. Broderick, J. V. Forrester, and G. J. Wright. 2001. "Distribution of OX2 antigen and OX2 receptor within retina." *Invest. Ophthalmol. Vis. Sci.* 42 (1):170-6.

Dubel, S., F. Breitling, R. Kontermann, T. Schmidt, A. Skerra, and M. Little. 1995. "Bifunctional and multimeric complexes of streptavidin fused to single chain antibodies (scFv)." *J. Immunol. Methods* 178 (2):201-9.

Elhelu, Mohamed A. 1983. "The Role of Macrophages in Immunology." *Journal of the National Medical Association* 75 (3):314-317.

Gabizon, A. A., Y. Barenholz, and M. Bialer. 1993. "Prolongation of the circulation time of doxorubicin encapsulated in liposomes containing a polyethylene glycol-derivatized phospholipid: pharmacokinetic studies in rodents and dogs." *Pharm. Res.* 10 (5):703-8.

Gorczynski, R. M., M. S. Cattral, Z. Chen, J. Hu, J. Lei, W. P. Min, G. Yu, and J. Ni. 1999. "An immunoadhesin incorporating the molecule OX-2 is a potent immunosuppressant that prolongs allo- and xenograft survival." *J. Immunol.* 163 (3):1654-60.

Gorczynski, R. M., K. Yu, and D. Clark. 2000. "Receptor engagement on cells expressing a ligand for the tolerance-inducing molecule OX2 induces an immunoregulatory population that inhibits alloreactivity in vitro and in vivo." *J. Immunol.* 165 (9):4854-60.

Hatakeyama, Hiroto, Hidetaka Akita, and Hideyoshi Harashima. 2013. "The Polyethyleneglycol Dilemma: Advantage and Disadvantage of PEGylation of Liposomes for Systemic Genes and Nucleic Acids Delivery to Tumors." *Biological and Pharmaceutical Bulletin* 36 (6):892-899.

Hayakawa, K., L. D. Pham, J. H. Seo, N. Miyamoto, T. Maki, Y. Terasaki, S. Sakadzic, D. Boas, K. van Leyen, C. Waeber, K. W. Kim, K. Arai, and E. H. Lo. 2016. "CD200 restrains macrophage attack on oligodendrocyte precursors via toll-like receptor 4 downregulation." *J. Cereb. Blood Flow. Metab.* 36 (4):781-93.

Hoek, R. M., S. R. Ruuls, C. A. Murphy, G. J. Wright, R. Goddard, S. M. Zurawski, B. Blom, M. E. Homola, W. J. Streit, M. H. Brown, A. N. Barclay, and J. D. Sedgwick. 2000. "Down-regulation of the macrophage lineage through interaction with OX2 (CD200)." *Science* 290 (5497):1768-71.

Kanke, M., I. Sniecinski, and P. P. Deluca. 1983. "Interaction of Microspheres with Blood Constituents: I. Uptake of Polystyrene Spheres by Monocytes and Granulocytes and Effect on Immune Responsiveness of Lymphocytes." *PDA J. Pharm. Sci. Technol.* 37 (6):210-217.

Kawasaki, Brian T., and William L. Farrar. 2008. "Cancer stem cells, CD200 and immunoevasion." *Trends in Immunology* 29 (10):464-468.

Kim, Y. K., R. Que, S. W. Wang, and W. F. Liu. 2014. "Modification of biomaterials with a self-protein inhibits the macrophage response." *Adv. Healthc. Mater.* 3 (7):989-94.

Knop, K., R. Hoogenboom, D. Fischer, and U. S. Schubert. 2010. "Poly(ethylene glycol) in drug delivery: pros and cons as well as potential alternatives." *Angew Chem Int Ed Engl* 49 (36):6288-308.

Li, C. C., Y. C. Hou, C. L. Yeh, and S. L. Yeh. 2014. "Effects of eicosapentaenoic acid and docosahexaenoic acid on prostate cancer cell migration and invasion induced by tumor-associated macrophages." *PLoS One* 9 (6):e99630.

Ljunggren, Hans-Gustaf, Robert P. A. Wallin, and Steven E. Applequist. 2002. "Variable expression of Toll-like receptor in murine innate and adaptive immune cell lines." *International Immunology* 14 (9):1065-1074.

Lyons, A., A. M. Minogue, R. S. Jones, O. Fitzpatrick, J. Noonan, V. A. Campbell, and M. A. Lynch. 2017. "Analysis of the Impact of CD200 on Phagocytosis." *Mol. Neurobiol.* 54 (7):5730-5739.

McMaster, W. R., and A. F. Williams. 1979. "Monoclonal antibodies to Ia antigens from rat thymus: cross reactions with mouse and human and use in purification of rat Ia glycoproteins." *Immunol. Rev.* 47:117-37.

Medzhitov, R., P. Preston-Hurlburt, and C. A. Janeway, Jr. 1997. "A human homologue of the Drosophila Toll protein signals activation of adaptive immunity." *Nature* 388 (6640):394-7.

Oh, Nuri, and Ji-Ho Park. 2014. "Endocytosis and exocytosis of nanoparticles in mammalian cells." *Int. J. Nanomedicine* 9 (Suppl 1):51-63.

Oldenborg, P. A., A. Zheleznyak, Y. F. Fang, C. F. Lagenaur, H. D. Gresham, and F. P. Lindberg. 2000. "Role of CD47 as a marker of self on red blood cells." *Science* 288 (5473):2051-4.

Pacheco, Patricia, David White, and Todd Sulchek. 2013. "Effects of microparticle size and Fc density on macrophage phagocytosis." *PloS one* 8 (4):e60989-e60989.

Pietilä, Mika, Siri Lehtonen, Elina Tuovinen, Kaarina Lähteenmäki, Saara Laitinen, Hannu-Ville Leskelä, Antti Nätynki, Juha Pesälä, Katrina Nordström, and Petri Lehenkari. 2012. "CD200 Positive Human Mesenchymal Stem Cells Suppress TNF-Alpha Secretion from CD200 Receptor Positive Macrophage-Like Cells." *PLoS ONE* 7 (2):e31671.

Qie, Y., H. Yuan, C. A. von Roemeling, Y. Chen, X. Liu, K. D. Shih, J. A. Knight, H. W. Tun, R. E. Wharen, W. Jiang, and B. Y. Kim. 2016. "Surface modification of nanoparticles enables selective evasion of phagocytic clearance by distinct macrophage phenotypes." *Sci. Rep.* 6:26269.

Rattan, Rahul, Somnath Bhattacharjee, Hong Zong, Corban Swain, Muneeb A. Siddiqui, Scott H. Visovatti, Yogendra Kanthi, Sajani Desai, David J. Pinsky, and Sascha N. Goonewardena. 2017. "Nanoparticle-macrophage interactions: A balance between clearance and cell-specific targeting." *Bioorganic & Medicinal Chemistry* 25 (16):4487-4496.

Remaut, K., B. Lucas, K. Braeckmans, J. Demeester, and S. C. De Smedt. 2007. "Pegylation of liposomes favours the endosomal degradation of the delivered phosphodiester oligonucleotides." *J. Control. Release* 117 (2):256-66.

Rodriguez, Pia L., Takamasa Harada, David A. Christian, Diego A. Pantano, Richard K. Tsai, and Dennis E. Discher. 2013. "Minimal "Self" Peptides That Inhibit Phagocytic Clearance and Enhance Delivery of Nanoparticles." *Science* 339 (6122):971-975.

Rosenblum, M. D., E. B. Olasz, K. B. Yancey, J. E. Woodliff, Z. Lazarova, K. A. Gerber, and R. L. Truitt. 2004. "Expression of CD200 on epithelial cells of the murine hair follicle: a role in tissue-specific immune tolerance?" *J. Invest. Dermatol.* 123 (5):880-7.

Salehi, N., and C. A. Peng. 2016. "Purification of CD47-streptavidin fusion protein from bacterial lysate using biotin-agarose affinity chromatography." *Biotechnol Prog* 32 (4):949-58.

Sanguedolce, M. V., C. Capo, P. Bongrand, and J. L. Mege. 1992. "Zymosan-stimulated tumor necrosis factor-alpha production by human monocytes. Down-modulation by phorbol ester." *J. Immunol.* 148 (7):2229-36.

Simon, S. I., and G. W. Schmid-Schonbein. 1988. "Biophysical aspects of microsphere engulfment by human neutrophils." *Biophys. J.* 53 (2):163-73.

Tabata, Y., and Y. Ikada. 1988. "Effect of the size and surface charge of polymer microspheres on their phagocytosis by macrophage." *Biomaterials* 9 (4):356-62.

Taylor, Neil, Karen McConachie, Claudia Calder, Rosemary Dawson, Andrew Dick, Jonathon D. Sedgwick, and Janet Liversidge. 2005. "Enhanced tolerance to autoimmune uveitis in CD200-deficient mice correlates with a pronounced Th2 switch in response to antigen challenge." *J. Immunol.* 174 (1):143-154.

Underhill, D. M., A. Ozinsky, A. M. Hajjar, A. Stevens, C. B. Wilson, M. Bassetti, and A. Aderem. 1999. "The Toll-like receptor 2 is recruited to macrophage phagosomes and discriminates between pathogens." *Nature* 401 (6755):811-5.

Wright, G. J., M. J. Puklavec, A. C. Willis, R. M. Hoek, J. D. Sedgwick, M. H. Brown, and A. N. Barclay. 2000. "Lymphoid/neuronal cell surface OX2 glycoprotein recognizes a novel receptor on macrophages implicated in the control of their function." *Immunity* 13 (2):233-42.

Yoo, J. W., E. Chambers, and S. Mitragotri. 2010. "Factors that control the circulation time of nanoparticles in blood: challenges, solutions and future prospects." *Curr. Pharm. Des.* 16 (21):2298-307.

Chapter 6. Decreased Macrophage Attachment on CD200 Coated Surfaces Supported by Polydopamine Film

6.1 Abstract

CD200 is an anti-inflammatory transmembrane glycoprotein in the immunoglobin superfamily. It interacts with its receptor CD200R which is expressed on the surface myeloid cells such as macrophages and neutrophils. The interaction of CD200-CD200R has shown to inhibit macrophage inflammatory response to foreign materials. polyethylene glycol (PEG) is a hydrophilic polymer used to reduce non-specific protein adsorption on biomaterial surface. The purpose of this study is to create a PEG/CD200 co-immobilized biomaterial surface through polydopamine coating to reduce macrophage cell attachment as well as inflammatory cytokine secretion by macrophages. In this study, tissue-culture treated polystyrene surface was modified with biotin-PEG through polydopamine coating. CD200-streptavidin fusion protein was then immobilized onto the biotin-functionalized surface through the high affinity between biotin and streptavidin. J774A.1 macrophages were seeded on PEG/CD200 co-immobilized surface to evaluate the effect of PEG/CD200 on macrophage attachment. The effect of CD200 on proinflammatory cytokine secretion from were measured by enzyme-linked immunosorbent assay. Our results showed that PEG/CD200 co-immobilized surface showed the effect of delayed macrophage attachment for 9 to 12 hours. The amount of IL-6 and TNF-α secreted from J774A.1 macrophages on PEG/CD200 surface was reduced by 36.3% and 32.4%, respectively.

6.2 Introduction

Implantation of medical device into human body initiates a series of inflammatory responses called foreign body reactions (Fournier et al. 2003). Foreign body reactions include protein and platelet adsorption, macrophage adhesion, formation of foreign body giant cells, etc (Anderson, Rodriguez, and Chang 2008). Foreign body reaction is one of the major causes of medical device failure, and it affects the lifetime and function of the device. Upon implantation, serum proteins tend to adsorb non-specifically onto the

material surface, followed by the infiltration of inflammatory cells such as macrophages and neutrophils (Anderson, Rodriguez, and Chang 2008).

Macrophages are myeloid cells that can detect foreign invaders. They are able to engulf microbes and foreign particles in the process of phagocytosis. Macrophages play essential roles in foreign body reactions. In the early stage of implantation, non-specific protein adsorption causes acute inflammation, and macrophages are recruited to the surface of medical device (Tang and Eaton 1993, Tang et al. 1996). Macrophages can fuse and form giant cells on biomaterial surface when they are activated (Zhao et al. 1991). Activated macrophages secret a wide array of cytokines: they include TNF-α, interleukin 1 beta (IL-1β), interleukin-6 (IL-6), interleukin-10 (IL-10), transforming growth factor β (TGF-β), etc (Jones et al. 2007, Fujiwara and Kobayashi 2005). Adherent macrophages and foreign body giant cells could cause biomaterial degradation, cracking of implanted device, fibrous thickening, etc (Anderson, Rodriguez, and Chang 2008, Zhao et al. 1990, Sutherland et al. 1993, Zhao et al. 1991, Stark, Gobel, and Jaeger 1990). Therefore, preventing inflammatory cell attachment is crucial in the design of biomaterial surface.

Traditionally, polyethylene glycol (PEG) is a widely used hydrophilic polymer for reducing non-specific adsorption of proteins and platelets on the biomaterial surface (Hashi et al. 2010, VandeVondele, Voros, and Hubbell 2003). The hydrophilic chains of PEG can expel the proteins and prevent cell adhesion. Surface immobilized PEG has shown reduce non-specific protein adsorption as well as platelet adhesion (Uchida et al. 2000, Park et al. 2000). PEG has also been used as a space linker together with anticoagulants to enhance the anticoagulant effect (Hashi et al. 2010, VandeVondele, Voros, and Hubbell 2003). However, PEG does not completely eliminate the problem of protein adsorption. Also, the effect of PEG at reducing macrophage activation is moderate; in some cases, PEG may even promote proinflammatory cytokine secretion of macrophages (Lynn, Kyriakides, and Bryant 2010). PEG coated surface has been made through polydopamine coating to prevent cell attachment (M. Hamming and B. Messersmith 2008). Dopamine self-polymerizes to create an ultrathin polydopamine film at the pH of 8.5 by dip coating objects into the dopamine solution (Lee et al. 2007). The catechol group of polydopamine film is able to react with amine or thiol functional

groups by simply immersing the polydopamine film into a solution containing amine or thiol functional groups (Lee et al. 2007). This makes the polydopamine film a versatile platform for surface modification.

More recently, naturally expressed self-proteins have been incorporated onto biomaterial surface to reduce inflammatory cell attachment and activation. CD47, also known as integrin-associated protein (IAP), is a marker of self protein that regulates macrophage phagocytosis by the interaction of CD47with its receptor SIRPα which is expressed on the surface of macrophage (Oldenborg et al. 2000). Stachelek et al. showed CD47 immobilized surfaces can successfully reduce the adhesion of inflammatory cells and platelets through CD47-SIRPα interaction (Stachelek et al. 2011). Another self protein CD200, also known as OX-2, is an anti-inflammatory transmembrane glycoprotein in the immunoglobin superfamily (Clark et al. 1985). CD200 interacts with CD200 receptor (CD200R), which is also expressed on the surface of myeloid cells such as macrophages, neutrophils, and microglia (Hoek et al. 2000, Wright et al. 2000). CD200-CD200R interaction has shown to transmit an inhibitory signal that downregulates macrophage activity (Hoek et al. 2000). Kim et al. have coated CD200 on biomaterial surface for reduced inflammatory cell responses (Kim et al. 2014). In their study, reduced macrophage activation was observed on CD200 modified surface.

The purpose of this study is to create a PEG/CD200 co-immobilized surface through polydopamine film. The purpose of co-immobilizing PEG spacer and CD200 is two-fold: PEG is able to physically reduce protein adsorption, while CD200 is able to reduce inflammatory cell responses through CD200-CD200R interaction. Macrophages will be seeded onto PEG/CD200 modified surface to evaluate the effect of PEG/CD200 on macrophage attachment. The effect of PEG/CD200 on IL-6 and TNF-α secretion from macrophages will be also be evaluated by enzyme-linked immunosorbent assay (ELISA).

6.3 Materials and Methods
6.3.1 Materials

Plasmid encoding CD200 and streptavidin gene was prepared as described in chapter 5. Tris (hydroxymethyl) aminomethane (Tris base), 1× phosphate buffer saline (PBS), B-PER bacterial protein extraction reagent, Halt protease inhibitor, lysozyme,

DNase I, HisPur Ni-NTA Resin, DMEM (Dulbecco's Modified Eagle Medium), Tween-20, mouse IL-6 ELISA Ready-SET-Go!™ kit and mouse TNF-alpha ELISA Ready-SET-Go!™ kit were purchased from were purchased from Thermo Fisher Scientific (Waltham, MA, USA). Dopamine hydrochloride, Ampicillin, Isopropyl β-D-1-thiogalactopyranoside (IPTG) and penicillin-streptomycin were purchased from Sigma-Aldrich (St. Louis, MO, USA). Biotin-PEG-NH$_2$ (MN 5000) was purchased from NanoCS (New York, NY, USA). Rosetta™(DE3) competent cells were purchased from Merck Millipore (Darmstadt, Germany). Imidazole and sodium chloride (NaCl) was purchased from ACROS (Fair Lawn, NJ, USA). J774A.1 macrophages were kindly provided by Professor Tanya Miura, University of Idaho. Anti-mouse CD200R antibody and anti-mouse CD200 antibody were purchased from BioLegend (San Diego, CA, USA).

6.3.2 Preparation of CD200 and PEG/CD200 coated surface

To make CD200 immobilized surface, 2 mg/mL dopamine was dissolved in 10 mM Tris buffer, and 2 mL of the solution was added into each well of the 6-well plate. The 6-well plate was kept at room temperature for overnight. After the formation of polydopamine film, the 6-well plate was rinsed extensively with DI water. 1 mL of 5 mg/mL biotin-PEG-NH$_2$ solution was added into each well of the 6-well plate. The 6-well plate was shaken at 50 rpm, room temperature for overnight. The biotin-PEG coated 6-well plate surface was washed with 1× PBS for three times. Expression and purification of CD200-SA protein was prepared as described in section 5.3.3. 1 mL of purified CD200-SA protein was added into the biotinylated 6-well plate. The plate was mildly shaken at 50 rpm, 4°C for 30 min. The protein was removed, and the 6-well plates were washed with 1× PBS for three times. The PEG/CD200 coated 6-well plate surface was sterilized with 70% ethanol for 15 min.

6.3.3 Macrophage cell attachment study on PEG/CD200 surface

J774A.1 macrophages were inoculated onto bare, polydopamine, and PEG/CD200 modified 6-well plate surface at 1.0 x 10^4 cells/cm^2 and incubated at 37°C in a 5% CO$_2$ incubator (Forma 310; Thermo Fisher Scientific, Waltham, MA, USA). J774A.1 macrophages were cultured with DMEM supplemented with 10% FBS and 1% penicillin-

streptomycin. Bright field images were taken with a Leica DMi8 microscope equipped with Leica EC3 camera (Leica Microsystems, Wetzlar, Germany). The unattached cells were collected and counted using a hemocytometer at 3 h, 6 h, 12 h, and 24 h, respectively.

J774A.1 macrophages were treated with anti-mouse CD200R antibody at the concentration of 0.5, 1, 2 µg/million cells to block CD200-CD200R signal. Briefly, cells were incubated in 1× PBS with 3% BSA containing anti-mouse CD200R antibody for 30 min. Cells were washed 3 times by centrifugation at 400× g for 5 min. Un-treated macrophages and CD200R blocked macrophages were seeded on PEG/CD200 coated 6-well plates at 1.0 x 10^4 cells/cm^2. Cell attachment behavior was observed by light microscope. CD200 coated 6-well plates was also treated with anti-mouse CD200 antibody at the concentration of 5 µg/well and 1 µg/well to block CD200-CD200R signal. The surfaces were washed with 1× PBS, and J774A.1 macrophages were seeded on PEG/CD200 coated and CD200 blocked 6-well plate surfaces at 1.0 x 10^4 cells/cm^2.

6.3.4 Proinflammatory secretion from macrophages on PEG/CD200 surface

To assess the effect of CD200 on proinflammatory cytokine secretion, J774A.1 macrophages were seed on bare, polydopamine, PEG and PEG/CD200 modified 6-well plate surfaces at 1.0 x 10^4 cells/cm^2. After the cells were cultured for 24 h, culture medium was collected for the detection of IL-6 and TNF-α by enzyme-linked immunosorbent assay (ELISA) kits. 100 µL coating buffer containing IL-6 and TNF-α capture antibody was added to each well of the ELISA 96 well plate and incubated overnight at 4°C. After overnight, coating buffer was removed and the wells were washed 3 times with washing buffer (1× PBS with 0.05% Tween-20). 200 µL 1× ELISPOT diluent was added to each well and incubated at room temperature for 1 h. The wells were washed 3 times with washing buffer, and 100 µL of J774A.1 culture medium collected above, IL-6 standards and TNF-α standards were added to each well and incubated at room temperature for 2 h. After 2 h, samples and standards were removed, and the wells were washed 3 times with washing buffer. 100 µL of 1× ELISPOT diluent containing IL-6 and TNF-α detection antibody was added to each well and incubated at room temperature for 1 h. After 1 h, detection antibody solutions were removed, and the wells

were washed 3 times with wash buffer. 100 µL of 1× ELISPOT diluent containing avidin-HRP was then added to each well and incubated at room temperature for 30 min. Avidin-HRP solution was removed, and the wells were washed 5 times with wash buffer. 100 µL of TMB solution was added to each well and incubated at room temperature for 15 min. The reaction was stopped with by adding 50 µL of 1 M phosphoric acid to each well, and absorbance was measured at 450 nm with a SpectraMax M2e Microplate Reader (Molecular Devices, Sunnyvale, CA, USA). The concentrations of IL-6 and TNF-α in the culture medium were quantified by IL-6 and TNF-α standard curves.

6.3.5 Statistical analysis

Statistical analysis was performed using Prism 8 software (Graphpad Software). Data were presented as mean ± standard deviation from three independent experiments. For the detection of IL-6 and TNF-α from J774A.1 macrophages on bare, polydopamine, PEG and CD200 coated surfaces by ELISA, one-way ANOVA followed by Tukey's post-hoc analysis was performed for comparisons between each group. $p < 0.05$ was considered statistically significant.

6.4 Results and Discussion

6.4.1 J774A.1 macrophage attachment study

On bare and polydopoamine control surfaces, J774A.1 macrophages attached to the surfaces within 2 to 3 h. At 3 h, most macrophages on PEG/CD200 modified surface remained unattached (Figure 6.1). Macrophages started to attach to CD200 modified 6-well plate surfaces at 6 to 9 h. A549 lung cancer cell and human MSCs were also inoculated onto CD200 immobilized surface as control cell lines (data now shown). As a result, A549 cells and MSCs attached to the surface within 2 to 3 h. The quick attachment of A549 cells and MSCs macrophages was due to the lack of CD200R on their surface. The delayed macrophage attachment effect on PEG/CD200 coated 6-well plate surface lasted up to 10 to 12 h. After 24 h, all the macrophages eventually attached to the PEG/CD200 coated surfaces. Stachelek et al. showed reduced attachment of THP-1 macrophages and HL-60 neutrophils on CD47 coated polyurethane (PU) surfaces for 3

days (Stachelek et al. 2011). The delayed macrophage attachment effect in this study does not last as long as 3 days, probably because the polystyrene 6-well plate surface facilitated cell attachment.
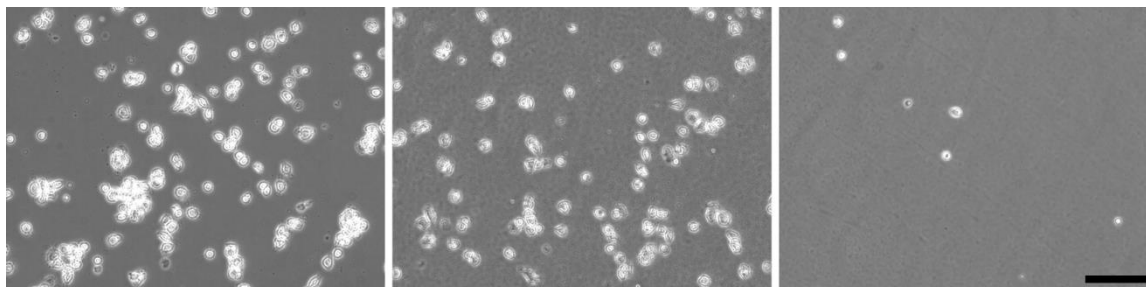

Figure 6.1. J774A.1 macrophages were seeded on (left) bare (middle) polydopamine and (right) PEG/CD200 coated surfaces for 3 h. Scale bar denotes 100 μm.

Anti-human CD200 and anti-human CD200R antibodies were used to block the signal of CD200-CD200R. J774A.1 macrophages were treated with 0.5, 1 and 2 μg anti-CD200R per million cells (Figure 6.2A). As a result, 0.5 μg/million cells still had the delayed effect, while macrophages treated with 1 and 2 μg anti-CD200R per million cells attached to CD200 surface within 3 h. CD200 immobilized surface was also treated with 1 and 5 μg anti-CD200 antibody to block the CD200-CD200R signal (Figure 6.2B). As a result, more macrophages attached to the CD200 surface treated with 5 μg anti-CD200 than the surface with 1 μg per well within 3 h. This further confirmed the decreased macrophage attachment was due to CD200-CD200R interaction.
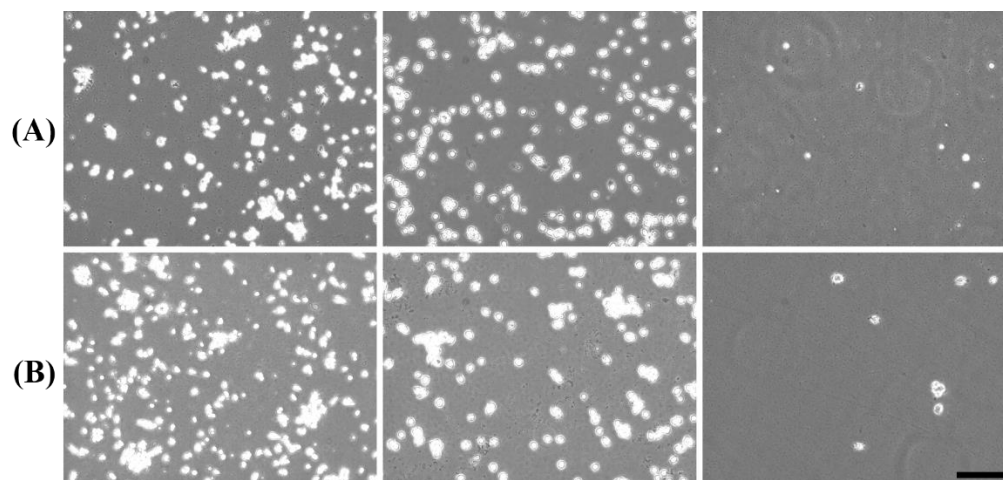
Figure 6.2. (A) J774A.1 macrophages were treated with anti-CD200 antibody at 2, 1 and 0.5 μg/million cells (from left to right) and then seeded on PEG/CD200 coated 6-well plate surfaces for 3 h. (B) PEG/CD200 coated 6-well plate surface was treated with 5, 1 and 0 μg anti-CD200 antibody per well (from left to right). J774A.1 macrophages were then seeded onto the anti-CD200 treated wells for 3 h. Scale bar denotes 100 μm.

6.4.2 IL-6 and TNF-α secretion from J774A.1 Macrophage on PEG/CD200 surface

The level of proinflammatory cytokine IL-6 and TNF-α secretion from J774A.1 macrophages was assessed by ELISA (Figure 6.3). J774A.1 macrophages in this study was not activated in order to simplify the experiment. Macrophages seeded on PEG/CD200 secreted 36.3% less IL-6 and 32.4% less TNF-α than the bare control group. It should be noted that surface modification of PEG slightly increased the secretion of IL-6 from J774A.1 macrophages. Kim et al. seeded bone marrow derived macrophages (BMDM) on CD200 coated surface (Kim et al. 2014). In their study, the secretion of IL-6 and TNF-α was significantly inhibited for both un-activated and activated macrophages on CD200 coated surface. They reported ~70% reduced TNF-α secretion from CD200 coated surface compared to control polystyrene surface. In another study, CD200 positive MSCs with was co-cultured with THP-1 macrophages to suppress TNF- α secretion (Pietilä et al. 2012). In their study, the level of TNF- α was decreased by ~50% from IFN-γ activated macrophages. In this study, 32.4% decreased TNF- α from J774A.1 macrophages was comparable to the 50% decrease from THP-1 macrophages. In short, our findings indicate that PEG/CD200 coating decreased the level of secreted IL-6 and TNF-α from J774A.1 macrophages.

(A)

IL-6

(B)

TNF-α
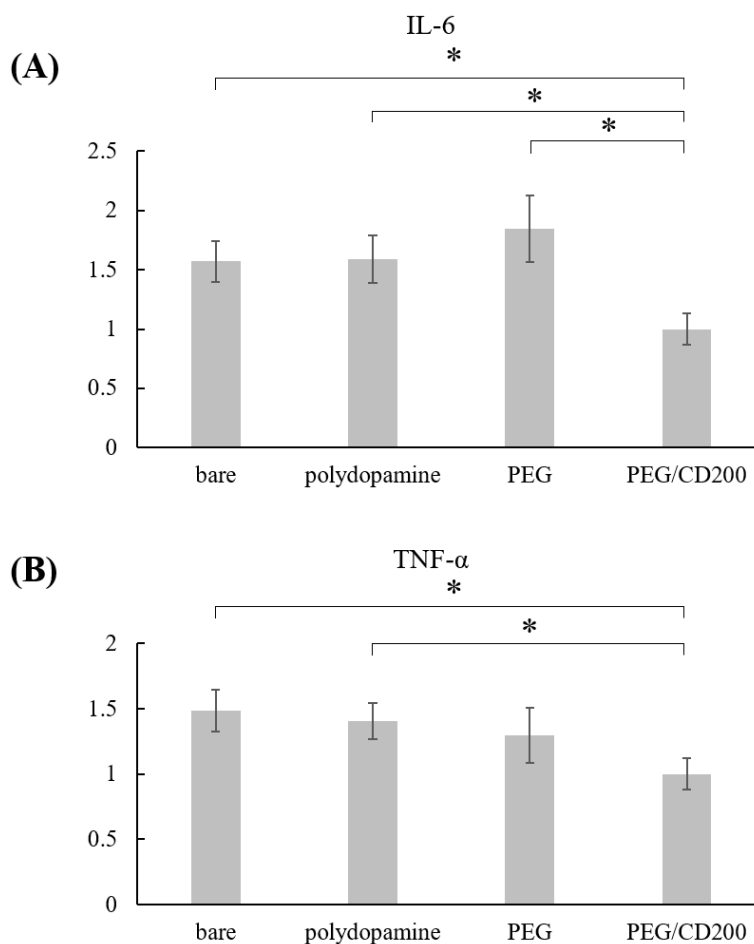
Figure 6.3. The level of (A) IL-6 and (B) TNF-α secretion from bare, polydopamine, PEG and PEG/CD200 surfaces. Each value is expressed as the mean ± standard deviation (n = 3). The amount of secreted proinflammatory cytokines were normalized to macrophages seeded on PEG/CD200 coated 6-well plate surface. * denotes $p <0.05$.

6.5 Conclusion

CD200-SA fusion protein was expressed by bacterial transformation and IPTG induction. A PEG/CD200 co-immobilized biomaterial surface was fabricated via polydopamine chemistry. PEG/CD200 coated surface was able to delay macrophage cell attachment for 9 to 12 hours. The secretion of IL-6 and TNF-α from macrophages was reduced on PEG/CD200 surface.

6.6 References

Anderson, James M., Analiz Rodriguez, and David T. Chang. 2008. "Foreign body reaction to biomaterials." *Seminars in immunology* 20 (2):86-100.

Clark, M. J., J. Gagnon, A. F. Williams, and A. N. Barclay. 1985. "MRC OX-2 antigen: a lymphoid/neuronal membrane glycoprotein with a structure like a single immunoglobulin light chain." *Embo j* 4 (1):113-8.

Fournier, E., C. Passirani, C. N. Montero-Menei, and J. P. Benoit. 2003. "Biocompatibility of implantable synthetic polymeric drug carriers: focus on brain biocompatibility." *Biomaterials* 24 (19):3311-31.

Fujiwara, N., and K. Kobayashi. 2005. "Macrophages in inflammation." *Curr Drug Targets Inflamm Allergy* 4 (3):281-6.

Hashi, C. K., N. Derugin, R. R. Janairo, R. Lee, D. Schultz, J. Lotz, and S. Li. 2010. "Antithrombogenic modification of small-diameter microfibrous vascular grafts." *Arterioscler Thromb Vasc Biol* 30 (8):1621-7.

Hoek, R. M., S. R. Ruuls, C. A. Murphy, G. J. Wright, R. Goddard, S. M. Zurawski, B. Blom, M. E. Homola, W. J. Streit, M. H. Brown, A. N. Barclay, and J. D. Sedgwick. 2000. "Down-regulation of the macrophage lineage through interaction with OX2 (CD200)." *Science* 290 (5497):1768-71.

Jones, J. A., D. T. Chang, H. Meyerson, E. Colton, I. K. Kwon, T. Matsuda, and J. M. Anderson. 2007. "Proteomic analysis and quantification of cytokines and chemokines from biomaterial surface-adherent macrophages and foreign body giant cells." *J Biomed Mater Res A* 83 (3):585-96.

Kim, Y. K., R. Que, S. W. Wang, and W. F. Liu. 2014. "Modification of biomaterials with a self-protein inhibits the macrophage response." *Adv. Healthc. Mater.* 3 (7):989-94.

Lee, H., S. M. Dellatore, W. M. Miller, and P. B. Messersmith. 2007. "Mussel-inspired surface chemistry for multifunctional coatings." *Science* 318 (5849):426-30.

Lynn, A. D., T. R. Kyriakides, and S. J. Bryant. 2010. "Characterization of the in vitro macrophage response and in vivo host response to poly(ethylene glycol)-based hydrogels." *J Biomed Mater Res A* 93 (3):941-53.

M. Hamming, Lesley, and Phillip B. Messersmith. 2008. *Fouling Resistant Biomimetic Poly(Ethylene Glycol) Based Grafted Polymer Coatings*. Vol. 3.

Oldenborg, P. A., A. Zheleznyak, Y. F. Fang, C. F. Lagenaur, H. D. Gresham, and F. P. Lindberg. 2000. "Role of CD47 as a marker of self on red blood cells." *Science* 288 (5473):2051-4.

Park, K., H. S. Shim, M. K. Dewanjee, and N. L. Eigler. 2000. "In vitro and in vivo studies of PEO-grafted blood-contacting cardiovascular prostheses." *J Biomater Sci Polym Ed* 11 (11):1121-34.

Pietilä, Mika, Siri Lehtonen, Elina Tuovinen, Kaarina Lähteenmäki, Saara Laitinen, Hannu-Ville Leskelä, Antti Nätynki, Juha Pesälä, Katrina Nordström, and Petri Lehenkari. 2012. "CD200 Positive Human Mesenchymal Stem Cells Suppress TNF-Alpha Secretion from CD200 Receptor Positive Macrophage-Like Cells." *PLoS ONE* 7 (2):e31671.

Stachelek, S. J., M. J. Finley, I. S. Alferiev, F. Wang, R. K. Tsai, E. C. Eckells, N. Tomczyk, J. M. Connolly, D. E. Discher, D. M. Eckmann, and R. J. Levy. 2011. "The effect of CD47 modified polymer surfaces on inflammatory cell attachment and activation." *Biomaterials* 32 (19):4317-26.

Stark, G. B., M. Gobel, and K. Jaeger. 1990. "Intraluminal cyclosporine A reduces capsular thickness around silicone implants in rats." *Ann Plast Surg* 24 (2):156-61.

Sutherland, K., J. R. Mahoney, 2nd, A. J. Coury, and J. W. Eaton. 1993. "Degradation of biomaterials by phagocyte-derived oxidants." *J Clin Invest* 92 (5):2360-7.

Tang, L., and J. W. Eaton. 1993. "Fibrin(ogen) mediates acute inflammatory responses to biomaterials." *J Exp Med* 178 (6):2147-56.

Tang, L., T. P. Ugarova, E. F. Plow, and J. W. Eaton. 1996. "Molecular determinants of acute inflammatory responses to biomaterials." *J Clin Invest* 97 (5):1329-34.

Uchida, K., M. Yamato, E. Ito, O. H. Kwon, A. Kikuchi, K. Sakai, and T. Okano. 2000. "Two different types of nonthrombogenic surfaces: PEG suppresses platelet adhesion ATP-independently but HEMA-St block copolymer requires ATP consumption of platelets to prevent adhesion." *J Biomed Mater Res* 50 (4):585-90.

VandeVondele, S., J. Voros, and J. A. Hubbell. 2003. "RGD-grafted poly-L-lysine-graft-(polyethylene glycol) copolymers block non-specific protein adsorption while promoting cell adhesion." *Biotechnol Bioeng* 82 (7):784-90.

Wright, G. J., M. J. Puklavec, A. C. Willis, R. M. Hoek, J. D. Sedgwick, M. H. Brown, and A. N. Barclay. 2000. "Lymphoid/neuronal cell surface OX2 glycoprotein recognizes a novel receptor on macrophages implicated in the control of their function." *Immunity* 13 (2):233-42.

Zhao, Q., M. P. Agger, M. Fitzpatrick, J. M. Anderson, A. Hiltner, K. Stokes, and P. Urbanski. 1990. "Cellular interactions with biomaterials: in vivo cracking of pre-stressed Pellethane 2363-80A." *J Biomed Mater Res* 24 (5):621-37.

Zhao, Q., N. Topham, J. M. Anderson, A. Hiltner, G. Lodoen, and C. R. Payet. 1991. "Foreign-body giant cells and polyurethane biostability: in vivo correlation of cell adhesion and surface cracking." *J Biomed Mater Res* 25 (2):177-83.

Chapter 7. Potentials and Future Applications

7.1 Future application of astaxanthin in regenerative medicine

In this dissertation, astaxanthin has shown to improve the proliferation as well as chondrogenic, adipogenic and osteogenic differentiation of human MSCs. In the future study, the expression level of proliferative protein such as PI3 K, p-MEK, p-ERK, and p-Stat3 needs to be investigated. Also, the expression level of genes specifically related to chondrogenesis, adipogenesis and osteogenesis can be evaluated with reverse transcriptase-polymerase chain reaction (RT-PCR) analysis. Some chondrogenic related genes include ACAN, COL2B, COL10, SOX9; some adipogenic related genes include peroxisome proliferator-activated receptor (PPAR) γ2, lipoprotein lipase (LPL), and fatty acid binding protein (aP2); some osteogenic related gene include osteopontin, Insulin-like growth factor binding protein 2 (IGFBP2). The enhanced effect of astaxanthin on MSC differentiation can be potentially applied in the area of regenerative medicine and tissue repairment.

7.2 Future application of CNT-MSC in photothermal therapy (PTT)

In this dissertation, a cell-based tumor targeted system was established using human MSCs and streptavidin functionalized CNTs. Future work will be focusing on the migration of CNT-MSCs toward different types of cancer cell lines. Photothermal therapy experiments *in vivo* can be done with mouse MSCs tethered with CNTs. The amount of CNTs on mouse MSCs can be optimized similarly described in this dissertation so that the migration capacity of mouse MSCs are unaffected. Mouse MSCs then can be administered to tumor sites *in vivo*, and the tumor sites will be shined with NIR light to eliminate tumor. Due to MSC's immunosuppressive property, the application of MSC in cancer therapy demands extreme caution since MSCs may have the chance of helping tumors hiding from immune surveillance. Moreover, therapeutic efficacy of MSCs needs to be carefully monitored because MSCs may secret various cytokines that may affect clinical effectiveness.

7.3 Future application of CD200 in cardiovascular graft material

Cardiovascular devices such as vascular grafts and drug-eluting stents have been used to treat cardiovascular diseases. During the treatment process, thrombosis is a major cause of failure for medical devices. It is estimated that 60,000 – 10,000 Americans die of deep vein thrombosis each year (Beckman et al. 2010). Coronary arteries are prone to getting clogged, especially when the device is small in size. Chronic inflammation is one of the causes of arterial and venous thrombosis (Martinelli, Bucciarelli, and Mannucci 2010, Aksu, Donmez, and Keser 2012, Poredos and Jezovnik 2007, Di Minno et al. 2012). Thrombosis and inflammation are closely related: inflammation can induce thrombosis while thrombosis can amplify inflammation (Libby and Simon 2001). Thus, anti-inflammatory therapies have the potential to fight thrombosis.

Surface modification with anticoagulants has proved to be efficient in preventing platelet adhesion and activation upon implantation of blood contacting devices. For example, heparin has been widely used to coat vascular grafts using Carmeda BioActive Surface (CBAS) technology (Dreyer et al. 2012). The efficacy of heparin in thrombosis prevention is due to the interaction of its active site and antithrombin III (Serruys et al. 1996). However, heparin modified grafts has limitations such as low patency rate and adverse side effects (Shen et al. 2008).

CD200 is known as an anti-inflammatory self protein. In this dissertation, modification of nano- and micro-sized particles with CD200 has shown to decrease macrophage phagocytosis. PEG/CD200 functionalized biomaterial surface has also shown to delay macrophage attachment and decrease macrophage activation. In future work, the surface of cardiovascular graft can be modified with PEG/CD200 to reduce thrombosis and restenosis during the treatment of cardiovascular diseases. Expanded polytetrafluoroethylene (ePTFE) surface can be modified with CD200 through polydopamine coating in the method described in this dissertation. Platelet and inflammatory cells attachment/activation can be tested on PEG/CD200 coated surface *in vitro*. The effect of PEG/CD200 modified ePTFE on thrombosis, acute/chronic inflammation and restenosis can be further tested *in vivo* in a mouse model.

7.4 References

Aksu, K., A. Donmez, and G. Keser. 2012. "Inflammation-induced thrombosis: mechanisms, disease associations and management." *Curr Pharm Des* 18 (11):1478-93.

Beckman, M. G., W. C. Hooper, S. E. Critchley, and T. L. Ortel. 2010. "Venous thromboembolism: a public health concern." *Am J Prev Med* 38 (4 Suppl):S495-501.

Di Minno, M. N., A. Tufano, W. Ageno, P. Prandoni, and G. Di Minno. 2012. "Identifying high-risk individuals for cardiovascular disease: similarities between venous and arterial thrombosis in perspective. A 2011 update." *Intern Emerg Med* 7 (1):9-13.

Dreyer, D. R., D. J. Miller, B. D. Freeman, D. R. Paul, and C. W. Bielawski. 2012. "Elucidating the structure of poly(dopamine)." *Langmuir* 28 (15):6428-35.

Libby, Peter, and Daniel I. Simon. 2001. "Inflammation and Thrombosis: The Clot Thickens." *Circulation* 103 (13):1718-1720.

Martinelli, I., P. Bucciarelli, and P. M. Mannucci. 2010. "Thrombotic risk factors: basic pathophysiology." *Crit Care Med* 38 (2 Suppl):S3-9.

Poredos, P., and M. K. Jezovnik. 2007. "The role of inflammation in venous thromboembolism and the link between arterial and venous thrombosis." *Int Angiol* 26 (4):306-11.

Serruys, P. W., H. Emanuelsson, W. van der Giessen, A. C. Lunn, F. Kiemeney, C. Macaya, W. Rutsch, G. Heyndrickx, H. Suryapranata, V. Legrand, J. J. Goy, P. Materne, H. Bonnier, M. C. Morice, J. Fajadet, J. Belardi, A. Colombo, E. Garcia, P. Ruygrok, P. de Jaegere, and M. A. Morel. 1996. "Heparin-coated Palmaz-Schatz stents in human coronary arteries. Early outcome of the Benestent-II Pilot Study." *Circulation* 93 (3):412-22.

Shen, Z., W. Wei, Y. Zhao, G. Ma, T. Dobashi, Y. Maki, Z. Su, and J. Wan. 2008. "Thermosensitive polymer-conjugated albumin nanospheres as thermal targeting anti-cancer drug carrier." *Eur J Pharm Sci* 35 (4):271-82.

Chapter 8. Summary and Conclusions

MSCs are extraordinary candidates for various cellular therapies due to their multiple characteristics such as multi-lineage differentiation, low immunogenicity, tumor-tropism, immunosuppression, etc. In this dissertation, astaxanthin encapsulated mPEG-PCL polymeric micelles have shown to improve the proliferation of human MSCs by 26.3% over an 8-day culture period. Astaxanthin can also enhance the chondrogenic, adipogenic and osteogenic differentiation of human MSCs at the concentration of 20 ng/mL. MSCs can be easily cultured *in vitro* and harvested from a temperature-sensitive PNIPAAm-*g*-polydopamine surface. Supplementing culture medium with astaxanthin followed by harvesting MSCs from PNIPAAm-*g*-polydopamine surface can help obtaining a large cell number of MSCs, which is crucial in clinical applications of MSCs. CNT tethered MSCs have shown to retain their migration capability toward the chemoattractant SDF-1α with optimized CNT amount on MSC surfaces. CNT tethered MSCs can be potentially used in photothermal therapy for cancer treatment. MSCs possess immunosuppressive properties partly because MSCs express anti-inflammatory protein CD200 on their surfaces. In this study, modification of nano- and micro-sized particles with CD200 has shown to reduce macrophage phagocytosis through CD200-CD200R interaction. Surface modification with CD200 can potentially help the drug/gene delivery vehicles evade immune surveillance and prolong their circulation time in human body. Moreover, PEG/CD200 coated biomaterial surface has shown to reduce macrophage attachment and proinflammatory cytokine secretion. Surface modification of biomaterials with PEG/CD200 can be potentially used as an anti-thrombotic surface in cardiovascular treatment.

Appendix A

Chapter 3 "Poly(N-isopropylacrylamide) modified polydopamine as a temperature-responsive surface for cultivation and harvest of mesenchymal stem cells" is reproduced by permission of The Royal Society of Chemistry. The link to the paper on the Royal Society of Chemistry's website:

https://pubs.rsc.org/en/content/articlelanding/2017/bm/c7bm00371d

Letter of permission from The Royal Society of Chemistry

Dear Jun,

The Royal Society of Chemistry (RSC) hereby grants Jun Zhang permission for the use of "Poly(N-isopropylacrylamide) modified polydopamine as a temperature-responsive surface for cultivation and harvest of mesenchymal stem cells" as Chapter 3 in the printed and microfilm version of your thesis.

Gill Cockhead

Publishing Contracts & Copyright Executive

Royal Society of Chemistry,

Thomas Graham House,

Science Park, Milton Road,

Cambridge, CB4 0WF, UK

Tel +44 (0) 1223 432134

Appendix B

Chapter 4 "Migration of mesenchymal stem cells tethered with carbon nanotubes under a chemotactic gradient" is reproduced by permission of The Royal Society of Chemistry. The link to the paper on the Royal Society of Chemistry's website: https://pubs.rsc.org/en/content/articlelanding/2019/ra/c8ra09768b

Letter of permission from The Royal Society of Chemistry

Dear Jun,

The Royal Society of Chemistry (RSC) hereby grants Jun Zhang permission for the use of "Migration of mesenchymal stem cells tethered with carbon nanotubes under a chemotactic gradient" as Chapter 4 in the printed and microfilm version of your thesis.

Gill Cockhead
Publishing Contracts & Copyright Executive
Royal Society of Chemistry,
Thomas Graham House,
Science Park, Milton Road,
Cambridge, CB4 0WF, UK
Tel +44 (0) 1223 432134